LEVEL II

Fredric C. Lynch

FREDRIC C. LYNCH, Major, USAF.
e   of Public Affairs

Air Force Institute of Technology (ATC)
Wright-Patterson AFB, OH 45433

PHOTOLUMINESCENCE STUDY

OF LASER INTERACTION WITH GaAs

THESIS

AFIT/GEO/PH/80-6   James M. Heitman

PHOTOLUMINESCENCE STUDY

OF LASER INTERACTION

WITH GaAs

THESIS

Presented to the Faculty of the School of Engineering

of the Air Force Institute of Technology

Air Training Command

in Partial Fulfillment of the

Requirements for the Degree of

Master of Science

by

James M. Heitman, B.S.

Graduate Electro-Optics

December 1980

Preface

Many aspects of this study involved technologies in which I had no previous experience. I consider the short time spent on this effort a valuable experience. The set up and refinement of both the photoluminescence and laser annealing systems used a large percentage of the 14 weeks of full time effort allotted. It was unfortunate that more time was not available to work on the exploration of laser annealing GaAs.

I would like to express my thanks to Dr. R. L. Hengehold for his suggestions and advice; thanks also to Dr. Y. S. Park (AFWAL/AADR), Dr. T. Luke, and Dr. D. Wille (AFWAL/AADO) for many technical discussions concerning this thesis. A special thanks to Dick Lane (AFWAL/AADO) for his help on many aspects of the laser annealing system. Ion implantation was performed by Jim Ehret; epitaxial samples were provided by Gary Mc Coy (AFWAL/AADR). The vacuum and cryogenic systems operated flawlessly thanks to Jim Miskimen, whose cheerful assistance was always available. Finally, to my wife, Marilynn, who has kept her sense of humor through all of this, I would like to express my appreciation for the typing of this report and for just being the person she is.

James M. Heitman

Contents

Contents (Cont'd)

List of Figures

v

List of Figures (Cont'd)

List of Tables

Abstract

A study was made on the effect of scanned C.W. laser radiation
on the photoluminescence (PL) of GaAs. PL data was taken at 5° K
using an argon ion laser (488 nm single line) as an illumination
source. Samples were irradiated at room temperature using a second
argon laser running multiline and TEM_{oo}. The sample spot size was on
the order of 25 microns, and the dwell time was approximately 1 msec.
A flowing cover gas was essential during scanning to prevent oxidation
of the scanned surface region. The damage threshold was primarily a
function of laser power and spot size; dwell time (in the 1 msec range)
was only of secondary importance. PL was not significantly altered
for virgin samples scanned below the damage threshold. VPE grown
samples were implanted, at room temperature, with Ge at a fluence of
1×10^{14} and 1×10^{15} cm^{-2}. Tightly overlapped scan sequences (2.5
micron spacing) were more effective in increasing PL than lightly
overlapped scans (15.2 micron spacing). The optimum power level was
approximately 95% of damage level. Approximately 4% of virgin
material PL was recovered after laser annealing of VPE samples
implanted at 1×10^{14} cm^{-2}. Approximately 6% of virgin PL was recover-
ed by thermal annealing with a Si_3N_4 protective overcoat. Laser
annealing was also performed on a sample which was capped with Si_3N_4,
and identical results were obtained as in the laser annealed, uncapped
sample. No sign of Ge activation was present in the PL spectra of
laser annealed samples. Hall measurements indicated the laser anneal-
ed samples had the same sheet resistance as the high resistivity

virgin material. Thermally annealed samples showed a Ge peak in the PL spectra, and electrically had a sheet resistance 2000 times lower than virgin material. Ellipsometry measurements showed that laser annealing had restored the index of refraction of the surface to the value associated with virgin material. UV reflectometry measurements indicated that substantial recrystallization of the surface had taken place. Laser Annealing was unsuccessful with samples implanted at 1×10^{15} cm^{-2}. Samples implanted at 1×10^{13} cm^{-2} were annealed to approximately the same degree as those implanted at 1×10^{14} cm^{-2}.

PHOTOLUMINESCENCE STUDY OF LASER INTERACTION WITH GaAs

I Introduction

Background

Gallium arsenide (GaAs) is a semiconductor material with experimentally demonstrated characteristics which are ideal for many device applications. GaAs has a relatively large direct bandgap of 1.435 ev at 294° K (Ref 1), which is important for high temperature operation and radiation damage resistance. GaAs also has high electron mobility and short minority carrier lifetime, which are important for efficient microwave devices. However, many problems have been encountered during efforts to establish reliable manufacturing techniques. Most problems stem from arsenic's high vapor pressure at elevated temperatures, which causes GaAs to decompose during heat treatment operations. Decomposition can be effectively stopped by placing an inert, non-porous, and uncontaminated coating on the surface of the GaAs wafer (Ref 2). Even more demanding coatings are required for dopant diffusion operations. Adherence of the protective coating has often proved to be a problem at high annealing temperatures (Ref 3).

Researchers have turned, therefore, to ion implantation, a room temperature doping operation. It is an ideal technique in all respects but one. When large impurity doses (greater than 1×10^{14} cm^{-2}) are implanted into a semiconductor surface, the surface crystallinity is destroyed, usually leaving the surface in an amorphous state (Ref 4). For most devices to be useful, the surface region must be returned

1

to its original crystalline form, and dopant atoms must substitute for host atoms in the host atoms' normal position in the lattice. One method to accomplish the recrystallization is the application of a protective coating followed by annealing in an oven (700-900° C for 15-30 minutes) (Ref 5). However, ion implantation was originally attractive because it avoided the complexities of thermal annealing.

An alternative to thermal annealing is laser annealing. Sufficient laser energy is applied to the semiconductor surface to rapidly raise the surface temperature, while not significantly affecting the temperature of the bulk of the crystal. The surface region to be heated is typically on the order of one micron in depth. For absorption to occur essentially at the surface, it is necessary that the laser operate in a region of the spectrum where the absorption coefficient of the material is very high. This region usually corresponds to a photon energy greater than the semiconductor bandgap. Both Q-switched and C.W. scanning techniques have been successful with silicon (Ref 6;4). Pulse techniques melt the surface rapidly, and recrystallization occurs by liquid phase epitaxy. C.W. scanning techniques do not melt the surface, but rely on solid phase epitaxy, at elevated temperatures, to reattain the previous surface crystallinity. Epitaxial regrowth, in both processes, proceeds from the amorphous/ crystalline material interface region formed by ion implantation.

Photoluminescence (PL) is a non-destructive optical technique which can be used to evaluate the surface region (approximately one micron in depth) of a semiconductor material. PL occurs as a result of the radiative recombination of electrons and holes. PL can be

stimulated by illuminating a sample with light of sufficient energy
to create electron/hole pairs. A spectrometer is used to disperse
the resulting recombination radiation. A PL spectra is produced by
detecting and recording the scanned output of the spectrometer. Opti-
cally active impurities can be identified by the position of certain
lines in the resulting spectra, and the degree of crystalline perfection
can be evaluated by the intensity of other lines. The effect on the
crystal lattice of any processing operation can be evaluated by com-
paring the spectra before and after the process has been completed.

Problem

The purpose of this experimental study was to investigate
the effects of a scanned C.W. laser on GaAs, using PL as a primary
diagnostic tool. This effort emphasized low power and small spot
size scanning of GaAs, since this had not been previously attempted.
Both the annealing and PL systems were assembled and calibrated.
Because of the attendant problems associated with the use of liquid
helium, PL operation at both liquid helium and liquid nitrogen tempera-
tures were compared to see if operation at liquid nitrogen temperature
was able to produce adequate PL intensities for this effort. The
effects of various parameters associated with laser annealing were
studied. Annealing power density, scan rate, number of repeated scans,
scan overlap, and effects of various atmospheres present during
scanning were the primary parameters studied. Implanted samples
spanned a fluence range of 1×10^{13} to 1×10^{15} cm^{-2}. The effects of
various doping species on the success of laser annealing of implanted

samples were not addressed. Laser annealing through a protective
overcoat was attempted. All annealing operations were conducted
with the substrate held at room temperature.

The exact relationship between PL performance and electrical
usefulness of processed material is not exactly known. It was assumed,
however, that good PL performance is important, therefore, the goal
of this effort was to optimize the laser annealing conditions so as
to maximize the PL intensity after annealing.

Previous Associated Research

A recent publication reported a significant increase in PL
from an unimplanted sample of GaAs after it was irradiated with a
relatively long (one millisecond) ruby laser pulse (Ref 7). The
energy density used was approximately 10 J/cm^2. Very little increase
in PL was seen when a very short (25 nsec) Q-switched pulse was used.
Exposure time apparently was a very important variable. Four recent
attempts were made to anneal GaAs using scanning techniques
(Ref 6;8;9;10). All researchers recommended annealing, using a
flowing inert cover gas, with the substrate preheated to approximately
500° C to minimize thermal shock. All reported that optimum annealing
resulted at power densities just below the damage threshold. These
same researchers also reported that poor electrical activation was due
to the formation of surface slip plane cracks. All researchers pre-
viously mentioned used large spot sizes (50-185 microns) and high
beam power (3-7 watts).

A PL spectral peak (1.36 ev) associated with lattice vacancies

4

(usually related to thermal decomposition) had been recorded from uncoated samples thermally annealed at temperatures in excess of 500° C (Ref 2). This emission band can be monitored in laser annealed samples to check for decomposition.

Recent work with silicon showed that laser annealing can restore, in implanted materials, the band edge PL originally measured in unimplanted material. However, the same annealing process performed on unimplanted material resulted in a decrease in PL (Ref 11). This suggested the possibility that further application of laser radiation to implanted material, that had been successfully annealed, could result in reduced crystal quality.

II Theory

Band Theory and Photoluminescence

Electrons occupy discrete energy levels in an isolated atom
(a low pressure gas, for instance). When many atoms are bound together
in a pure semiconductor crystal lattice, the allowed energy positions
split into bands of levels which are separated by an energy gap
where occupation is forbidden (Ref 12). Transitions from one band
to another are allowed if energy greater than the gap energy is
absorbed or lost. At absolute zero temperature, the highest occupied
band is completely full (valence band), and the next higher band
(conduction band) above the energy gap is completely empty. When
sufficient energy is applied to the material to allow some valence
electrons to jump into the conduction band, empty levels (called
holes) will be left at the top of the valence band and the occupied
levels will be at the bottom of the conduction band. If the conduc-
tion band is weakly populated at low temperatures, a downward tran-
sition would have a high probability of occurring from the bottom
of the conduction band to the top of the valence band, and the energy
released would have a small spread around the gap energy. As the
conduction band becomes more heavily populated, or the temperature
is raised, the occupied region in the conduction band and the vacant
levels in the valence band spread. This spreading results in a spread
in the released energy on downward transitions.

Defects or impurities in the crystal structure can introduce
allowed energy levels within the forbidden gap. Levels on the con-

duction band side of the intrinsic fermi level (approximately gap center) generally form donors (n-type impurities), and those on the valence band side of the intrinsic fermi level form acceptors (p-type impurities) (Ref 13). In GaAs impurities from the elements in Group II of the Periodic Table are acceptors, and those from Group VI are common donors. Ge (Group IV) produces both p-type and n-type activity, depending on the concentration introduced (Ref 14).

Energy, sufficient to excite transitions between levels, can come from many sources. There are two energy sources involved in transitions that are of importance to this study: thermal energy (phonons), and optical radiation energy (photons). Energy greater than the bandgap is required to excite electrons from the valence band to the conduction band. Energy greater than the ionization energy is required to free carriers from impurity levels. Impurity levels are normally 100% thermally ionized at room temperature. Downward transitions are either radiative or non-radiative. Non-radiative transitions, which are due to electron/phonon interactions, are more probable at high temperatures, and their presence decreases the yield of radiative transitions.

PL in semiconductors occurs when upper energy levels are optically excited and subsequent recombination of electrons and holes releases optical radiation. Emission lines associated with radiative recombinations are narrowest and most intense when thermal energy is reduced. This is usually accomplished by cooling the sample with liquid helium (4.2° K) or liquid nitrogen (77° K).

Transitions involving excitons, band to impurity levels, donor

to acceptor pairs, and phonon replicas are of primary interest in this study. Figure 1 illustrates the important radiative transitions as they relate to the conduction and valence bands. The symbols ΔE_d and ΔE_a are, respectively, the donor and acceptor ionization energies. Conduction band to valence band radiative transitions have not been seen in GaAs produced by today's techniques.

Information given in the following subsections will be specifically for GaAs near liquid helium temperatures.

Excitons. An exciton is an electron and hole bound together by their attractive electrostatic force, similar to an electron bound to a proton in a hydrogen atom (Ref 12). Excitons are of two main types, free and bound. A free exciton is created from a free electron and a free hole, and it is able to move throughout the crystal lattice until annihilated as the result of recombination. In GaAs, free exciton radiative recombination produces radiation at 1.5156 ev (Ref 15). Bound excitons remain in the presence of impurity atoms. The following bound exciton recombinations are observed in GaAs; exciton bound to a neutral donor (1.5145 ev), exciton bound to an ionized donor (1.5133 ev), and exciton bound to a neutral acceptor (1.5125 ev) (Ref 15). Different donors and acceptors produce a small shift in the bound exciton energy position. Strong exciton emission, at low temperatures, is characteristic of high quality crystals.

Band to Impurity Transitions. The most prominent band to impurity transition is the transition from the conduction band to a bound acceptor level. The conduction band to acceptor transition broadens as the concentration of the impurity increases. The dif-

8
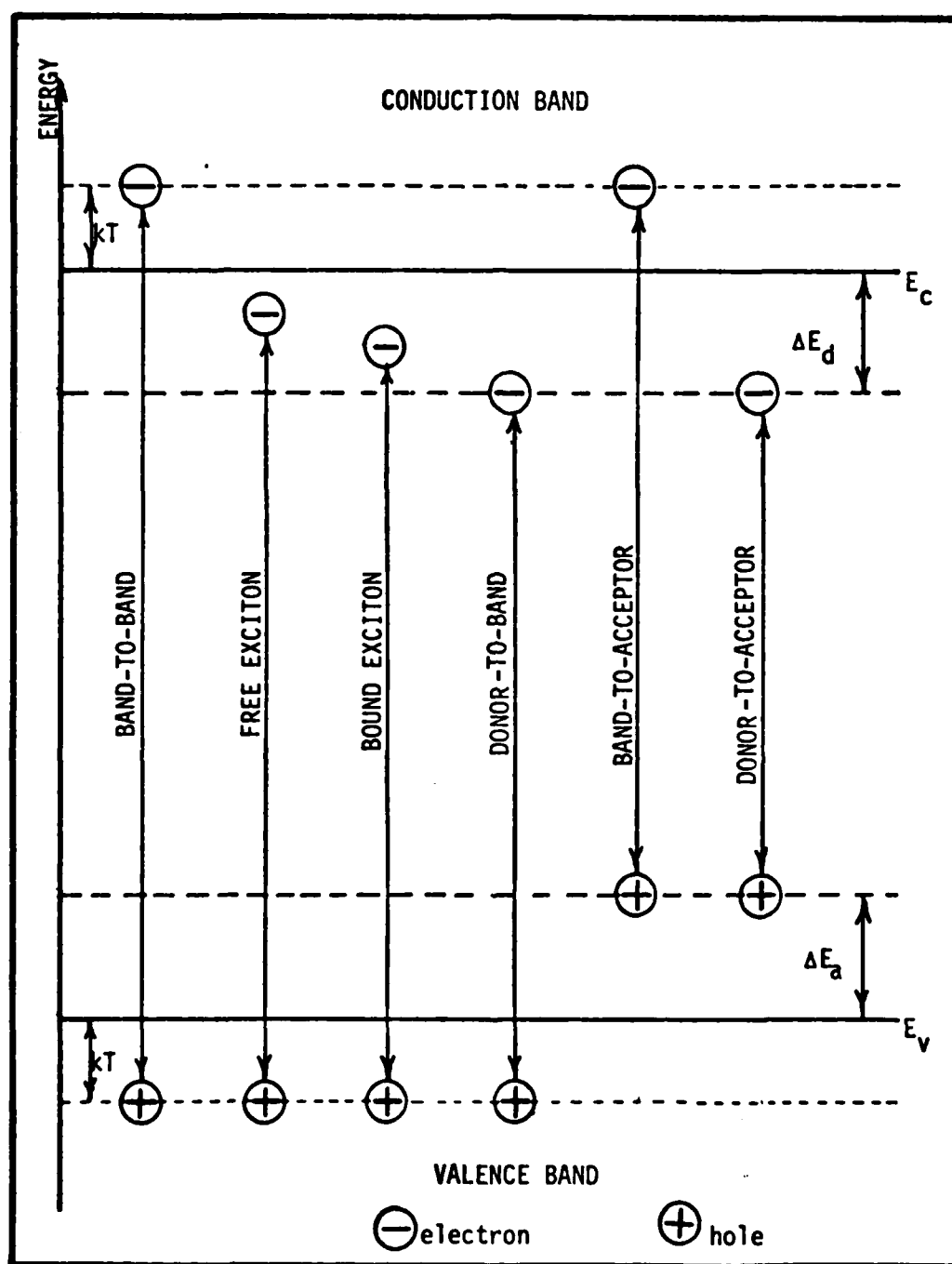
Figure 1. Radiative Transitions

9

TABLE I

Band to Bound Acceptor Transitions
(Ref 16)

Acceptor	Transition Energy ev
Carbon	1.4935
Silicon	1.4850
Germanium	1.4790
Zinc	1.4888

ferences between acceptor ionization energy for different elements are large enough to allow easy identification of acceptor impurity species which are optically active in the crystal lattice. Some transitions are listed in Table I.

In GaAs, all donor impurity levels are very close together, and donor to valence band transitions are very weak, making them difficult to detect and separate. A faint line can be observed at approximately 1.5137 ev for most donors (Ref 15).

Donor-Acceptor Pair Recombination. Donor-acceptor pair recombination involves an electron bound to a donor and a hole bound to an acceptor. Since energy levels associated with substitutional donor impurities are all very close to one another and just beneath the conduction band edge, every band to acceptor line can have a donor-acceptor pair transition (on the low energy side) if a donor is present. The donor-acceptor pair PL peak usually shifts to a higher

TABLE II

Arsenic Vacancy-Acceptor Centers
(Ref 15)

Acceptor	Emission Peaks ev
Silicon	1.417
Germanium	1.454
Zinc	1.368

energy as the excitation energy increases, usually about 1 mev per decade (Ref 15), and rapidly decreases in intensity as the temperature increases above the liquid helium range.

Emission lines associated with arsenic vacancies are listed in Table II. Arsenic vacancies act as donors and form complex recombination centers (Ref 15). Arsenic vacancy-acceptor lines are wider than all the other transitions previously mentioned, and they roll off slowly on the low energy side.

Phonon Replicas. As the binding energy of a carrier bound to a substitutional impurity increases, the electron-phonon coupling increases. Radiation from a recombination which has been phonon assisted is reduced in energy by the integer number of phonon assists times 36.4 mev (the energy of a LO phonon) (Ref 1). In GaAs most transitions involving acceptors can have phonon replicas. These replicas appear on the low energy side of the acceptor related transition, and they decrease in intensity as more phonons are involved.

Ion Implantation

As mentioned in the introduction, ion implantation is an attractive method of introducing dopants into a semiconductor material for device construction. Ion implantation has several advantages: precise and reproducible control of the amount of impurities introduced; ability to implant almost any single species; control of the depth distribution of the impurities introduced; and a clean, low temperature environment for dopant introduction.

A dopant is ionized, and subsequently accelerated, through a high potential field. Various species present in the beam are separated in a magnetic field, and only the desired ions are allowed to impact the material to be implanted. Electrostatic deflection coils are used to raster scan the ions over the material. Total dose can be controlled by varying the beam current and the length of time the material is scanned.

The impurity depth distribution is Gaussian shaped, with the peak below the material's surface. The implant distribution parameters for various ion/substrate combinations can be calculated from the theory developed by Lindhard, Scharff, and Schrott (Ref 17). Range tabulations have been prepared for various ion/substrate combinations (Ref 18), and it is accepted practice to use these values for a specific implanted species. The mean projected range (Rp) and the standard deviation are listed in these tables as a function of accelerating potential. As a result of the collisions between the high kinetic energy ions and the crystal lattice atoms, vacancies, interstitials, and various other defects are formed in the crystal's

surface. It is necessary to recrystallize the damaged surface region and place the introduced atoms into substitutional sites before the implant is electrically active.

C.W. Laser Annealing

In order to repair the damaged layer caused by ion implantation, the material's surface region must be elevated in temperature so that epitaxial regrowth can proceed. Because of the short interaction time (less than 100 nsec) of pulse annealing systems, the surface must be melted to take advantage of the extremely fast epitaxial growth rates associated with the liquid state. Under scanned C.W. annealing conditions the interaction time is much longer (approximately 1 msec), and complete recrystallization is possible, at temperatures lower than melting, by solid phase epitaxy. Elevated temperatures are achieved by irradiating with a laser. For efficient operation, the laser transition must be in a spectral region where the material to be annealed has a high absorption coefficient (photon energy greater than the material's bandgap). The kinetic energy of the stimulated free electrons is transferred to the crystal lattice, resulting in a rise in temperature.

One successful published effort in scanned C.W. laser annealing was conducted by Gat on ion implanted silicon (Ref 6). The main effect of the laser radiation was the supply of the energy needed to raise the temperature of the material being annealed. The annealing mechanism was solid-phase epitaxial regrowth, which started at the amorphous/crystalline interface and proceeded toward the surface. Regrowth rates were comparable to those obtained with conventional

thermal annealing. Gat reported that the surface temperature was proportional to the laser power divided by the beam diameter. It was assumed that, during the dwell time (defined as the beam diameter divided by the scanning velocity) of the laser spot, a thermal steady state condition was established. The required dwell time was determined by the ratio of the amorphous layer thickness and the epitaxial growth rate at the temperature achieved. Since the dwell time was short (approximately 1 msec) and the regrowth rate increased with increasing temperature, it was important to achieve as high a temperature as possible without damaging the crystal (temperature lower than melting). As long as the concentration of impurities was below the solid solubility level, the impurities were fully electrically activated. After the anneal there was no redistribution of implanted atoms (not true for pulse systems). Shallow implanted regions (less than the absorption length of the laser) were recrystallized. Deep implanted regions were converted to polysilicon by laser annealing. Apparently, the region of elevated temperature did not extend to the undamaged crystal region below the implanted layer, therefore, epitaxial regrowth could not proceed from a single crystal structure.

Previous attempts at scanning GaAs have resulted in some success in terms of crystal damage repair. However, electrical activation has never been close to that obtained by thermal annealing. As previously mentioned, surface cracks resulted from laser scanning, and these were suggested as the limiting phenomena. No known studies have reported the effects of laser annealing on the PL properties of GaAs.

III Laser Annealing System

The laser annealing system was set up to be completely auto-matic once a scanning cycle was initiated. Figure 2 is a schematic of the complete system. A C.W. laser was used to provide the necessary optical power. The laser beam was spread slightly, using a negative lens, and then focused, using a positive lens. The laser beam remained stationary throughout the scanning operation. Scanning of the sample was accomplished by having motor driven translation stages move the sample holder (with the sample) in a vertical and horizontal stepping motion. A computer was programmed to control both the scanning stages and a solenoid activated mirror. The mirror was used to deflect the beam away from the optics and into a beam stop, whenever the actual scanning cycle was not in progress. A television system was used to monitor the sample during scanning. Figure 3 is a photograph of the optical portion of the annealing system.

Laser Beam

A C.W. argon ion laser (Spectra Physics, Model 165) was used as a source of optical power. The resonator, which had a one meter cavity length, was composed of a flat rear mirror and a 400 cm radius of curvature output mirror (a half symmetric configuration). The mirrors were broadband coated, and the laser was operated multiline (pri-mary lines were 488.0 and 514.5 nm). The laser was equipped with an internal aperture for transverse mode control. The laser pro-duced multimode power on the order of 5 W with the aperture wide
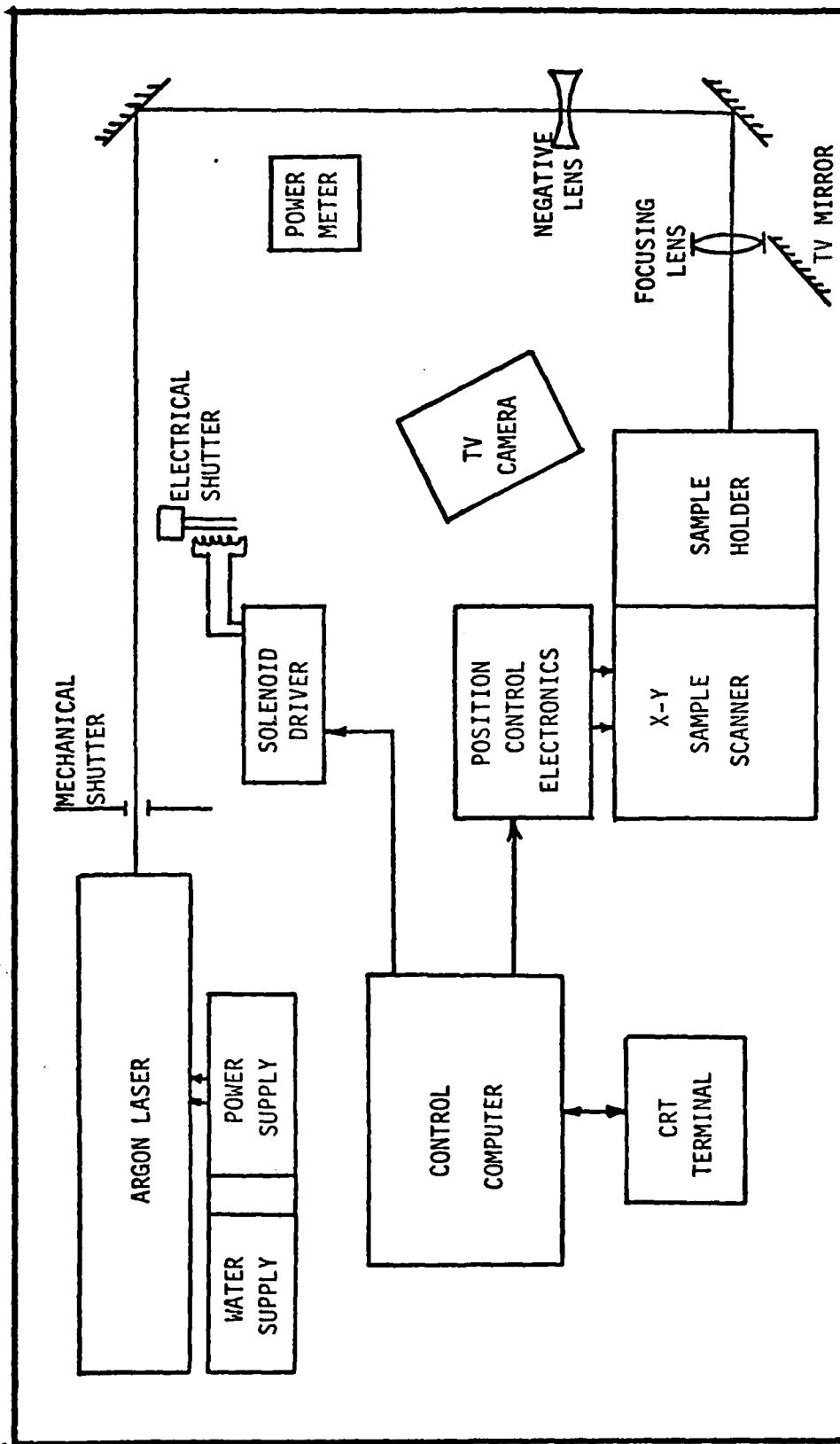
Figure 2. Laser Annealing System Diagram
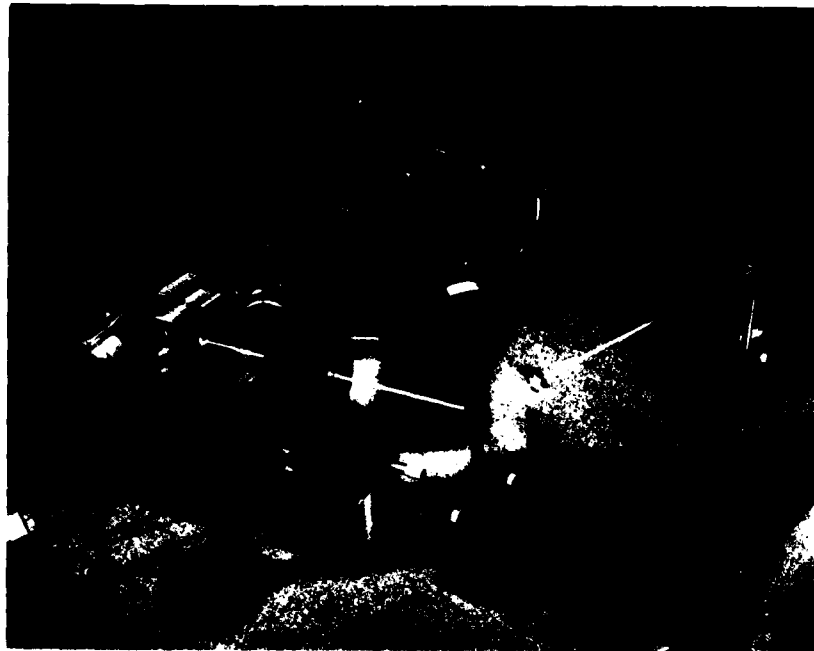
Figure 3. Laser Annealing System
(Double exposure technique used to show beam)

open, and 2.2 W TEM_{00} with the aperture closed to a dial setting of
120 (unknown units).

Beam diameter and divergence were calculated (using complex
radius of curvature techniques) to be 1.20 mm and .67 mrad respective-
ly (at the 1/e points) for the 514.5 nm line. Appendix A contains
details of these calculations. These values are approximately 3%
lower than the published specifications for the laser. The beam
profile was scanned using a fiber optic probe photometer (Gamma
Scientific, Model 2900). The beam shape was more flat topped than
a Gaussian distribution with the same peak and $1/e^{-2}$ width. The
beam was scanned at a distance of 1.5 m from the output mirror, and

the beam diameter was approximately 12% larger than the calculated width for that location.

A small grating spectrometer (Bausch and Lomb, Model 37-06-02) was set up to allow each laser line to be monitored separately with a high speed photodiode (Spectra Physics, Model 403) and an R.F. spectrim analyzer (Hewlett Packard, Model 141T). With the aperture set to 120, only the C/2L mode beats (150 mHz) were observed. When the aperture was opened to a setting of 160, many lines were observed between the C/2L beats, indicating multimode operation. Multimode spatial distributions were also observed using the fiber optic beam scanner previously mentioned. All laser annealing trials were run with the aperture set at 120, resulting in TEM_{00} operation.

Optics

In order to verify waist calculations for the focused beam, a test system was set up to measure the focused spot size for two candidate lenses (15.24 cm and 36.0 cm focal length). A microscope objective was mounted on a positioning stage, which was then mounted on an optical rail, and aligned with the laser beam axis. A 25 micron diameter pin hole was imaged on the scanning fiber optic probe previously mentioned, and the image was scanned to calibrate the system. The microscope objective's and the fiber optic probe's mounts were locked together, and the beam image was scanned at various locations to define the waist position. The waist produced by the two lenses was approximately 15% smaller than the calculated value, which was expected since the unfocused beam was larger than the calculated value. Because of the difficulty in making waist

measurements, and the demonstrated accuracy of the waist calculations, calculated values were used to determine the spot size for all annealing trials.

A high quality multi-element lens (15.24 cm focal length) was selected as the focusing element for the annealing spot. The longer focal length lens was considered at first because of the long associated Rayleigh range. However, preliminary tests indicated that the large spot size and limited laser power were not adequate to reach the damage threshold. GaAs damage was observed, however, using the short focal length lens. Therefore, it was finally selected as the focusing element.

The measured spot size produced by the 15.24 mm lens was approximately 30 microns (36 microns calculated) when the lens was placed 169 cm from the laser output mirror. The spot size was further reduced by placing a simple negative lens in front of the focusing lens. The negative lens expanded the beam passing through the focusing element which resulted in a smaller focused spot. Figure 4 is a plot of spot size versus negative lens focal length. These calculations are valid as long as the divergence angle of the ex- panded beam from the negative lens satisfies the conditions for the paraxial approximation (divergence angle less than 10 degrees). When using a -10 cm lens, placed 34 cm in front of the focusing lens, the spot produced by the focusing lens was measured to be 16 microns (calculated value was 13 microns). The smallest spot size used for annealing was approximately 24 microns.

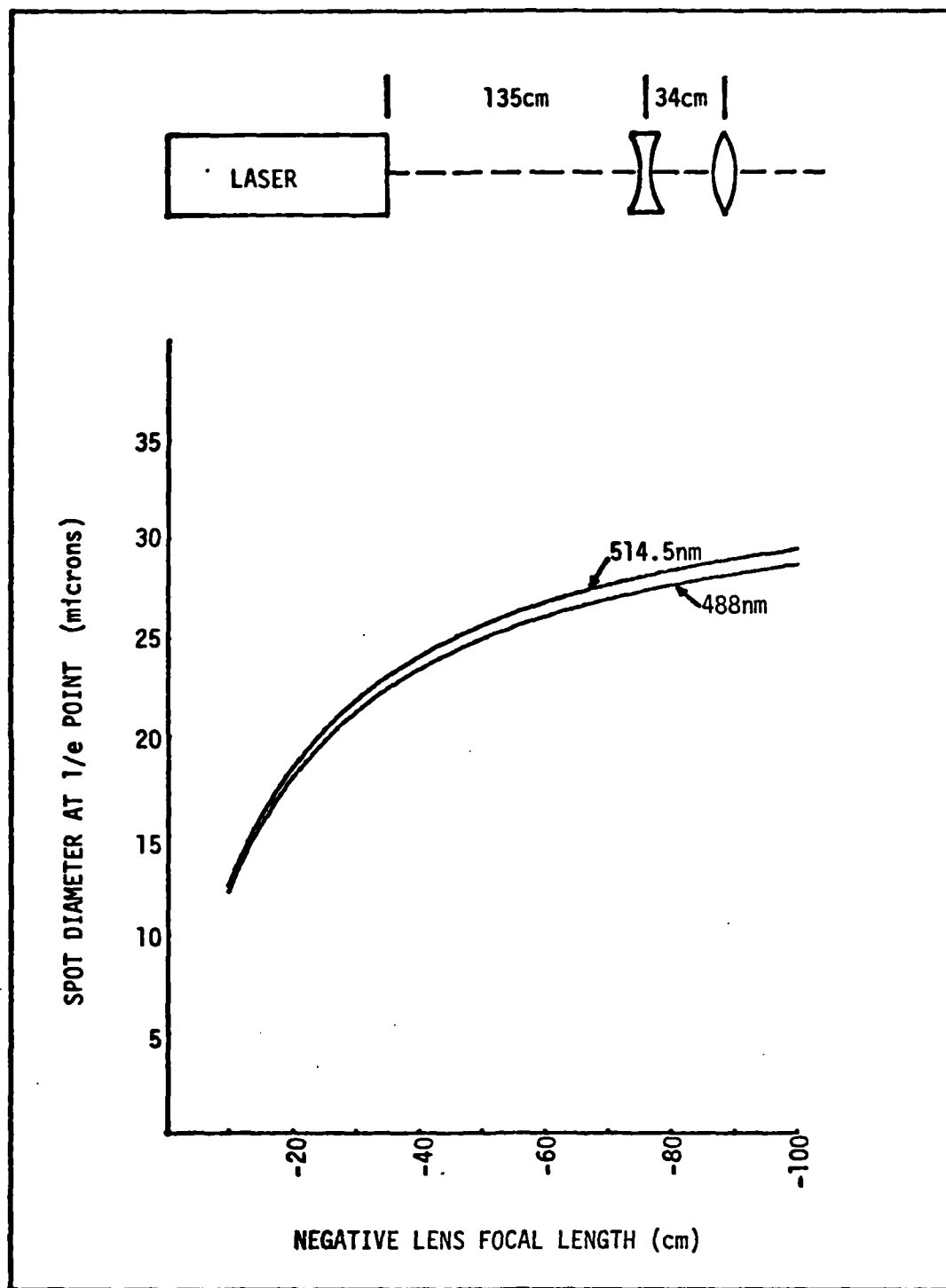Since anticipated scanning rates could be achieved with trans-

Figure 4. Beam Waist Versus Negative Lens Focal Length

lation stages, it was decided to physically scan the sample and avoid focusing field curvature problems (Ref 6) which result when the beam itself is deflected.

Scanner and Electronics

The sample scanner was composed of two orthogonally mounted motorized positioning stages (Aerotech). The vertical stage (fast axis) had a step size of 12.7 microns, and could scan from 0.6 to 6.0 cm/sec. The low speed limit was established by vibrations which caused the stage mount to move on the table. The horizontal stage (slow axis) had a step size of 2.54 microns. Both stages were driven by their controllers when signaled by a minicomputer (Digital Equipment Corp., PDP/11-05). An electrically activated beam deflector was built and interfaced with the computer. The beam deflector was comprised of a small mirror mounted on the armature of a solenoid. When not in a scan cycle, the solenoid was de-energized and the beam was deflected away from the optical system and into a beam stop. During a scan cycle the mirror was moved out of the path of the beam, and the beam was allowed to reach the sample. All power measurements were made after the first beam steering mirror (Figure 2). The transmission of the optics following the first beam steering mirror was measured to be 69%.

A television camera, with a silicon sensing element (response cut off at approximately 1100 nm), was mounted so that the sample would be seen continuously during scanning. The laser light was attenuated with a 650 nm high pass filter placed in front of the camera. Therefore, the spot illuminated by the laser was only

21
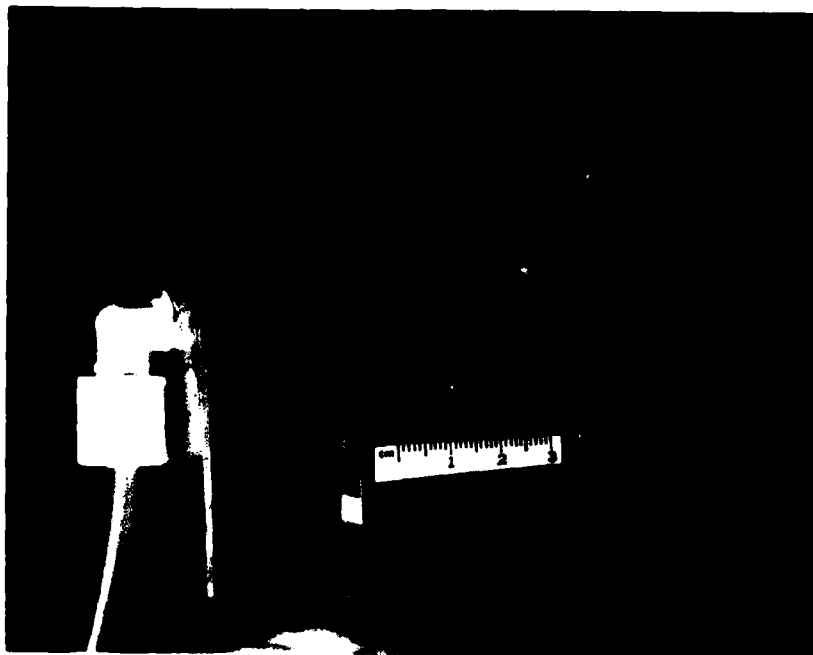
Figure 5. Sample Holder

visible on the television monitor when the surface of the sample was

heated enough to reradiate sufficient radiation in the near IR. A

bright spot on the television image of the sample was always indica-

tive of damage to the sample surface.

Figure 5 is a picture of the laser annealing sample holder.

The aluminum block was rough cut on a lathe to 4. x 4. x 1.5 inches.

A vacuum line was drilled in the side of the block. The block was

tapped and a fitting was attached so that a vacuum hose could be

connected. Two .66 mm diameter holes (3.5 mm separation) were

drilled into the top surface down to the vacuum hole. The top

surface of the sample holder was lapped with successively smaller

grits, with the final surface being lapped with 8 micron size grit.
This surface finish was adequate to ensure good thermal contact with
the polished rear surface of the GaAs samples. An indexing fixture
was bolted to the top surface of the laser sample holder so that the
vacuum holes would be evenly spaced along the diagonal of an indexed
5 mm square sample. The use of this indexing fixture allowed easy
and reproducible sample positioning. Two stainless steel razor
blades were mounted on the top surface of the indexing fixture
(approximately 1 cm from the polished surface), forming a mask to
prevent damage caused by scanning over the sample's edge. Samples
were scanned to within approximately .4 mm of their edges. The
beam would normally scan approximately 2.5 mm onto the razor blades,
in each direction. This allowed the direction change of the fast
axis, and the indexing of the slow axis to the next line position, to
be accomplished off the sample. Since these scanning variations
occurred on the razor blades and not on the sample itself, the scan
lines on the sample were straight, and the sample was scanned at a
constant velocity.

A five inch diameter flexible hose was connected to an exhaust
hood and positioned over the sample holder to draw off any toxic
fumes possibly produced during damage threshold tests. A small
flexible hose was positioned between the sample block and the sample
mask (razor blades) during scanning. A cover gas was allowed to
flow through the hose and over the sample.

23

Procedure

The first step was to accurately locate the waist position of the focused beam. The focusing lens was mounted on a translation stage and its position (Position A) was recorded. With the laser beam illuminating the lapped surface of the sample holder, the entire scanning assembly was manually positioned along the laser beam axis until maximum back scatter speckle size was obtained. Speckle cells from a non-specular surface will increase in size as the illumination spot size decreases. Using this technique, the waist position was located within the Rayleigh range of the focused beam (typically 2.3 mm). A sample was positioned in the sample holder and illuminated by the focused laser beam. The scanning system was manually rotated to position the reflection from the sample onto the blades of the mechanical shutter. The mechanical shutter aperture was only opened enough to allow the laser output beam to pass un-affected. Therefore, the reflection only needed to be offset from the output beam by approximately one beam diameter. This alignment prevented the reflected beam from bouncing off the laser output mirror and returning to the sample. Thus, only the power indicated on the power meter reached the sample, with only the variations normally produced by the laser itself. This procedure also placed the sample in a near normal orientation to the laser beam, which resulted in a round-shaped spot on the sample.

To refine the location of the focus, the following procedure was used. The focusing lens was then moved along the beam axis about 10 mm toward the laser from Position A. The laser was turned

24

up to a power that was known to damage GaAs (greater than 1.4 W in a 25 micron diameter spot). Scanning was then started (without a flowing cover gas) and the lens was slowly translated back toward its previous position, Position A. The sample was monitored on the television, and lens translation was stopped when visual damage (a diffuse white line on the sample) was seen. The laser was interrupted with the mechanical shutter, and the lens micrometer position was recorded. The lens was then moved 10 mm to the sample side of Position A, and the mechanical shutter was opened. The lens was again gradually translated in toward Position A until damage was seen. The laser power was reduced approximately 5%, and the procedure was repeated within the damage range found on the previous iteration. When the damage range had been reduced to less than 1.0 mm of lens travel, the center of this range was assumed to be the focal position. The micrometer position was altered to account for the test sample's thickness. The resulting micrometer position placed the beam waist at the surface of the sample holder. The micrometer was then advanced by the thickness of the sample to be tested.

If no previous information was available on the effect of various laser powers on a specific sample type, then a set of scans, at various power levels, were run to determine the damage threshold. Usually eight lines would be scanned at each power level, and each group of scanned lines would be offset from each other group to facilitate identification with a microscope. When the desired power level was determined, the actual annealing was performed.

The sample to be annealed was positioned on the sample holder

with a pair of tweezers, and the vacuum pump was turned on. The sample was then pushed against the indexing fixture while being held by the vacuum. The power meter (Coherent Radiation, Model 201) was moved into position, and the beam deflector manually deactivated. The required power level (1.43 times greater than the power incident on the sample) was set, and the beam deflector was returned to computer control. The power meter was removed from the beam path. The scanner was positioned at a previously determined start point, and the desired number of scan lines and scan speed were entered into the computer through the CRT terminal. Upon entering the last piece of data, the beam deflector was removed from the beam path, and scanning commenced. During the last scan line the deflector was activated, and the translation stages were stopped at the end of the last line. The vacuum pump was turned off and air was bled into the sample holder to release the sample. The sample was removed with vacuum tweezers and returned to its box.

IV Photoluminescence System

The PL system was composed of a group of components which were carefully integrated to provide fast, accurate, reproducible, and reliable data acquisition on a daily basis. A block diagram of the entire PL system is shown in Figure 6. The center of the system was a cryogenic dewar in which the samples to be tested were mounted. A vacuum system was used to continuously pump the inner baffles of the dewar. A C.W. laser was used to illuminate a spot on a diffuser plate, placed near the dewar, which, in turn, was used as the illumination source for the samples. The particular sample to be tested was imaged onto the entrance slit of a spectrometer and the dispersed light was detected using a photomultiplier tube (P.M.T.). The P.M.T. was cooled with liquid nitrogen (LN). The resultant current pulses were threshold detected, and then recorded with a multi-channel analyzer (M.C.A.). The spectrometer and the M.C.A. were stepped at integer related frequencies, and the result was a digitized plot of PL as a function of wavelength.

Dewar and Vacuum Subsystems

A research dewar (Janis, Model DT) was positioned on a vertically adjustable platform whose framework was securely fastened to the wall of the room. A mechanical vacuum pump (Welch Scientific Co., Model 1397) was attached to a manifold from which individually valved lines were connected to the sample chamber, helium canister, dewar baffle region, and a diffusion pump (Consolidated Vacuum,
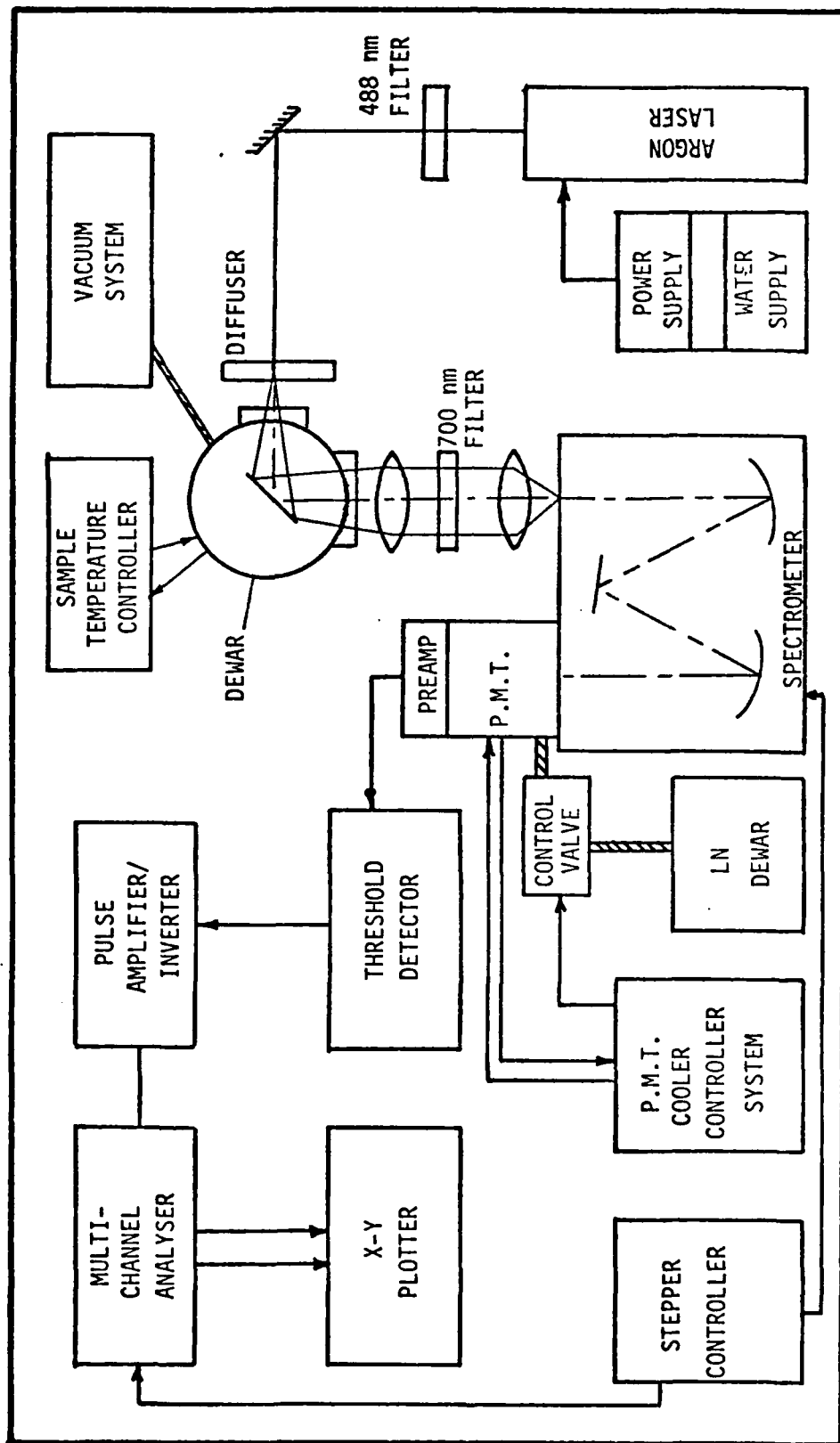
Figure 6. Photoluminescence System Diagram

28

Type PMC-115). The diffusion pump was connected to the dewar inner baffle region and was run continuously over the period of dewar use (baffle region was originally roughed using the mechanical pump).

The dewar consisted of a stainless steel housing with two vacuum insulated canisters: a 3-1/2 liter LN container surrounding a three liter LHe container. LHe was allowed to flow from its canister, through a capillary tube, to a flow control valve. When this valve was opened, LHe was allowed to flow into the bottom of the sample chamber.

Samples were mounted on a flat area cut out of a cylindrical copper block which was attached to the end of a stainless steel rod. A previously calibrated silicon diode was mounted in the rear of the sample holder, directly behind the region where the samples were mounted, and was used as a temperature sensor. Three 30 ohm resistive heaters were placed in the top portion of the sample block to allow control of the sample temperature. The silicon diode and heaters were connected to a closed loop temperature controller (Lakeshore Cryotronics, Model DTC-500). The sample holder assembly could be easily removed and replaced to facilitate a change of samples. Four samples could be held in place by a piece of thin sheet copper, with an aperture for each sample. The samples were sandwiched on the sample holder by the copper sheet which was attached to the copper block with brass screws. The sample chamber was not evacuated during operation, but was continuously purged by the vaporizing LHe entering the sample chamber.

Illumination and Optical Subsystem

An argon ion laser (Spectra Physics, Model 164) was used as the source of pump radiation to excite PL in the samples to be tested. The laser was operated on a single line (488 nm) with a nominal output power of 100 mW. A 1 nm bandpass filter, centered at 488 nm, was placed at the laser output to attenuate all spurious discharge induced radiation, which otherwise might enter the spectrometer and be confused with excited PL. The beam was directed onto a glass plate with one diffuse surface. The diffuse surface was placed approximately 5 cm from the center of the sample holder. The diffuser acted as a quasi-lambertian source and was used to produce a region of uniform irradiance directly over the spot illuminated by the laser. Typical irradiance over the samples was approximately 10 mW/cm^2. Power incident on the diffuser was monitored, before and after a data run, using a thermopile (EPPLY) and a 10% transmissive filter.

A two lens relay system was placed between the samples and the spectrometer. The collection lens was placed its focal length (76.2 mm) away from the samples, and the imaging lens was placed its focal length (200 mm) away from the entrance slit plane. A 700 nm high pass filter was placed between the lenses to prevent scattered laser light from entering the spectrometer, and to function as an order sorting filter. The spectrometer (SPEX, Model 1702) was used with a 1200 groove/mm grating, blazed at 500 nm. The f/7 entrance aperature was overfilled by the imaging lens. The spectrometer bandpass was measured to be linear over a slit width range

of .05-3 mm with a slope of 1.07 nm/mm. Slit height was 10 mm, which was slightly less than the height of the sample image.

Detection and Data Acquisition

The output of the spectrometer was detected by a P.M.T. (RCA, Model C70007A, with an S-1 type photocathode). The P.M.T. was mounted in a refrigeration chamber (Products for Research, Model TE-176-RF) which was bolted onto the exit slit assembly of the spectrometer. A temperature controller (Products for Research) was used to regulate the flow of LN to the P.M.T., and to maintain the photocathode at a preset temperature, normally -100°C. The P.M.T. bias supply (Princeton Applied Research High Voltage Supply, Model HVS-1) was set at a nominal value of 1250 v. The P.M.T. output was connected to an amplifier/discriminator (Princeton Applied Research, Model 1121) which was operated in a single threshold level mode. Event counts were prescaled down by a factor of ten. The output pulse of the discriminator was amplified by a factor of five, inverted to positive going, and stretched to 150 nsec in duration, using a pulse amplifier (Tennelic, Model TC200). The pulse amplifier output was connected to the M.C.A. (Canberra, Model 8100/e). The spectrometer stepper signal was frequency divided and used to trigger the M.C.A. channel advance. A single spectrometer step corresponded to .001735 nm. The M.C.A. continuously counted threshold detection pulses until a predetermined number of spectrometer wavelength steps had been taken. At this point the M.C.A. advanced to the next channel and continued counting. When the scan was completed (1023 channels), the data was plotted on an

X-Y plotter (Hewlett Packard, Model 7045A). Peak counts associated with recorded PL and corresponding channel locations were transferred from the M.C.A. display to the data plot, by hand.

For this experiment, only relative PL between samples was of importance. Therefore, no attempt was made to correct the data for non-uniform system response.

Procedure

The LN canister of the dewar was kep full of LN for approximately two hours, to precool the dewar, before LHe was transferred to the dewar. The samples were placed on the sample holder block and a mask, with four 4 mm diameter apertures, was bolted over the samples to hold them in place. The sample holder assembly was then lowered into the dewar, where it was suspended in front of quartz windows, and sealed at the top with a clamp. Electrical connenction to the temperature controller was made with a single multipin connector. The LHe canister, capillary tube, and sample chamber were purged with dry helium gas prior to filling with LHe. An evacuated, double-walled, flexible tube was used to transfer LHe from a storage dewar to the system dewar. Once full, the LHe canister was sealed off, and was self-pressurized by LHe vaporization. This pressurization increased the flow rate of LHe into the sample chamber. Once the botton of the sample chamber reached LHe temperature, liquid began to rise in the sample chamber. The temperature controller was set to maintain the samples at 5° K, which kept the liquid level from rising above the bottom of the sample holder. The temperature of LHe is 4.2° K, so a slight amount of heat (approximately 40 mW) was required to keep the samples

at 5° K. The LHe flow valve was gradually closed until the lowest stable heater power point was reached. This combination of low flow and required heater power resulted in a small thermal gradient across the sample holder and efficient use of LHe (five hours of operation per single charge of LHe).

With the order sorting filter removed, the specular reflection from the samples was used to position a particular sample's image on the entrance slit. The laser beam position was adjusted on the diffuser so as to produce the maximum illumination condition across the sample. The order sorting filter was then replaced and the P.M.T. bias was turned on. The spectrometer was tuned to a strong PL line and the optics were adjusted for a maximum signal.

Before data collection was initiated, the laser output power was adjusted to a nominal level of 100mW. The PL spectra was then recorded in the M.C.A., and subsequently transferred to a paper plot. Laser power was also recorded at the end of the data run to check for any power offsets which may have occurred during the run.

At the start of each run, an argon calibration lamp was uncovered, near the relay optics, to introduce two peaks of known wavelength. The introduced lines were at 800.6157 and 801.4786 nm. After these peaks were recorded, the calibration lamp was again covered to prevent other calibration lines from entering the data.

V Experimental Results

As an initial step, the PL of virgin material was investigated. Virgin material was then irradiated at various power levels, and the effects of laser exposure on virgin samples were studied. Baseline PL data was collected from ion implanted samples. Various surface effect thresholds, resulting from laser irradiation, were observed for implanted material. Finally, optimum scanning conditions were established for laser annealing implanted GaAs. Under these optimum conditions, ion implanted GaAs samples were annealed; control samples were thermally annealed. Samples (all of which were 5 x 5 mm) annealed by both methods were them compared, using PL and other techniques.

PL of Virgin Material

All epitaxial layers were grown by vapor phase epitaxy (VPE) in facilities at AFWAL/AADR. Two separate PL spectra were made, at LHe temperature, to illustrate the characteristics of VPE material. Figure 7 shows the spectrum from approximately 1.55 ev to 1.27 ev. The individual peaks were identified and are listed in Table III. A high resolution (.05 nm FWHM) scan of the exciton region is shown in Figure 8. Table IV is a list of the transitions believed to be responsible for these lines.

In analyzing the effects of laser annealing ion implanted material, it was not possible to resolve the exciton lines because the signal levels were too low. The most common slit widths
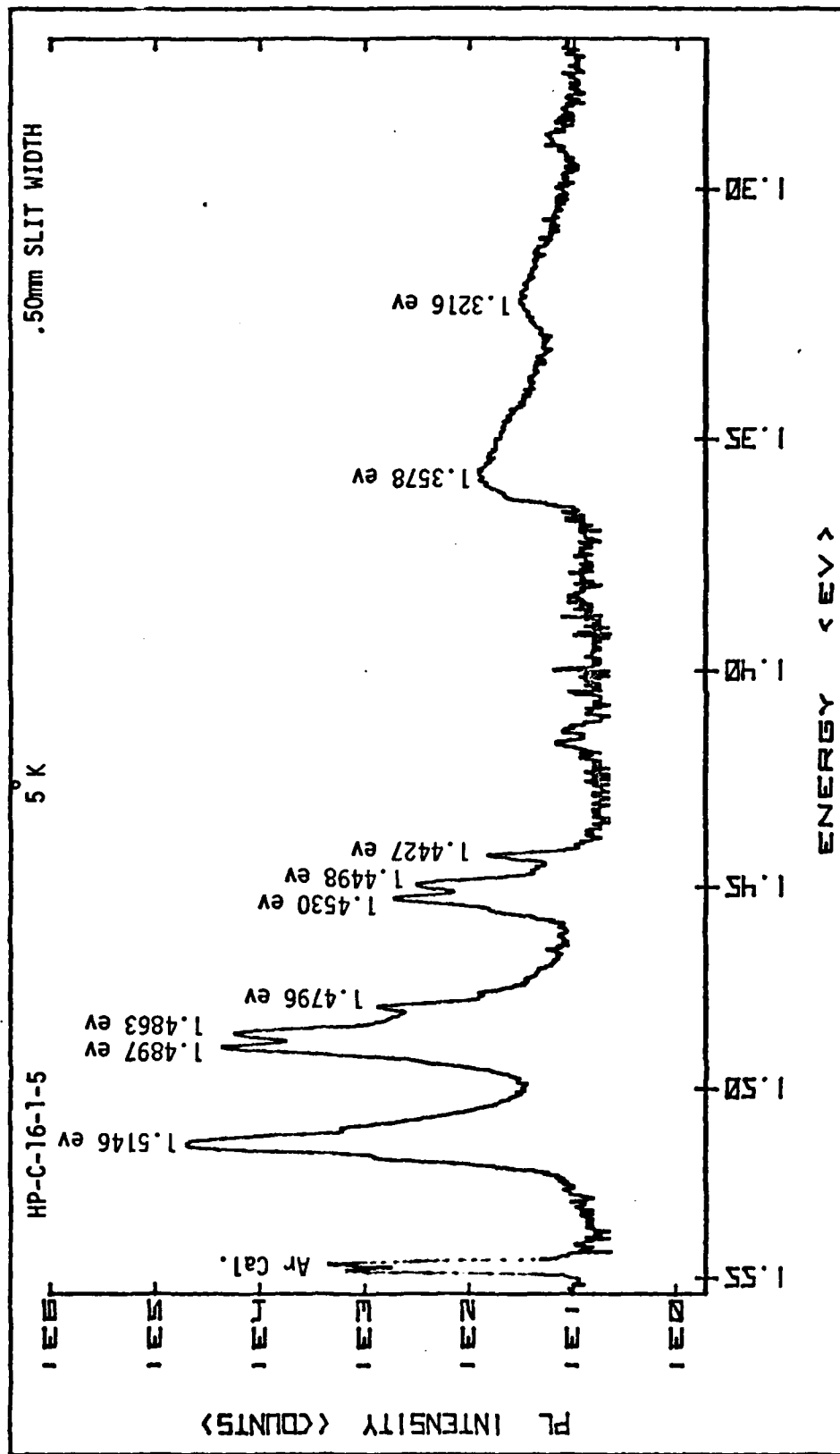
Figure 7. PL of Virgin VPE GaAs

TABLE III

VPE PL Spectral Lines

Line #	Energy (ev)	Transition
1	1.5138	Exciton Transitions
2	1.4891	Band to Zn Acceptor
3	1.4852	Donor to Zn Acceptor
4	1.4791	Band to Ge Acceptor
5	1.4526	Phonon Replica of #2
6	1.4490	Phonon Replica of #3
7	1.4423	Phonon Replica of #4
8	1.3582	Vacancy Complex to Zn Acceptor
9	1.3215	Phonon Replica of #8

TABLE IV

VPE Exciton Spectral Lines

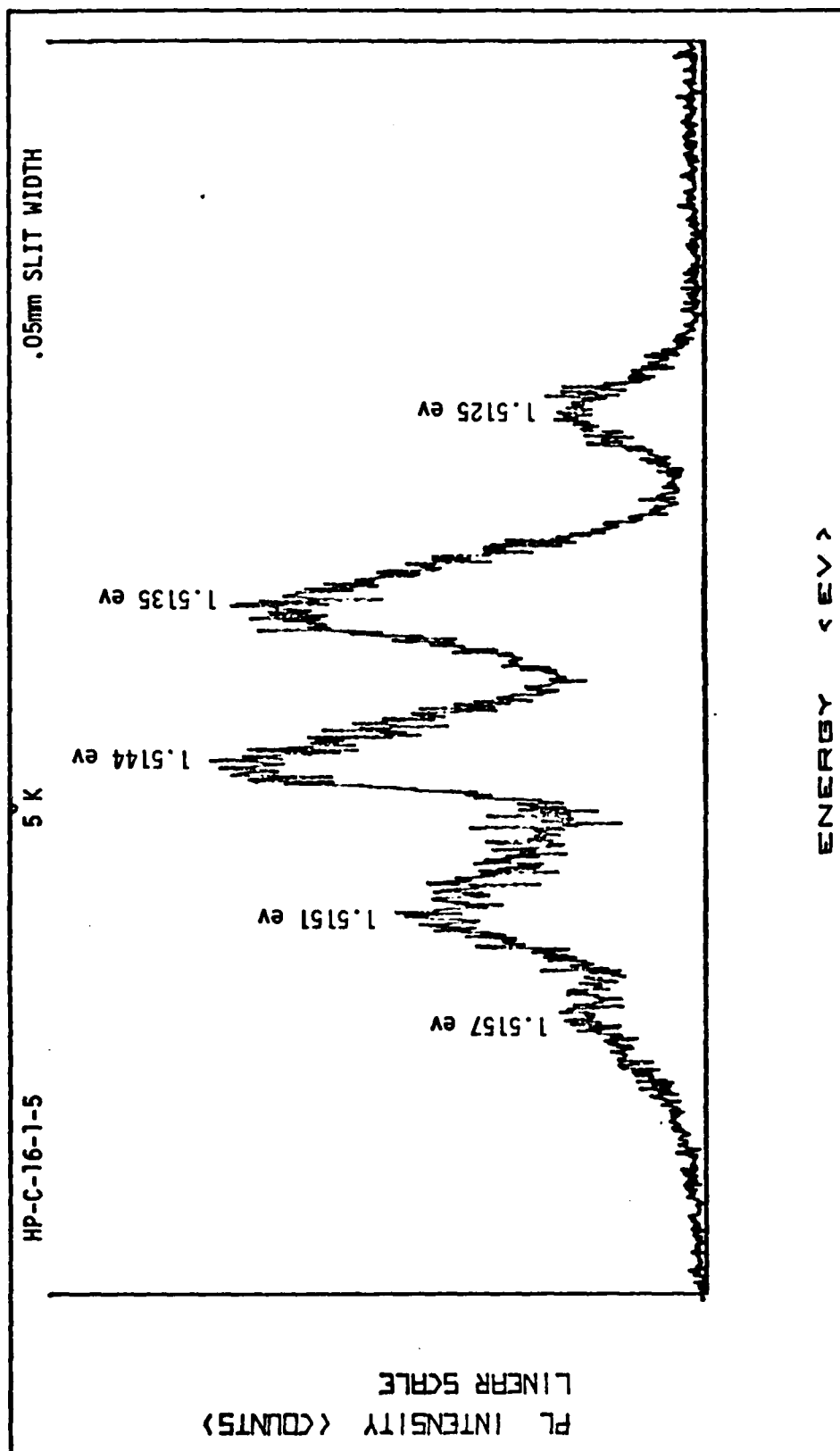| Energy (ev)	Transition
1.5157	Free Exciton
1.5151	Unknown Origin
1.5144	Exciton Bound to Neutral Donor
1.5135	Exciton Bound to Ionized Donor
1.5125	Exciton Bound to Neutral Acceptor

Figure 8. High Resolution of Exciton Band in Virgin VPE GaAs

(.25 to .50 mm) produced spectra similar to Figure 7, in which the individual exciton peaks overlapped to form essentially one peak. In general, the band to acceptor and combined exciton transitions were monitored to measure relative PL performance.

The same VPE sample, used for the data shown in Figure 7, was also run at LN temperature (Figure 9). A different set of argon calibration lines were accidentally introduced; this resulted in a shift to the left of the energy scale, relative to other spectral plots. The band edge transitions are very low in intensity and the vacancy complex band has widened appreciably. The acceptor related transitions are barely detectable. Since the PL of annealed implanted samples was expected to be lower than that for virgin samples, it was decided to collect all subsequent spectra at LHe temperature.

Data on VPE samples was collected at various temperatures and illumination intensities; this data was used to identify the acceptor related peaks. The peak at 1.4852 ev rapidly decreased in intensity as the temperature increased (Figures B-1 to B-4), and it shifted to higher energy (.7 mev/decade) as the illumination intensity increased (Figures B-5 to B-7). As previously mentioned, these are characteristics of donor-acceptor pair transitions (Ref 15). The donor species were unknown, and the acceptor element proved to be Zn, since it was the only acceptor identified. The line at 1.4891 ev at first increased with increasing temperature, and then decreased. This line did not shift significantly as the
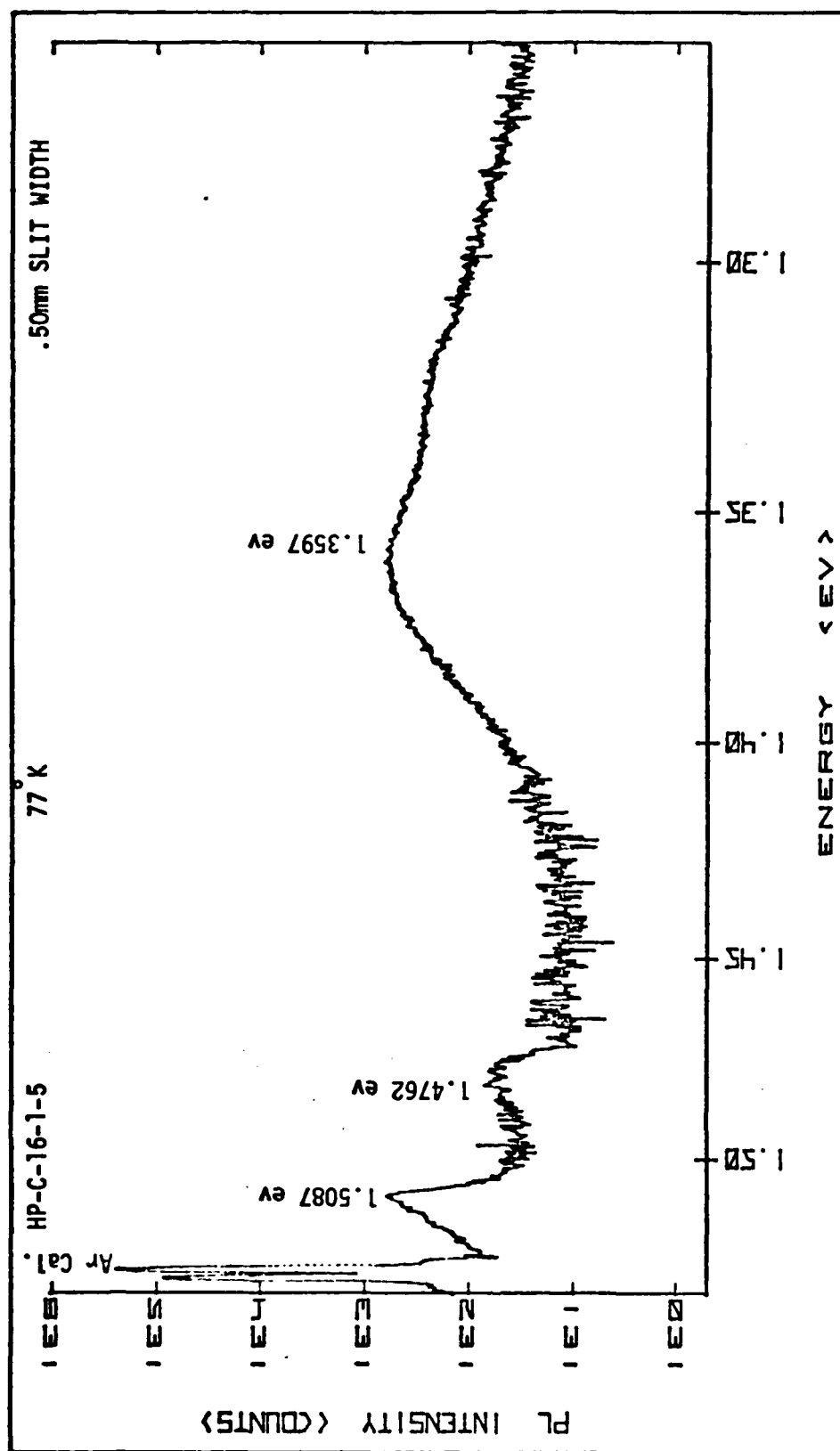
38

Figure 9. Virgin VPE GaAs at Liquid Nitrogen Temperature

illumination level changed. This line, therefore, was associated with a band to Zn acceptor transition.

Spectra of both VPE wafers used for the implantation/annealing part of this study are shown in Figures 10 and 11. These spectra show no evidence of Ge contamination as was found in the previous test sample. This will make Ge acceptors resulting from implantation easy to identify in PL spectra taken after annealing. The sample in Figure 11 had a small acceptor line at 1.4920 ev, which was probably due to carbon contamination.

Figure B-8 is a spectrum for virgin, uncompensated Bridgeman grown material used in this study. This material has intense, broad PL lines at 1.4662 ev and 1.4466 ev, which are believed to be caused by vacancy complexes. The Bridgeman material was, therefore, less desirable than the VPE material, but it was useful (because of its intense band to acceptor PL) for preliminary laser annealing tests where the scarce, high quality VPE material was not necessary.

Damage Phenomena

Samples were initially irradiated in an air atmosphere. If the laser power was above a certain threshold (believed to be the onset of melting), the scanning would destroy the sample surface. A smoke-like, dark, diffuse deposit extending on the sample's surface approximately 100 microns from the laser spot. Therefore, once the deposit appeared, the laser spot would always be moving onto a smoke covered area as it scanned. The absorption of the smoke covered surface was higher than that for clean material.
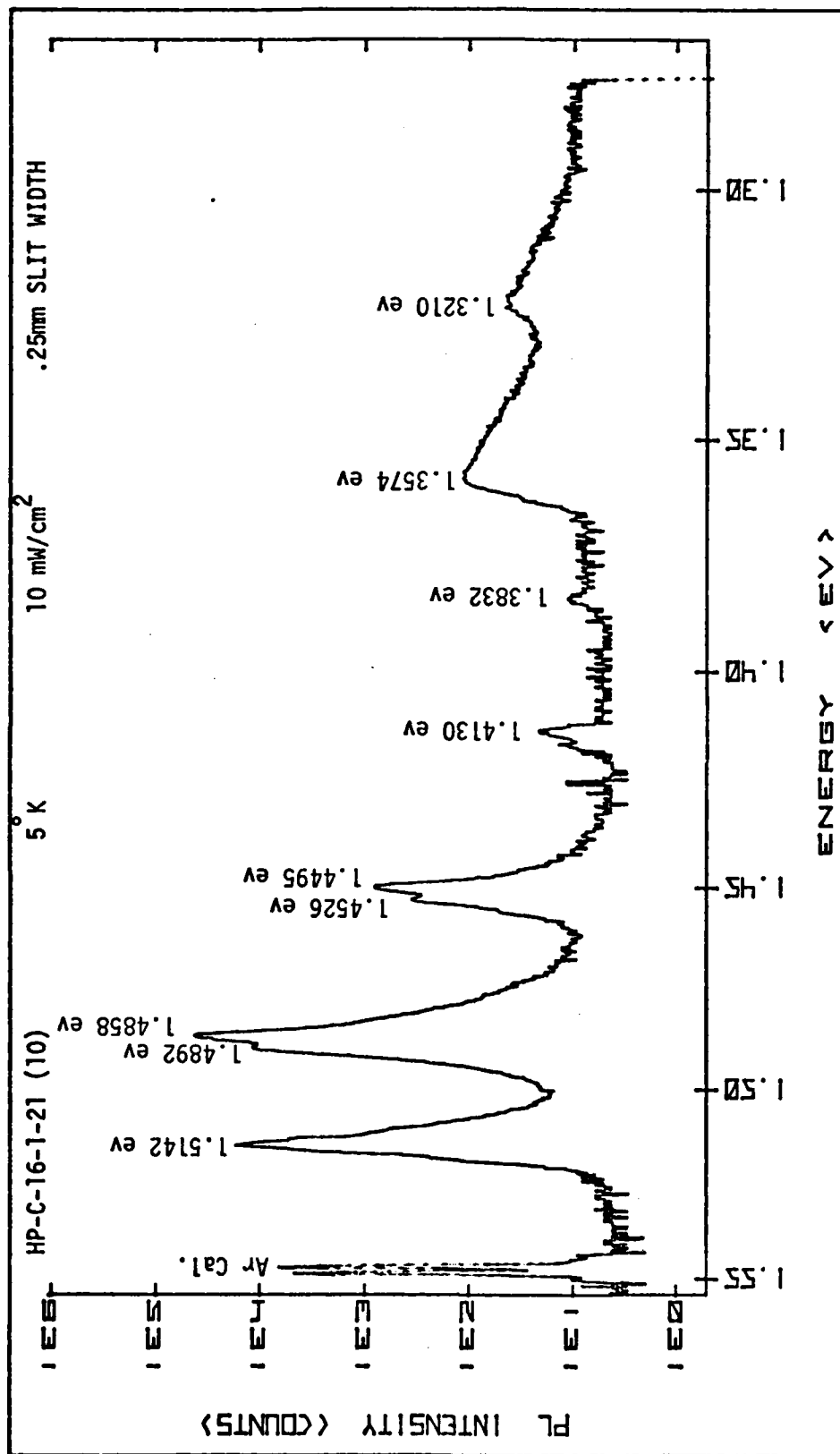
Figure 10. Virgin VPE GaAs (Other Samples from this Wafer Used for Ion Implantation)
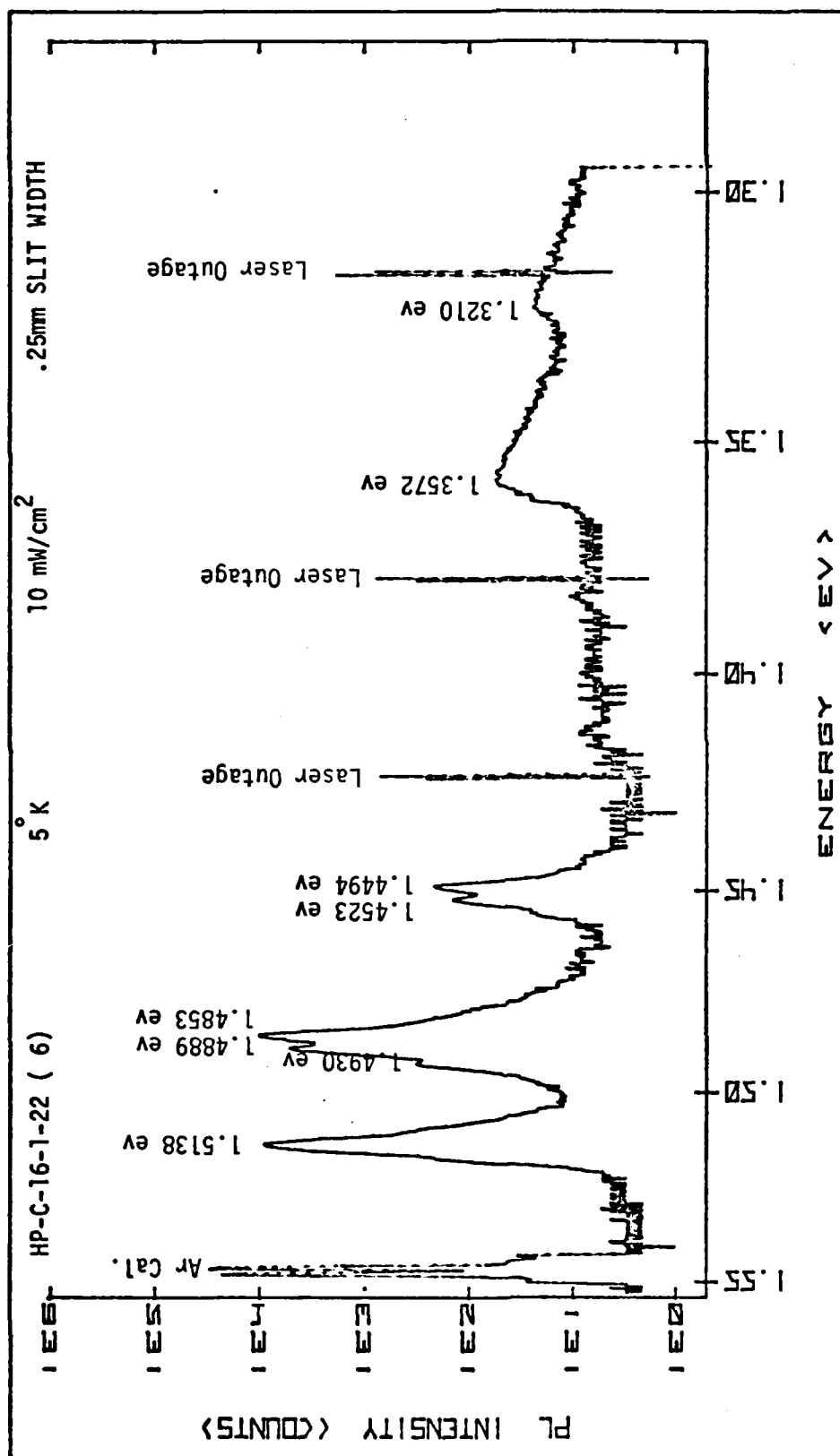
Figure 11. Virgin VPE GaAs (Other Samples from this Wafer Used for Ion Implantation)

The absorbed power (when the deposit was present) was sufficient to cut a scribe line at the peak of the scanning spot and char the surrounding area. The smoke could be washed off, but damage extending the width of the beam was permanent. The samples easily fractured along the scribe line. At power levels below the threshold value, the destructive process could still be started by scanning over a higher absorption defect on the surface of the sample. Once the scanning spot crossed a defect, the previously described process would start up and sustain itself until the beam was shut off.

Although it was planned to use power levels below the damage threshold, any defect on the sample's surface could cause the entire sample to be ruined. Therefore, during scanning, a pure cover gas was allowed to flow over the sample to minimize the reaction of ambient gases with the laser heated spot on the sample surface. Both helium and nitrogen successfully inhibited the destructive reaction. Nitrogen was chosen for subsequent laser annealing experiments because of its availability. If a defect was scanned, with the cover gas flowing, the immediate defect area was damaged, but the damage was not extended beyond the defect. The sample could also be damaged, even with a cover gas in use, by scanning over the sample's edges. The razor blades, previously mentioned, effectively prevented the beam from scanning over the sample's edges in the fast scan direction, and the scan pattern was always arranged such that the unmasked edges of the sample were never scanned.

Even with the flowing cover gas, microscopically visible surface effects were sometimes caused by the scanning beam.

TABLE V

VPE Surface Effect Thresholds

Threshold Identifier	Threshold Level (W/cm)	Effects
A	310	Onset of surface darkening
B	370	Onset of surface rising
C	530	Onset of depression in raised area, and significant increase in surface rise
D	590	Onset of structure in depression

Table V lists the various thresholds for VPE material implanted with Ge at 1×10^{14} cm^{-2} and laser scanned with a 1.11 msec dwell time and a 23.7 micron spot diameter. Threshold levels are given in terms of power divided by spot diameter (Ref 6). Each effect continued to occur at power levels above that at which the effect started. The darkening starts out very faintly at Threshold A, and is maximized at Threshold B. A raised surface was detected at Threshold B using a Nomarski differential phase contrast microscope (which greatly emphasizes height differences). As the power was increased from Threshold B, the raised area of the surface slowly increased in height. At Threshold C, depressions, believed to be the result of surface melting, were seen in the raised area, and there was a large increase in the height of the raised area.

A sample was cleaved perpendicular to the scan lines and photographed in cross section (Figure 12). The seven flat-topped
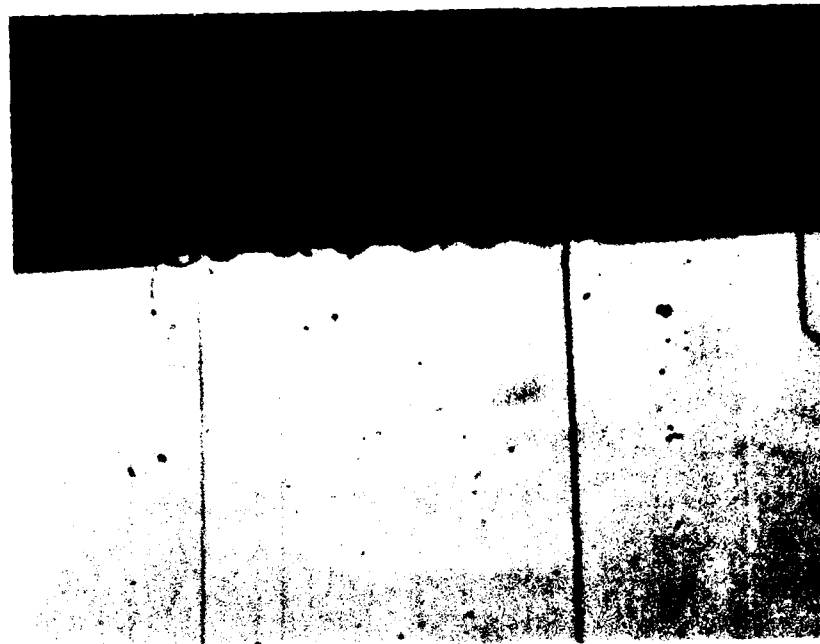
Figure 12. Surface Rising Effect
(Magnification 375x)

scan lines were separated by 20.3 microns; the raised areas were 3.5

microns high. The raised areas (Figure 12) were scanned at 590 W/cm.

The structure associated with Threshold D had various characteristics.

An example of such structure is shown in Figure 13, which is an SEM

photograph of a scan line produced at 620 W/cm. Threshold C (melt

threshold) is approximately 5% higher in virgin material than in

implanted material.

The melt threshold, Threshold C, was measured as a function

of dwell time. It was assumed that Threshold C was indicative of

the surface reaching the melt temperature. A 513% decrease in

dwell time (3.23 msec to .63 msec) resulted in a 6% increase
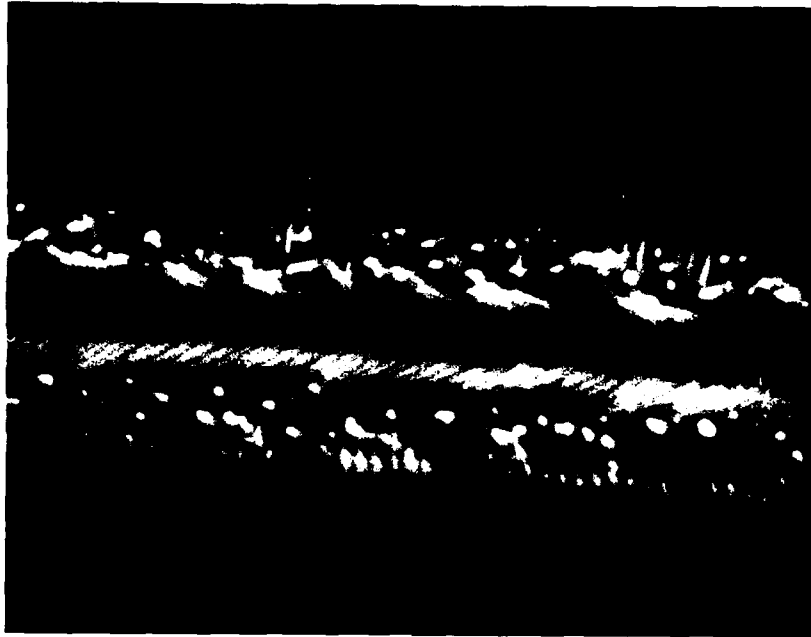
Figure 13. SEM Photo of GaAs Scanned at
620 W/cm (Magnification 5750x)

(500 to 530 W/cm) in Threshold C. This data demonstrates the

surface's strong temperature dependence on laser power (at a fixed

spot size) and not on total energy.

Virgin Material Irradiation

Figures B-9 to B-12 show the PL results of VPE samples

irradiated at various power levels. This material's melt related

threshold was approximately 535 W/cm (Threshold C). Virgin

material was scanned with a 26.8 micron spot, 1.26 msec dwell time,

and 50% scan overlap. A sample exposed at 500 W/cm (Figure B-9)

had the identical PL intensity as an unexposed virgin sample.

46

The vacancy related luminescence (1.36 ev) was also not signif-
icantly affected by the scanning. The laser scanning was apparently
not damaging to the crystal structure of the material at these
power levels. Scanning at very low power (17 W/cm) produced a
50% increase in PL intensity (Figure B-10).

Uncompensated and chromium compensated material, grown by
the Bridgeman technique, and uncompensated Czochralski grown
material were also tested. All sample types showed a 50-100%
increase in PL, which was maximized at approximately 25 W/cm.
Previously reported results (Ref 7) showed approximately a 1000
fold increase in PL after laser illumination at 10 J/cm^2. The
dwell time for both efforts was on the order of 1 msec, but the
previous work was accomplished with a long pulse ruby laser.

Annealing of Ion Implanted Samples

A sample implanted with carbon at 120 Kev (Rp = .25 microns
with a standard deviation of .11 microns) was laser annealed.
This implant produced a damage region which was much deeper than
the absorption length of the annealing radiation (approximately
1 micron). Scan lines appeared to have higher reflectivity than
the unscanned area. No PL was detected before or after the
annealing. If properly annealed, the surface reflectivity should
have decreased.

The first VPE grown samples to be tested were implanted
with krypton (Kr). Kr was used because it has the approximate
weight of the primary dopant to be evaluated (Ge), and it was

easy to set up on the ion implantation machine. Kr was expected
to produce a similar damage distribution (no data available) as Ge
would have produced, but Kr was not expected to become electrically
active, nor, perhaps, even remain in the crystal after implantation.
The annealing objective was, therefore, to restore the original PL as
much as possible. Samples were implanted at one of two fluences
$(1 \times 10^{14} cm^{-2}$ and $1 \times 10^{15} cm^{-2}$ at 90 Kev). A sample of each
fluence was scanned at various powers to determine their melt thres-
holds. The damage thresholds found for these samples were almost
identical. Samples implanted at each fluence were scanned with
approximately a 1.26 msec dwell time, 26.8 micron spot, and 520
W/cm power level (just below the damage level). PL, after scanning,
was compared to a similarly implanted, but unannealed, sample. The
PL of the scanned sample, implanted at $1 \times 10^{15} cm^{-2}$, was reduced
by 50% (Figures B-13 and B-14). The scanned sample, implanted
at $1 \times 10^{14} cm^{-2}$, had approximately four times the PL intensity
of the unannealed, similarly implanted sample (Figures B-15 and
B-16). The reflectivity of the scanned lines was lower, for
samples of each fluence, than that of the unscanned area.

Undoped, Bridgeman grown samples were implanted with Ge at
$1 \times 10^{13} cm^{-2}$ and $1 \times 10^{14} cm^{-2}$. The Bridgeman samples implanted
at $1 \times 10^{14} cm^{-2}$ were used for preliminary tests to optimize the dwell
time and scan pattern. PL spectra were recorded, after implantation,
on a sample of each fluence to establish the as implanted PL inten-
sities (Figures B-17 and B-18). One Bridgeman sample was then
laser scanned with a dwell time of .63 msec, and a second sample

48

was scanned with a 3.23 msec dwell time. Both samples were scanned at a power level just below Threshold C, with approximately a 50% scan line overlap (six horizontal stage steps per line). Both dwell times produced the same PL intensities (Figures B-19 and B-20), and it was concluded that dwell time was not an important factor within the range of values tested. Therefore, a scan speed of 2.14 cm/sec (1.11 msec dwell time) was selected as the baseline rate for the rest of this study (scanning stage operated with the least vibration at this speed).

Another sample was then similarly scanned at the same power but with a horizontal spacing of only 2.5 microns between lines (one horizontal stage step). The resulting PL was the same as the previous sample with 50% overlap. Another sample was scanned with six horizontal steps (15.2 microns) per scan line. The scan pattern was repeated five additional times, with different starting positions, so that all horizontal step positions were individually scanned (Figure 14). The objective of this scan pattern was to achieve a high degree of scan line overlap, but to minimize the thermal interaction between successive scan lines in time (one scan does not significantly preheat the track of the next line). The PL from this sample (Figure B-21) was approximately double that achieved previously.

VPE samples were taken from two separate wafers (both grown along the <100> orientation). The samples were implanted with Ge at 90 Kev (Rp equals .0355 microns, and the standard deviation was .0176 microns). Spectra were recorded, after implantation,
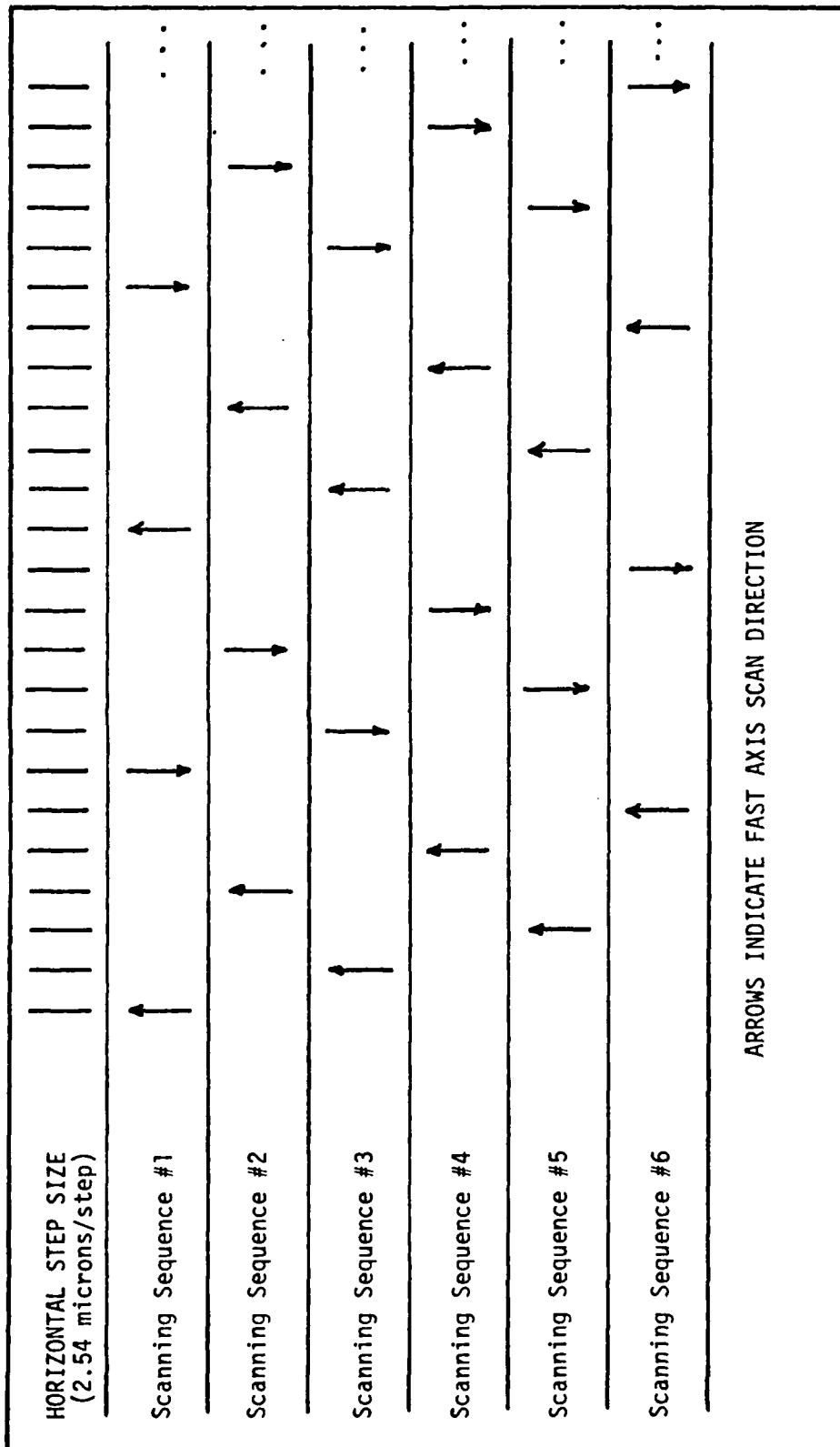
Figure 14. Optimum Scan Pattern

50

for samples from both wafers (Ge implanted at 1×10^{14} cm^{-2}), and are shown in Figures 15 and 16. No PL was detected from a VPE sample implanted at a fluence of 1×10^{15} cm^{-2}. The scan pattern of Figure 14 was run on an epitaxial sample implanted at 1×10^{14} cm^{-2}. The pattern was also run on a second sample, and then repeated after the sample was rotated 90° in the sample holder. Both samples produced about the same PL intensities (Figures 17 and 18). Therefore, the scan pattern of Figure 14 was adopted as the baseline pattern for the rest of the study.

Previous samples had been scanned at about 95% of the level of Threshold C. Two VPE samples were scanned to test the optimum annealing power. The first sample was scanned at Threshold C, and the second was scanned at approximately 83% of the Threshold C level. Results of both sample scans produced lower PL intensities than the scan performed at 95% of Threshold C level (Figures B-22 and B-23). Therefore, the baseline power level was established at 95% of the level of Threshold C, since this level produced the highest PL intensities of the levels tested.

Two ion implanted VPE samples were capped using plasma deposited Si_3N_4 (100 nm thick). One sample was laser annealed using the optimum parameters, previously established. The cap was then stripped and the PL spectra was obtained (Figure 19). The PL intensity was identical to that of the uncapped sample of Figure 17. Two other samples (one from each wafer) were capped and thermally annealed (hydrogen gas, 15 min., @900° C). The Zn acceptor related transition intensities of these samples (Figures 20 and 21) were
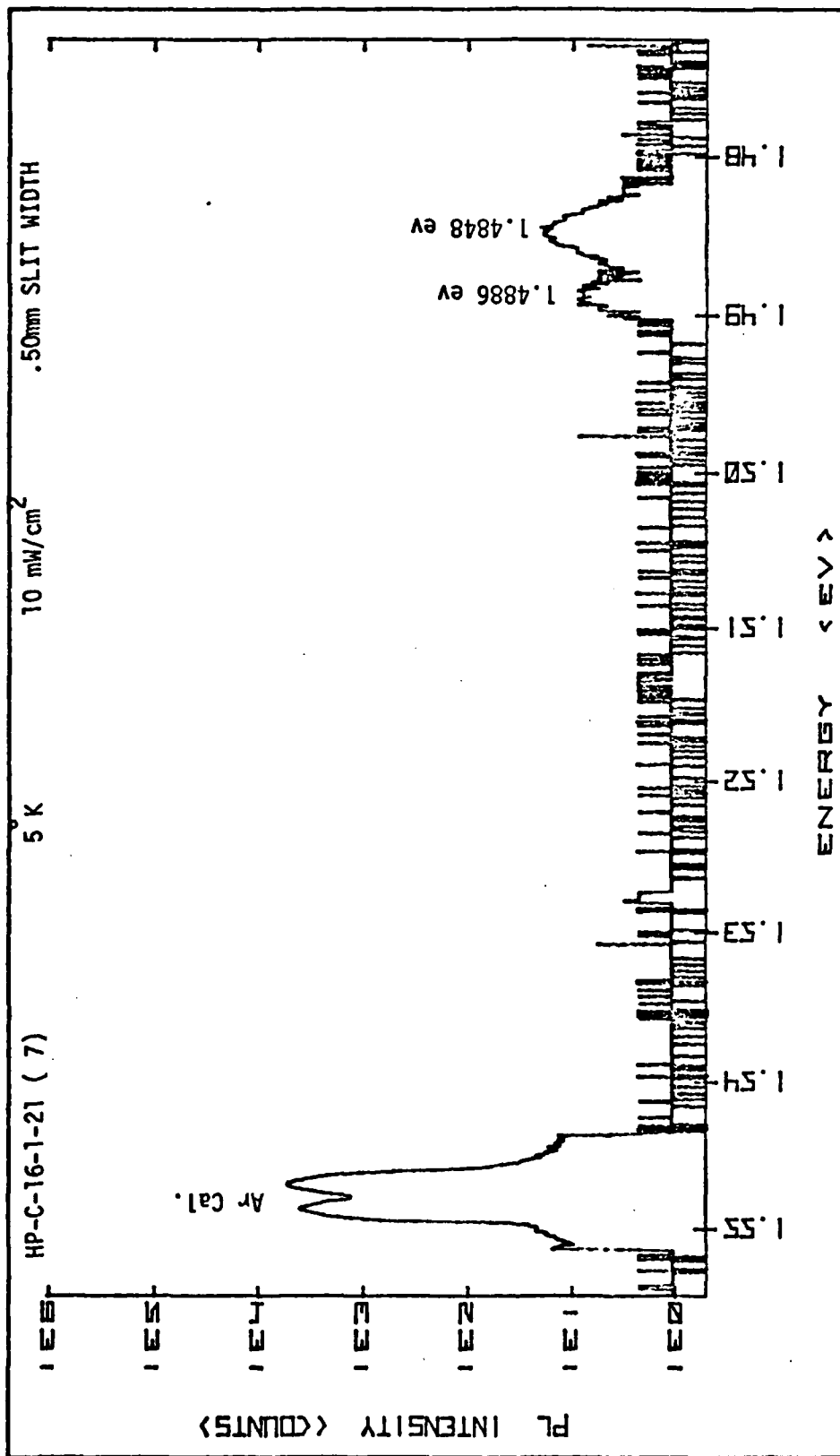
51

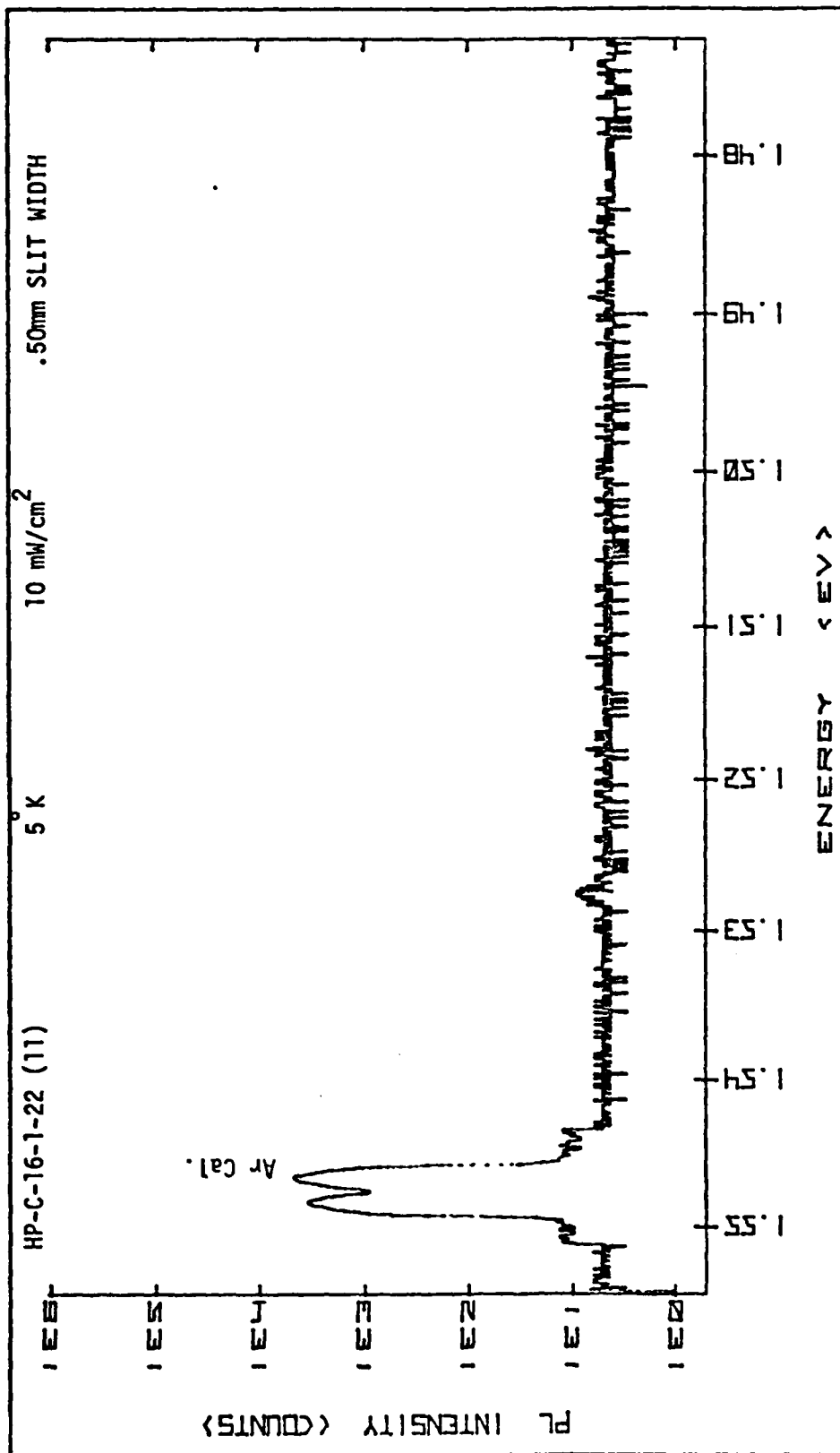Figure 15. PL of GaAs After Implantation with Ge (10^{14} cm^{-2}, 90 Kev)

52

Figure 16. PL of GaAs After Implantation with Ge (10^{14} cm^{-2}, 90 Kev)
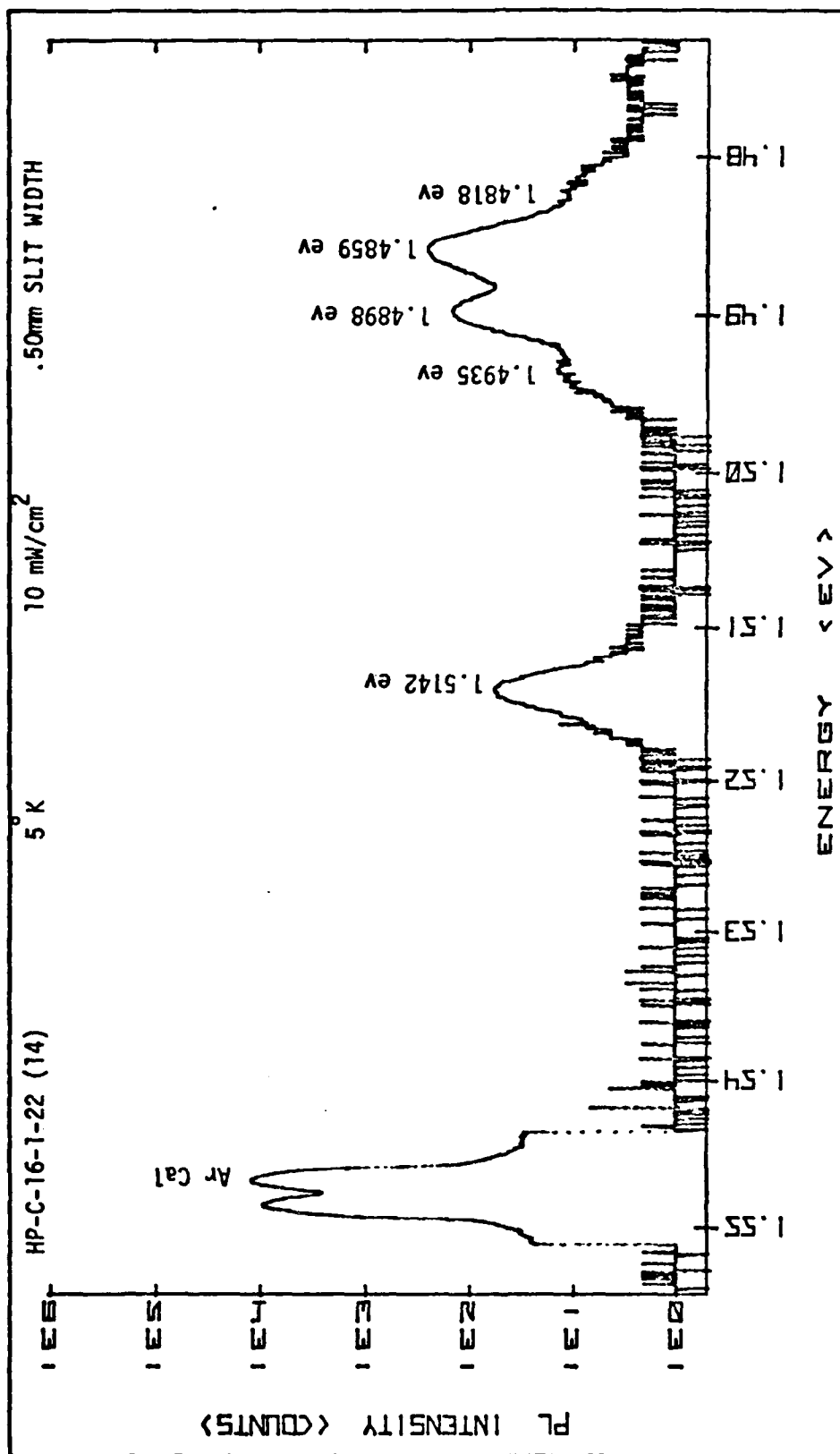
53

Figure 17. PL of Implanted GaAs After Laser Annealing Using Optimum Scan Pattern
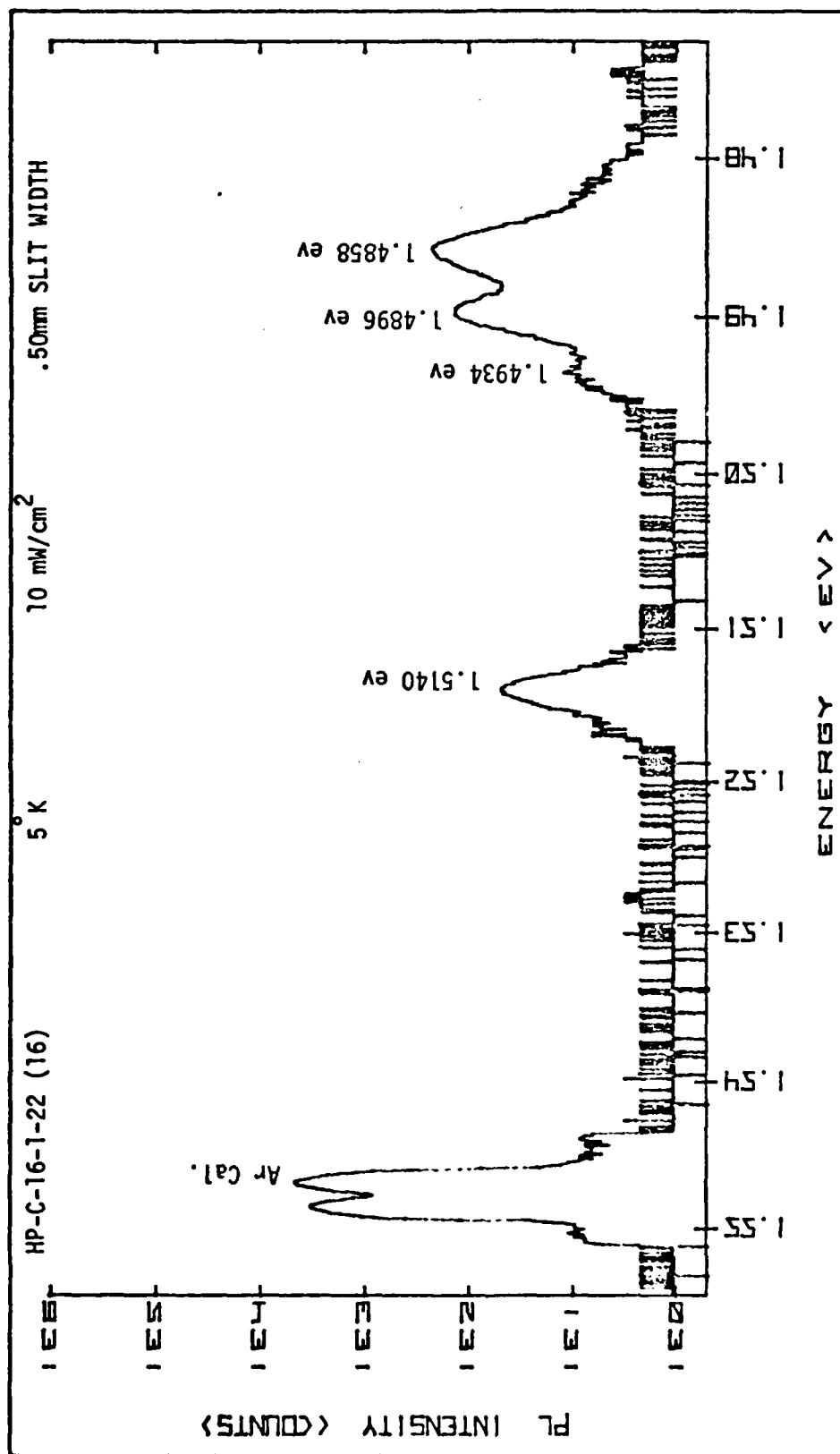
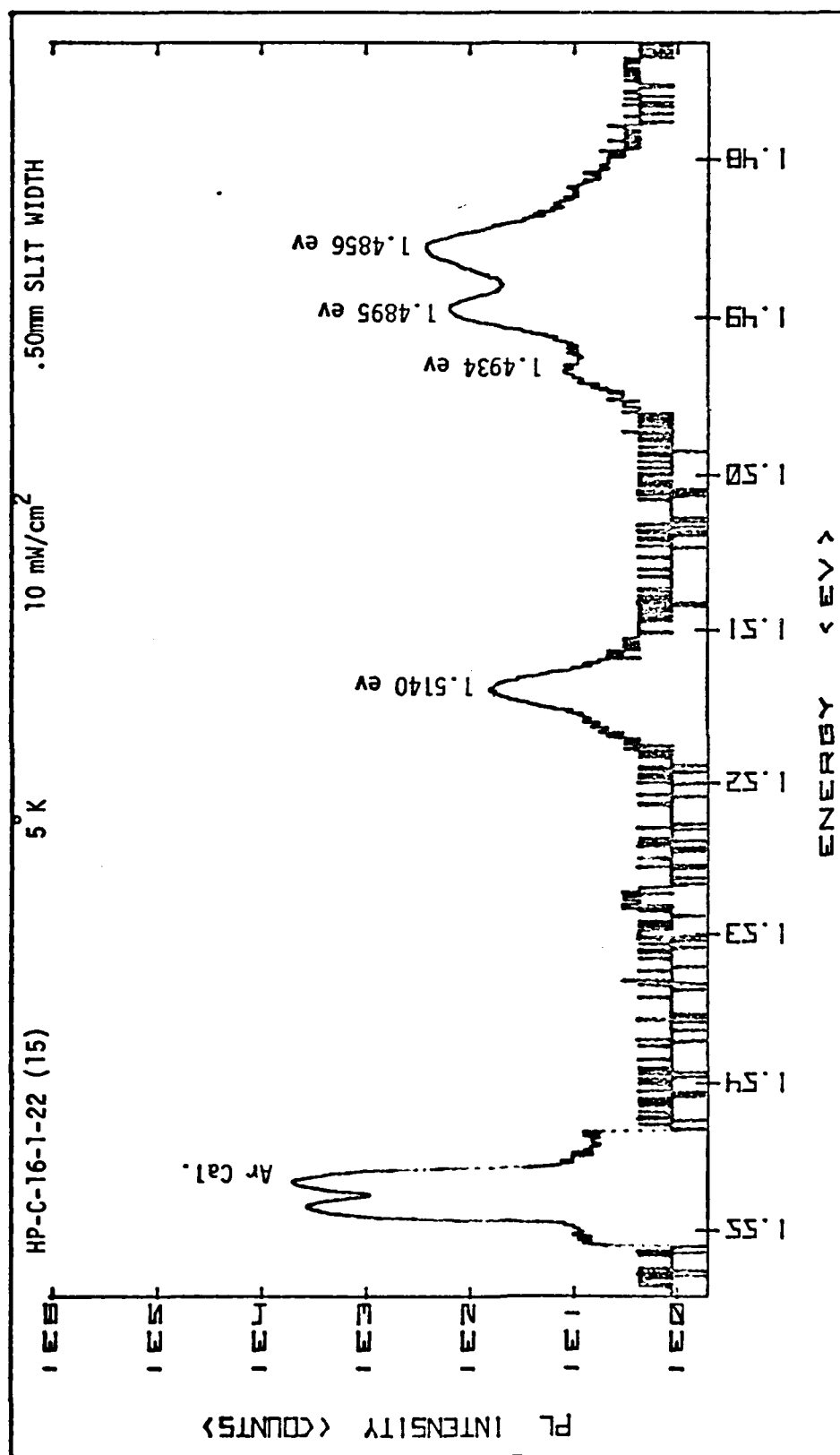Figure 18. PL of Implanted GaAs After Laser Annealing Twice With Optimum Scan Pattern

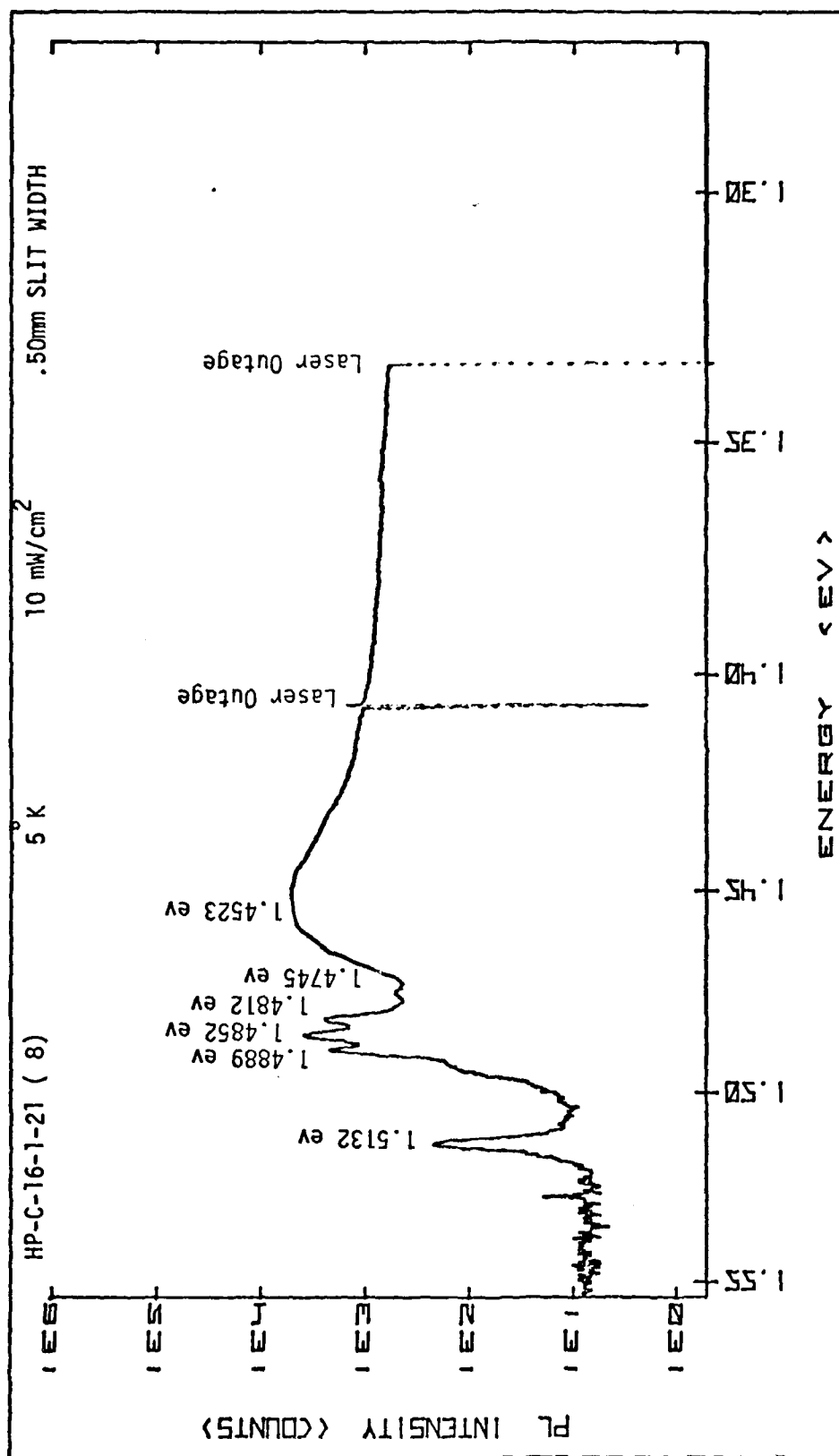Figure 19. PL of Implanted GaAs After Laser Annealing Through Si₃N₄ Protective Overcoat

56

Figure 20. PL of Implanted GaAs After Thermal Anneal With Si₃N₄ Protective Overcoat
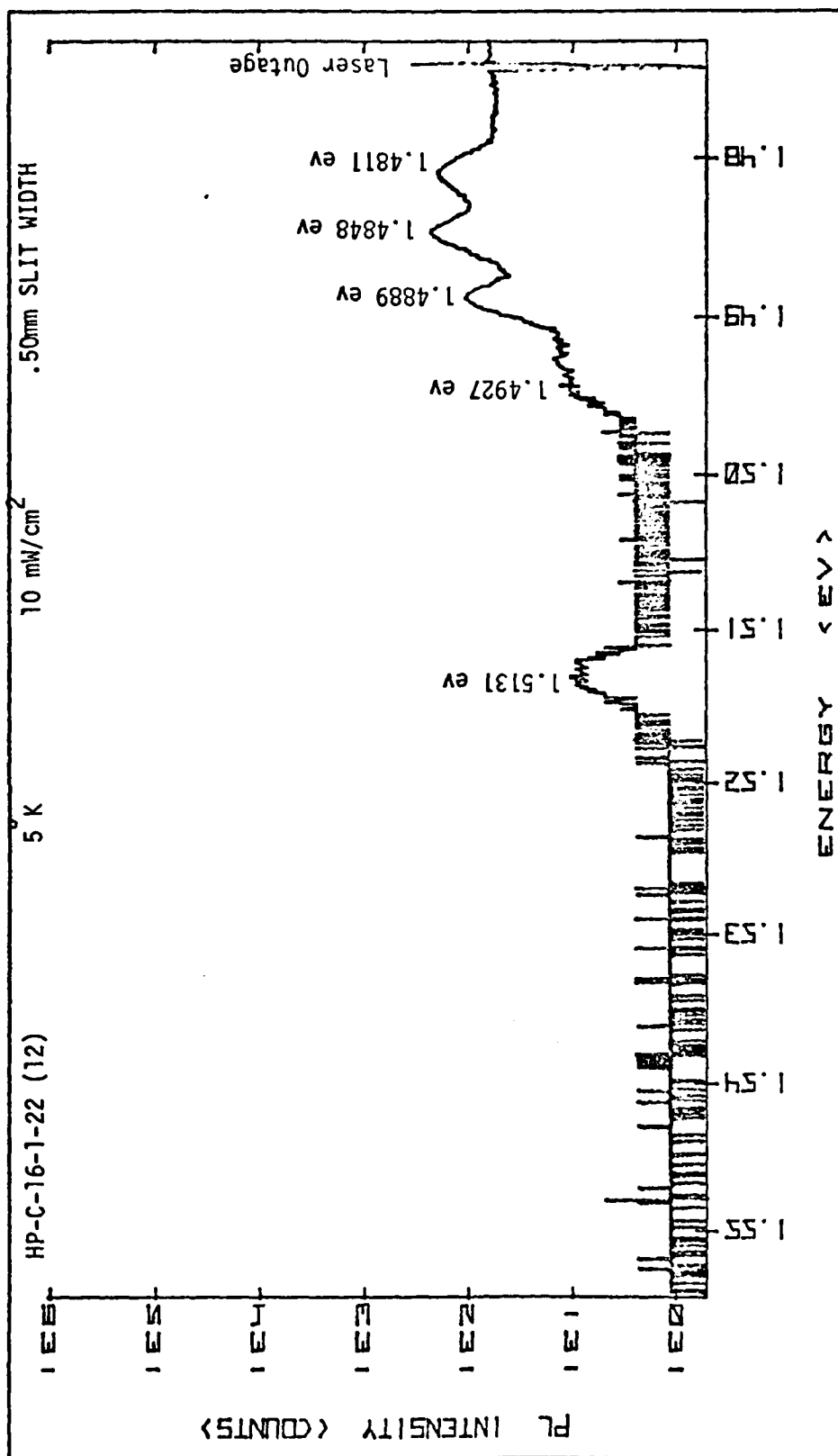
Figure 21. PL of Implanted GaAs After Thermal Anneal With Si_3N_4 Protective Overcoat

approximately the same as that obtained with laser annealing. However, a band-Ge acceptor peak (1.481 ev) was present (indicating Ge activation). There was also a very broad and intense peak centered at 1.4523 ev from the thermal annealed sample. This broad peak could not be positively identified, but was thought to be vacancy related.

Ellipsometry data, collected at AFWAL/AADR, using a He-Ne laser, showed that the capped and uncapped laser annealed samples had the same index of refraction as virgin material. Using the ellipsometry data, the calculated reflectivity was 34% for virgin material, and 41% for material ion implanted at 1×10^{14} cm^{-2}. Only the scanned region of the uncapped sample had a lower reflectivity. The capped sample had the reflectivity value of virgin material over the entire surface. Apparently, the index change was caused during the capping operation, where the sample was heated to 300° C. UV reflectometry data was collected on both the capped and uncapped samples. The resultant data (collected by another AFIT student) showed that both samples still had some residual damage in the surface region.

Hall measurements, performed at AFWAL/AADR, showed that sheet resistivity for laser annealed samples was only a factor of three lower than that obtained for the high resistivity virgin VPE material (5.3×10^6 ohm/$\square$). The thermal annealed sample had a sheet resistivity approximately 2000 times lower (2.7×10^3 ohm/$\square$) than virgin material (which indicates 36% activation of the implanted Ge). All samples tested were p-type. The samples

implanted at 1×10^{13} and 1×10^{15} cm^{-2} were scanned using the baseline parameters (Figures B-24 and B-25). The high fluence sample showed no sign of repair, but the low fluence sample recovered approximately the same percentage of PL as the samples implanted at 1×10^{14} cm^{-2}. Both samples had a region of lower reflectivity in the area scanned by the laser.

An ion implanted VPE sample was run at Threshold B level (310 W/cm) where sharp, dark lines were formed on the surface of the sample. However, the PL was the same as it had been before scanning. UV reflectometry data indicated no surface recrystal-lization had been accomplished.

A summary of the results on Ge implanted samples compared to unimplanted samples is presented in Table VI. Sample numbers which begin with "HP" are VPE samples, and those which begin with "CS" are Bridgeman grown samples.

TABLE VI

Laser Annealing Summary

Wafer #	Ge Dose	Surface Cap	Anneal	Band To Acceptor Peak	Exciton Peak	Figure
HP-C-16-1-21	None	None	None	100.0 %	100.0 %	10
HP-C-16-1-21	10^{14}	None	None	0.05%	X	15
HP-C-16-1-21	10^{14}	Si_3N_4	Thermal	8.0 %	0.5 %	20
HP-C-16-1-21	10^{14}	None	Laser	2.8 %	0.5 %	B-26
HP-C-16-1-22	None	None	None	100.0 %	100.0 %	11
HP-C-16-1-22	10^{14}	None	None	X	X	16
HP-C-16-1-22	10^{15}	None	None	X	X	-
HP-C-16-1-22	10^{15}	None	Laser	0.6 %	0.08%	B-25
HP-C-16-1-22	10^{14}	None	Laser	5.5 %	1.6 %	17
HP-C-16-1-22	10^{14}	Si_3N_4	Laser	5.5 %	1.6 %	19
HP-C-16-1-22	10^{14}	Si_3N_4	Thermal	3.3 %	0.2 %	21
CS-4422	None	None	None	100.0 %	X	B-8
CS-4422	10^{14}	None	None	X	X	B-18
CS-4422	10^{13}	None	None	0.05%	X	B-17
CS-4422	10^{14}	None	Laser	4.0 %	X	B-21
CS-4422	10^{14}	Si_3N_4	Thermal	137.0 %	X	B-27
CS-4422	10^{13}	None	Laser	2.5 %	X	B-24

VI Conclusions and Recommendations

Photoluminescence (PL), taken at LHe temperature, proved to be a useful, although tedious, method for optically evaluating the relative effects of varying C.W. laser scanning parameters. The PL absolute line position accuracy was verified to be better than .3 mev. Measured peak energy values agreed well with published data. Spot size of the annealing focusing lens was found to be easily adjusted by using a negative lens positioned in front of the focusing lens. A cover gas (nitrogen or helium) was successful at inhibiting the formation of a dark, diffuse deposit on the sample's surface, when scanning near the melt threshold. Surface reflectivity of ion implanted GaAs (1×10^{14} cm^{-2}) was measured to be 41%, and, in virgin material, it was 34% (at 633 nm). The lower value of surface reflectivity could be recovered in ion implanted material by scanning at power levels above 2/3 of the damage threshold. Scanning above the melt threshold causes the surface, along the scan track, to swell about 3.5 microns above the unscanned surface. A sample scanned above the melt threshold was sectioned and examined on edge with an SEM. No structural differences were observed when the cross section of the swelled area was compared to the unscanned area. However, the swelled area would not fracture cleanly indicating a loss of crystalline structure.

PL of virgin VPE material was not affected by laser scanning at power levels below the melt threshold. If the GaAs absorption

length, at the PL excitation wavelength, is greater than the implant depth, then PL can be generated from material below the damaged region. PL from material as implanted with Kr was more intense than that obtained from material implanted with Ge. LSS theory predicts that a heavier species (Kr, for instance) will be stopped closer to the surface, at a given implant energy, than a lighter species (Ge). Therefore, heavier atoms produce shallower implants, and thus allow more PL from the region beneath the implant.

Spot dwell time was seen to be of little importance (in the 1 msec region). Laser power and spot size were primary factors in establishing surface damage thresholds, which is consistent with associated work on silicon and first order thermodynamics. Optimum (maximum recovery of virgin PL lines) scanned laser annealing was performed at a power level just below the melt threshold. Successive scan lines should not overlap by more than 50%. Repeated scans, offset from one another, are beneficial (up to about six re-scans). No crack-like lines were observed on the surface of GaAs as the result of laser scanning. Approximately 5.5% of the virgin PL spectrum was reattained in implanted material (1×10^{14} cm^{-2}) after laser scanning. However, no Ge acceptor related PL was observed. No significant electrical activation was measured for the laser annealed sample. Identical results were obtained when an implanted sample was coated with Si_3N_4 before laser annealing. Thermally annealed samples recovered the same percentage of virgin PL as laser annealed samples, but, unlike the laser annealed sample, a Ge acceptor line was present at 1.481 ev. Hall measurements showed

63

36% electrical activation for the thermally annealed sample. Previous measurements of thermally annealed Ge implants achieved about 7% of virgin PL (Ref 19). It appears that C.W. scanned laser annealing is capable of annealing implant damage to the same degree achieved with thermal annealing. Laser annealing did not, however, activate implanted atoms as thermal annealing did. Atoms were either not positioned substitutionally in the lattice or were placed substitutionally and were nullified by neighboring non-radiative vacancy complexes. Very deep implants (deeper than the absorption length of the annealing laser) and a very heavy implant dose (1×10^{15} cm^{-2} and greater) showed little or no PL after exposure to laser scanning.

The goal of the present effort was to evaluate the effect of scanned laser annealing, performed at room temperature and with a short dwell time, on uncapped, ion implanted samples. These are the most desirable annealing conditions, from a manufacturing point of view, but they do not seem conducive to good results. In order to establish a baseline process, it is recommended that laser annealing be attempted on capped samples held at elevated temperature (perhaps 500° C) during annealing. Longer dwell times can be used to move the process in the direction of the higher yielding (in terms of electrical activation) thermal annealing conditions. If a successful process prescription is found, then one can study the trade off between activation and manufacturability.

64

Bibliography

1. Gershenson, M. "Radiative Recombination in the III-V Compounds," Semiconductors and Semimetals, Volume 2, edited by R. K. Willardsen and Albert C. Beer. New York and London: Academic Press, 1966.

2. Birey, Hulya et al. "Photoluminescence of Gallium Arsenide Encapsulated with Aluminum Nitride and Silicon Nitride," Applied Physics Letters, 35: 623-625 (15 October 1979).

3. Eisen, F. H., et al. Ion Implantation in Semiconductors and Other Materials, edited by B. L. Crowder. New York: Plenum, 1973.

4. White, C. W., et al. "Laser Annealing of Ion-Implanted Semiconductors," Science, 204: 461-468 (May 1979).

5. Zucca R. "Effects of Heat Treatment on Semi-Insulated GaAs," Proceedings of the Sixth International Symposium on Gallium Arsenide and Related Compounds, 228-235 St. Louis, Missouri (26-29 September 1976).

6. Gat, A., et al. "CW Laser Annealing of Boron and Arsenic Implanted Silicon; Electrical Properties, Crystalline Structure and Limitations," Solid State Technology, 24: 59-68 (November 1979).

7. Rostworowski, J. A., et al. "Improving the Radiative Yield of GaAs by Laser Annealing," Applied Physics Letters, 35: 934-937 (15 December 1979).

8. Kachurin, G. A., et al. "Annealing of Implanted Layers by a Scanning Laser Beam," Soviet Physics of Semiconductors, 10: 1128-1130 (October 1976).

9. Pan, John C. C., et al. "Annealing of Se-Implanted GaAs and InP by Scanned Nd:Yag Laser Irradiation," Seventh International Symposium on GaAs & Related Compounds. (preprint copy), St. Louis, Missouri (September 1978).

10. Anderson, C. L., et al. "Laser-Annealed Si and Se Implants for GaAs Microwave Devices," Proceedings of the American Institute of Physics Conference, 50: 585-589 Murray Hill, New Jersey (April 1979).

11. Nakashima, Hisao et al. "Photoluminescence Study of Laser Annealing in Phosphorous-Implanted and Unimplanted Silicon," Journal of Applied Physics, 50: 5966-5969 (September 1979).

12. Kittel, Charles. Solid State Physics (Fifth Edition). New York: John Wiley and Sons, Inc., (1976).

13. Grove, A. S. Physics and Technology of Semiconductor Devices. New York: John Wiley and Sons, Inc., (1967).

14. Yeo, Y. K., et al. "Amphoteric Behavior of Ge Implants in GaAs," Applied Physics Letters, 35 (2): 197-199 (15 July 1979).

15. Williams, E. W. and H. Barry Bebb. "Photoluminescence II; Gallium Arsenide," Semiconductors and Semimetals, Volume 8, edited by R. K. Willardsen and Albert C. Beer. New York and London: Academic Press, (1972).

16. Ashen, D. J., et al. "The Incorporation and Characterization of Acceptors in Epitaxial GaAs," Journal of Physics and Chemistry of Solids, 36: 1041-1053 (1975).

17. Lindhard, J., et al. "Range Concepts and Heavy Ion Ranges," Mat. Fys. Medd. Dan. Vid. Sclsk 33 1 (1963).

18. Gibbons, James F. Projected Range Statistics. Stroudsburg, Pa.: Dowden, Hutchinson and Rose, Inc., (1975).

19. Yu, Phil Won. "Deep Emission Centers in Ge-Implanted GaAs," Journal of Applied Physics, 50: 7165-7167 (November 1979).

20. Siegman, A. E. An Introduction to Lasers and Masers, New York: McGraw-Hill Book Company, (1971).

Appendix A

Summary of Gaussian Beam

Propagation Calculations

This appendix contains a review of Gaussian beam propagation calculations using complex radius of curvature (CRC) techniques (Ref 20). The CRC is defined as follows:

$$1/\bar{q} \triangleq 1/R - i\lambda/\pi w^2 \tag{1}$$

where

$\bar{q}$ = complex radius of curvature

R = wavefront radius of curvature

w = spot size (radius at $1/e^2$ point)

λ = wavelength of the propagating beam

If the ray transfer matrix of an optical system is known, then the CRC can be propagated from the input to the output planes using the following:

$$\bar{q}_{out} = \frac{A \, \bar{q}_{in} \times B}{C \, \bar{q}_{in} \times D} \tag{2}$$

Therefore, once a beam's CRC is known at some location, the wavefront radius of curvature and spot size can be calculated at any other point along the beam (as long as the Fresnal approximations are valid). A beam waist (w_0) is defined as the spot size of a beam at a point where the wavefront radius of curvature is infinite (plane wavefront). The Rayleigh range (z_R) of a beam is defined as the distance away from a waist at which the spot area is twice the waist area. It is expressed as:

$$z_R = \frac{\pi w_0^2}{\lambda} \tag{3}$$

The CRC at a beam waist is therefore:

$$\bar{q}_0 = \frac{i\pi w_0^2}{\lambda} \triangleq iz_R \tag{4}$$

The optical schematic of the laser annealing system is shown in Figure A-1. The cavity beam waist is located at the position of the flat rear mirror. The TEM_{oo} waist size is given by:

$$w_{o1} = (\lambda/\pi)^{1/2} \, (L_1 \, (R - L_1))^{1/4} \tag{5}$$

and the associated Rayleigh range is:

$$z_{R1} = (L_1 \, (R - L_1))^{1/2} \tag{6}$$

The ray transfer matrix of the laser optical system from the rear mirror to the outside surface of the output mirror is as follows:

$$\begin{bmatrix} A & B \\ C & D \end{bmatrix} = \begin{bmatrix} 1 & 0 \\ 0 & n \end{bmatrix} \begin{bmatrix} 1 & d \\ 0 & 1 \end{bmatrix} \begin{bmatrix} 1 & 0 \\ (n-1)/nR & 1/n \end{bmatrix} \begin{bmatrix} 0 & L_1 \\ 0 & 1 \end{bmatrix}$$
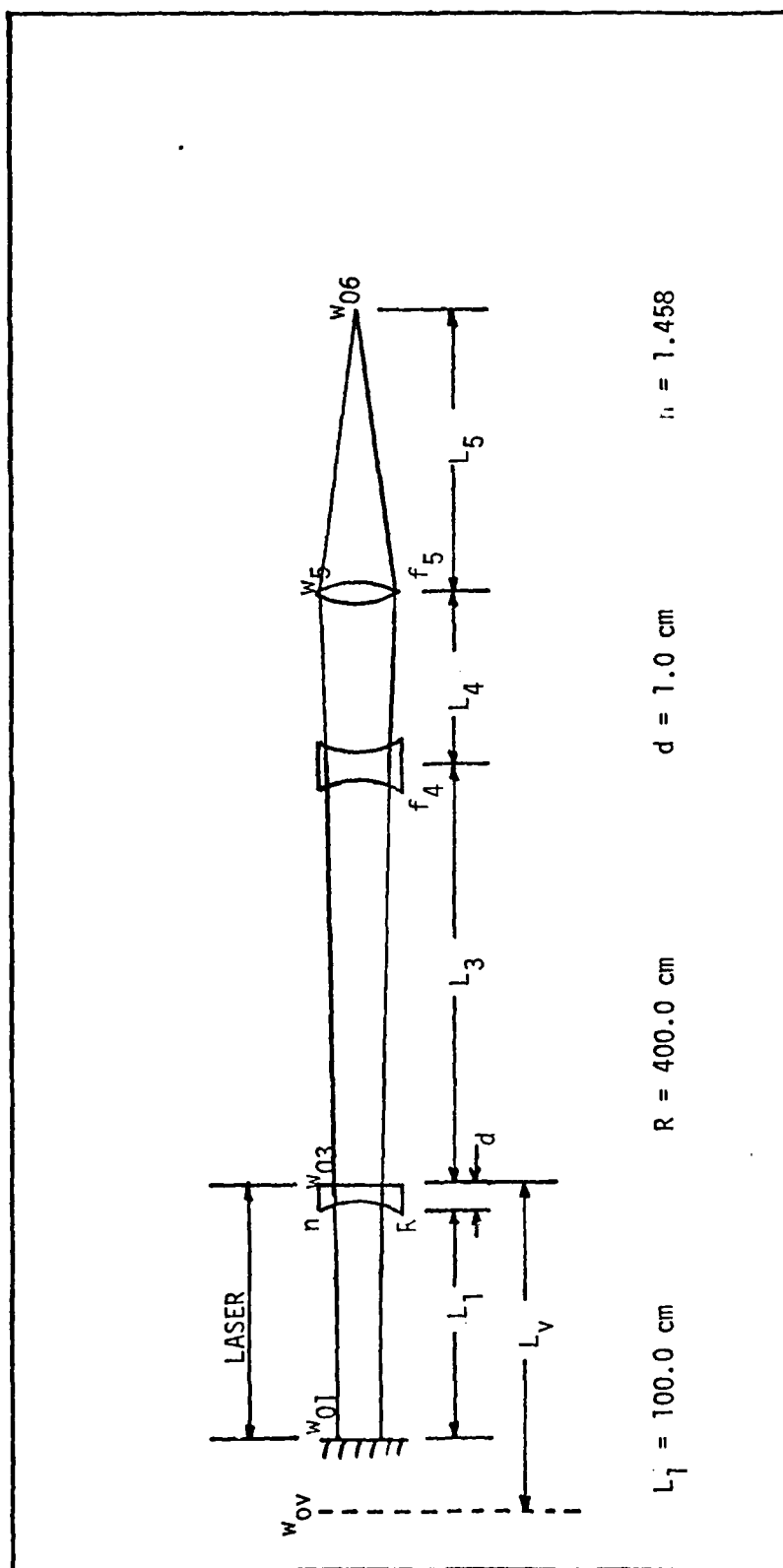
Figure A-1. Laser Annealing Optical Schematic

$$A = 1 + d(n-1)/nR \tag{7}$$

$$B = L_1 + (d/n) + L_1 \, d((n-1)/nR \tag{8}$$

$$C = (n-1)/R \tag{9}$$

$$D = 1 + L_1(n-1)/R \tag{10}$$

Solving for the real and imaginary parts of q_3

$$q_3 = \frac{BD + ACz_{R1}^2 + i \, z_{R1} \, (AD - BC)}{D^2 + (Cz_{R1})^2} \overset{\Delta}{=} L_v + iz_{Rv} \tag{11}$$

The real part of q_3 is equal to the distance back from the output surface to the virtual laser waist, and the imaginary part is the laser virtual Rayleigh range (z_{Rv}). The far field divergence half angle for the laser is approximated by:

$$\theta = \lambda/\pi w_{ov} \tag{12}$$

where

w_{ov} = virtual waist size

The ray transfer matrix to the second surface of the focusing lens (from the laser virtual waist) is:

$$\begin{bmatrix} E & F \\ G & H \end{bmatrix} = \begin{bmatrix} 1 & 0 \\ -1/f_5 & 1 \end{bmatrix} \begin{bmatrix} 1 & L_4 \\ 0 & 1 \end{bmatrix} \begin{bmatrix} 1 & 0 \\ -1/f_4 & 1 \end{bmatrix} \begin{bmatrix} 1 & L_v+L_3 \\ 0 & 1 \end{bmatrix}$$

$$E = - (L_4/f_4) \tag{13}$$

$$F = L_v + L_3 + L_4 \left(1 - (L_v + L_3)/f_4\right) \tag{14}$$

$$G = -(E/f_5) - (1/f_4) \tag{15}$$

$$H = 1 - B/f_5 - (L_v + L_3)/f_4 \tag{16}$$

Solving for the real and imaginary parts of q_5

$$q_5 = \frac{FH + EG\, z_{Rv}^2 + iz_{Rv}\,(EH - GF)}{H^2 + (G\, z_{Rv})^2} \stackrel{\Delta}{=} L_5 + iz_{R6} \tag{17}$$

The real part of q_5 is the distance from the focusing lens to the beam waist (L_5) and the imaginary part is the associated Rayleigh range (z_{R6}) for the focused spot. The actual waist size (w_{o6}) is found from the following:

$$w_{o6} = \frac{\lambda(EH - GF)}{\pi(H^2 + (Gz_{Rv})^2)} \tag{18}$$

where:

$$z_{Rv} = \frac{z_{R1}\,(AD - BC)}{D^2 + (C\, z_{R1})^2} \tag{19}$$

$$z_{R1} = (L_1\,(R_2 - L_1))^{1/2} \tag{6}$$

72

Appendix B

Photoluminescence Experimental Data
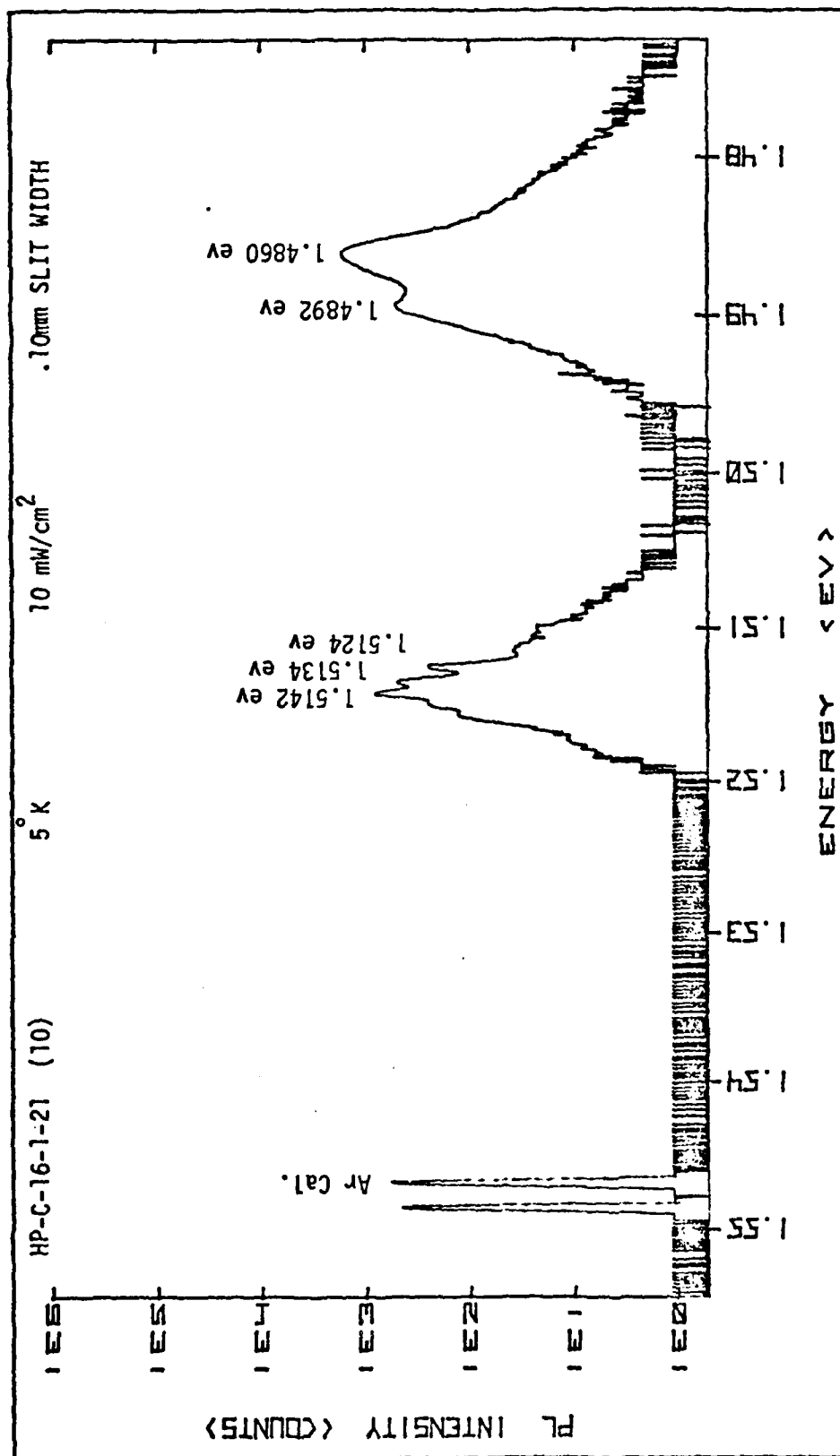
Figure B-1. PL of Virgin VPE GaAs at 5° K

74
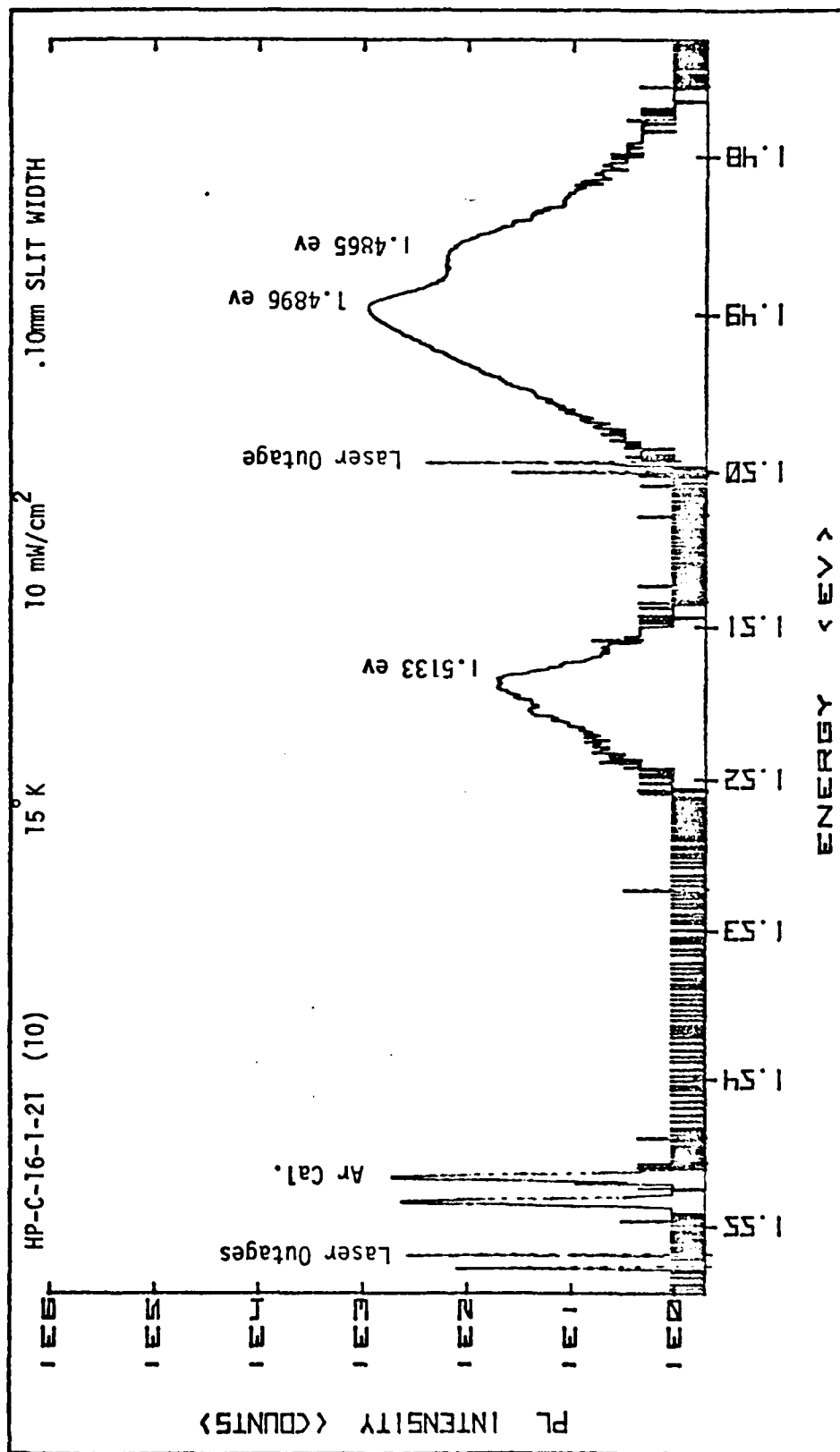
Figure B-2. PL of Virgin VPE GaAs at 15° K

75
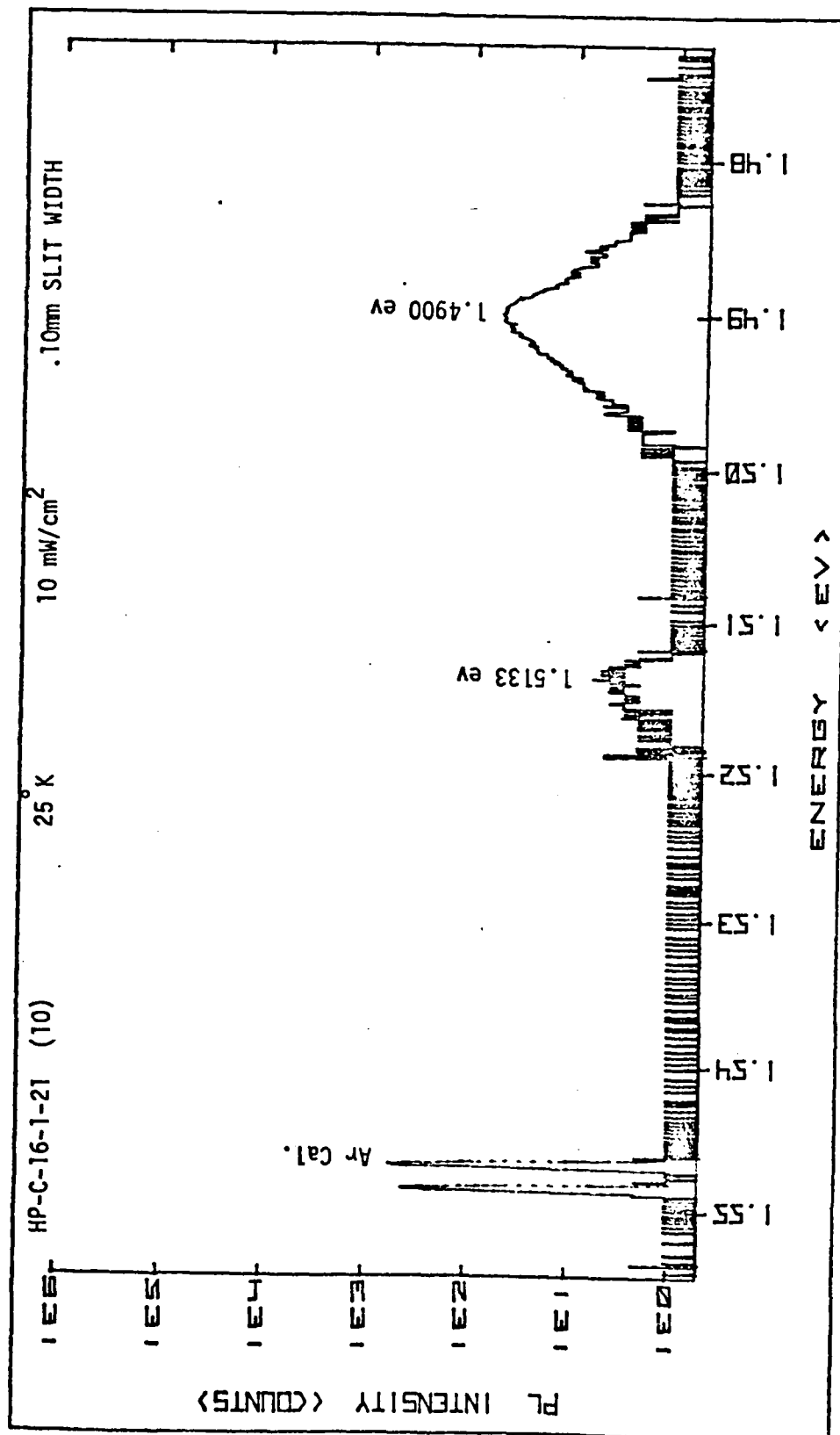
Figure B-3. PL of Virgin VPE GaAs at 25° K
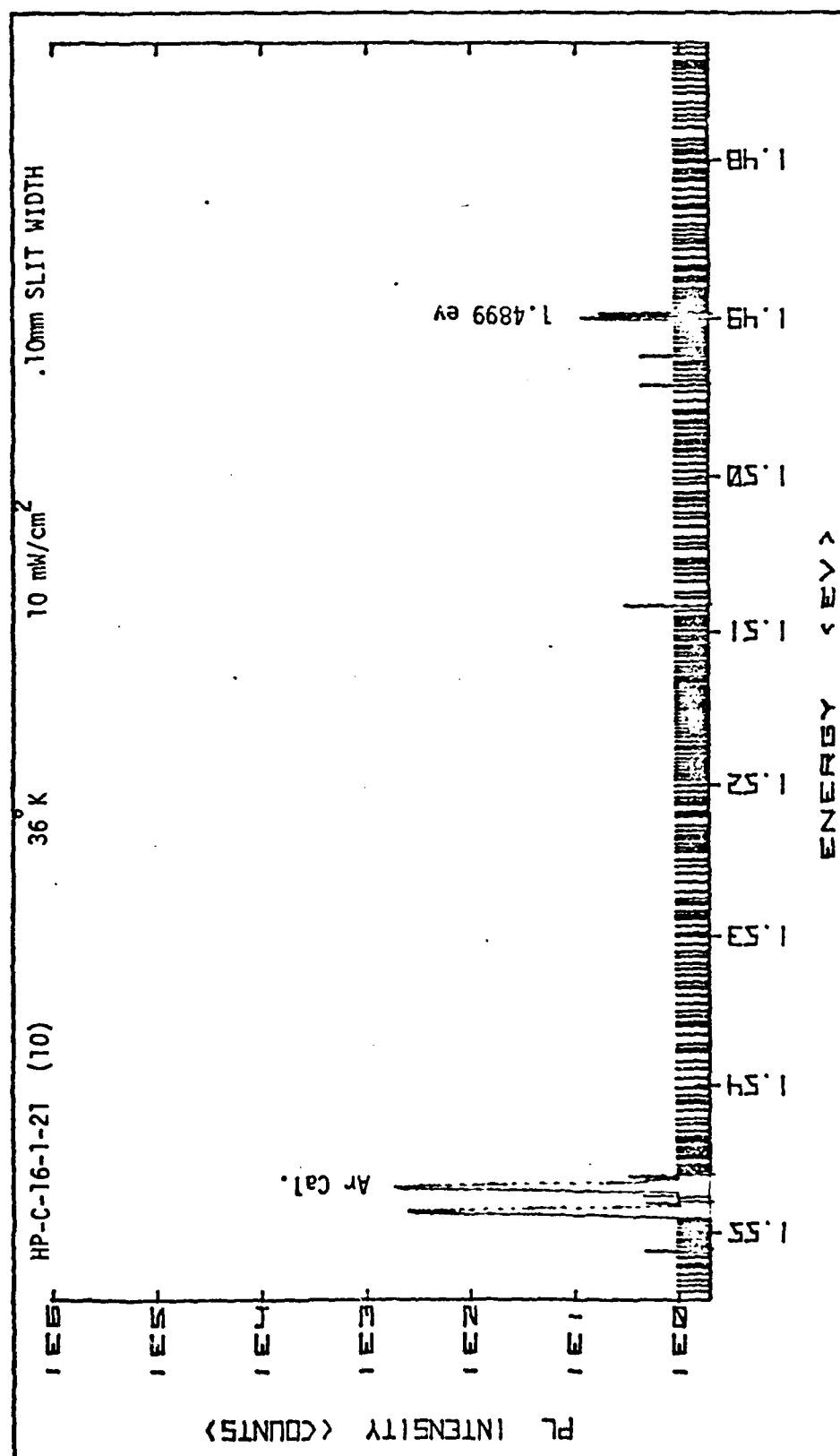
Figure B-4. PL of Virgin VPE GaAs at 36° K
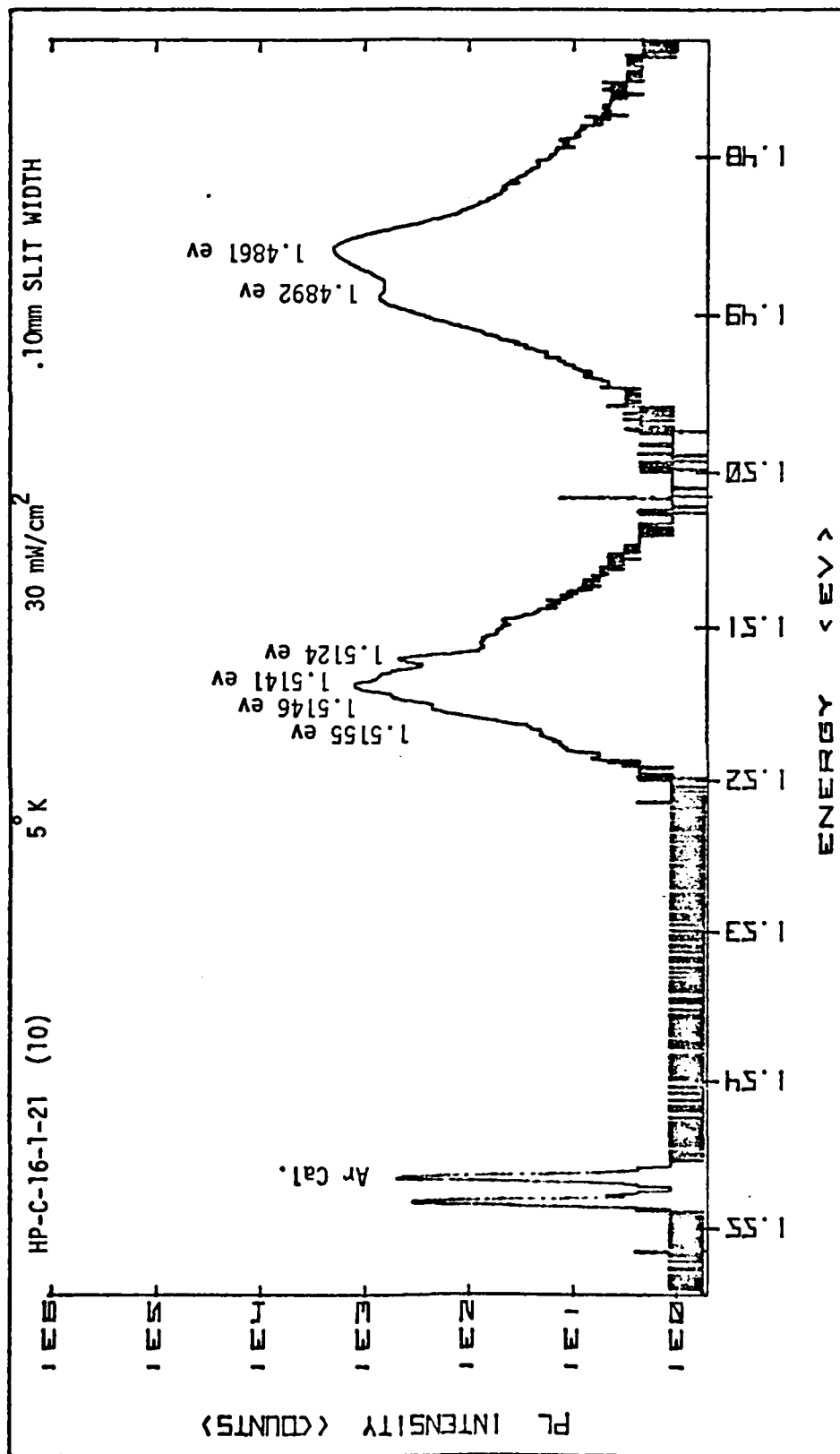
Figure B-5. PL of Virgin VPE GaAs at 30 mW/cm^2 Pump Irradiance

78
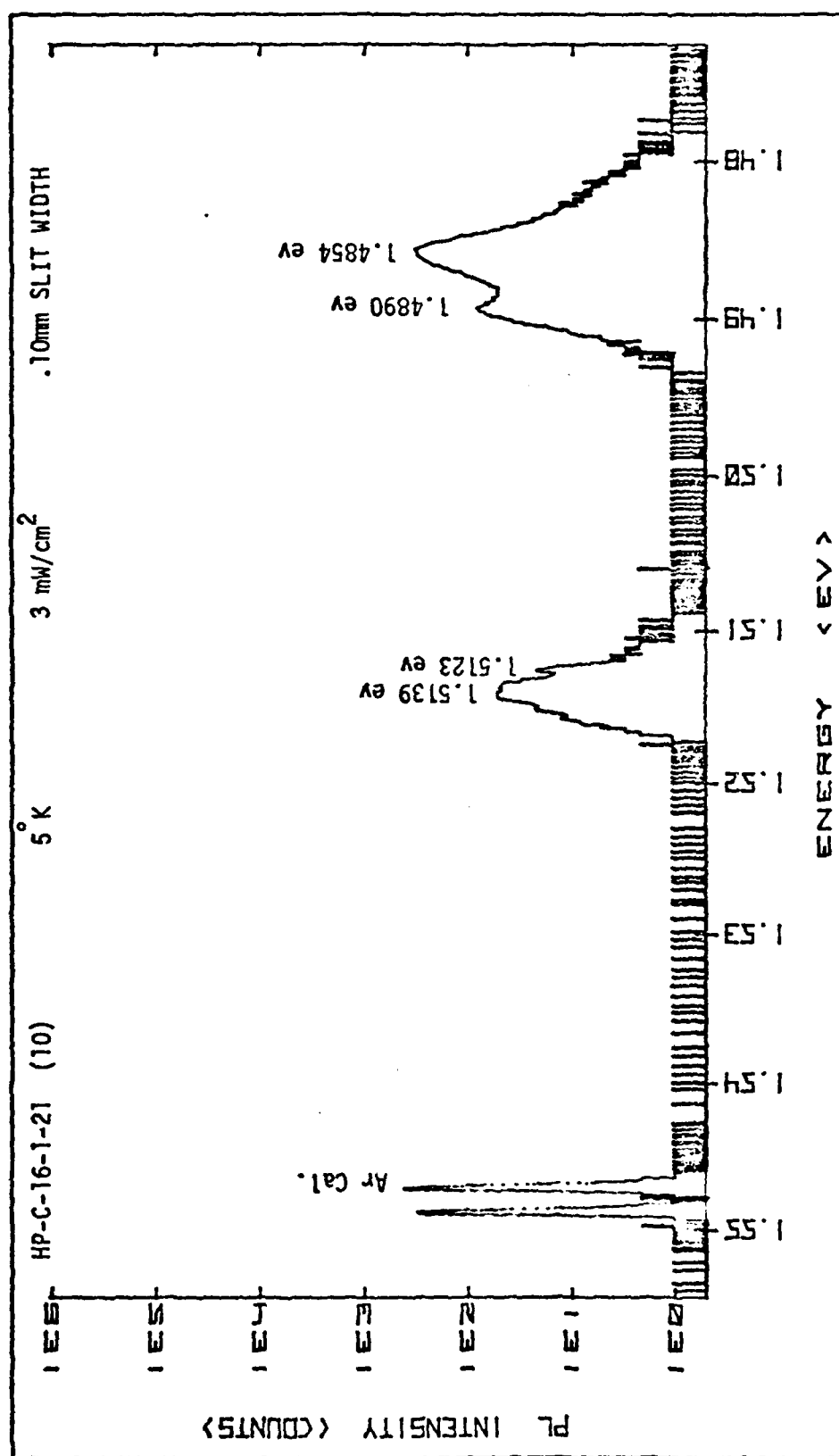
Figure B-6. PL of Virgin VPE GaAs at 3 mW/cm^2 Pump Irradiance
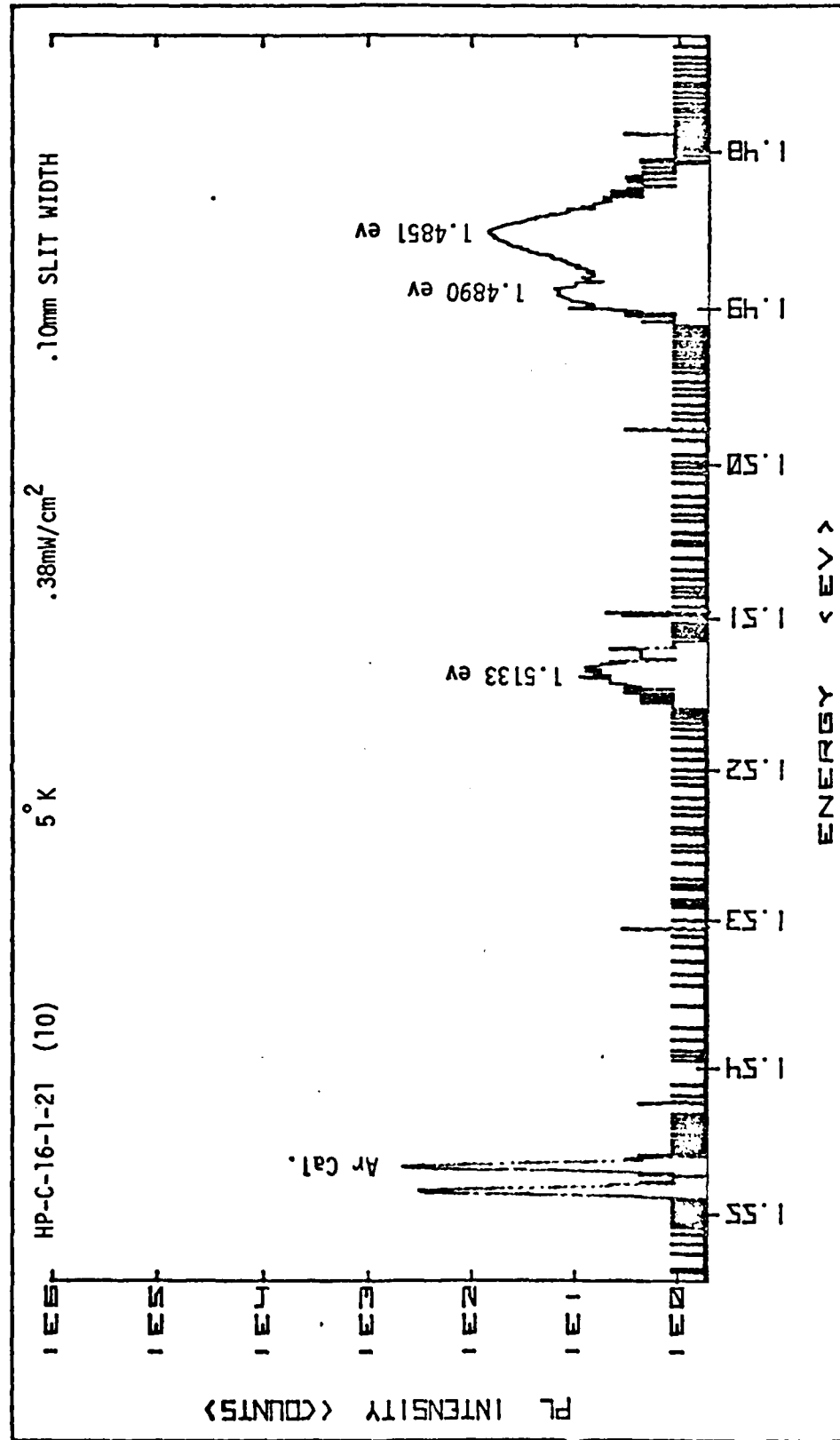
Figure B-7. PL of Virgin VPE GaAs at Approximately .38 mW/cm² Pump Irradiance
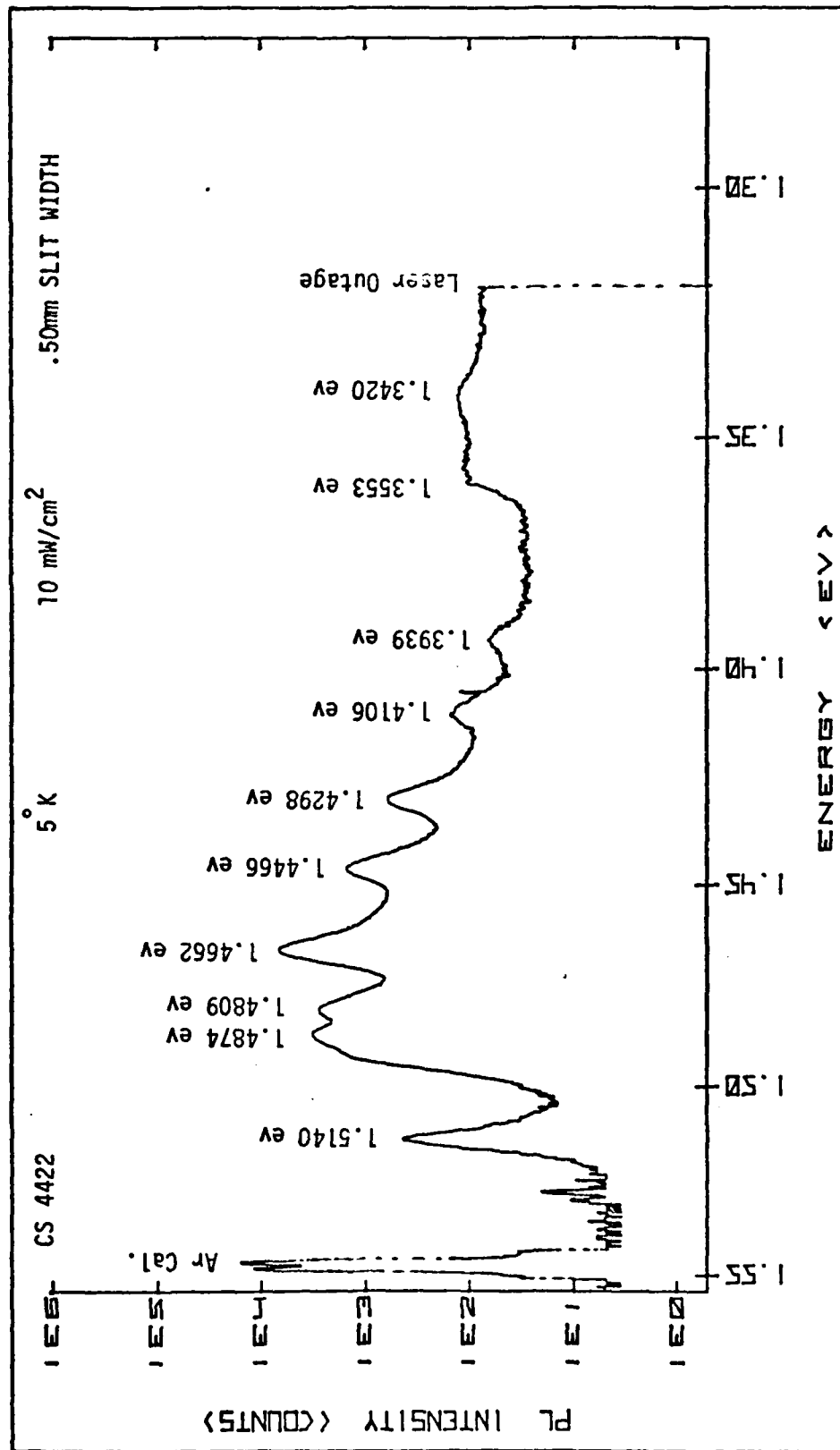
Figure B-8. PL of Virgin Bridgeman Grown GaAs
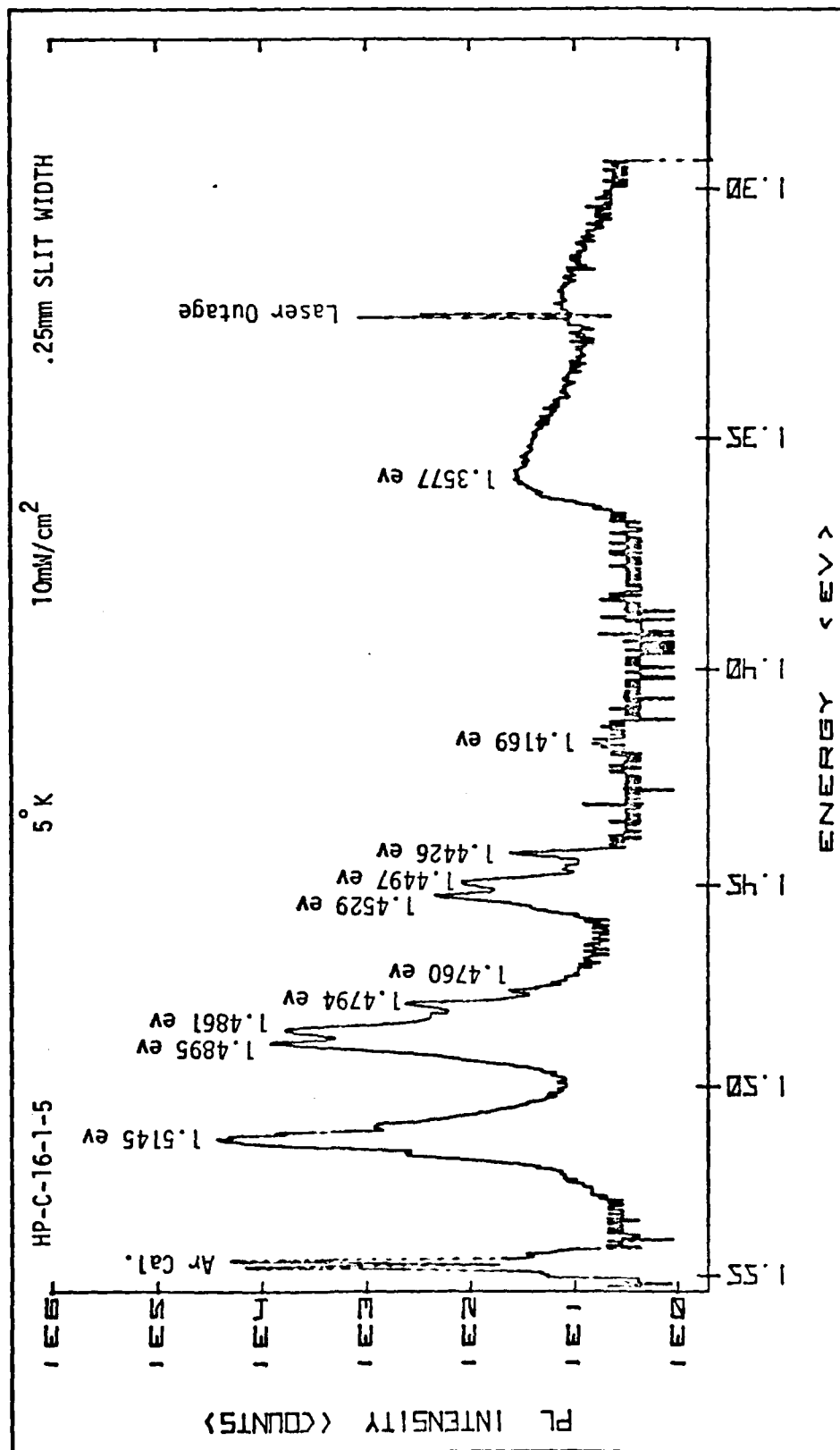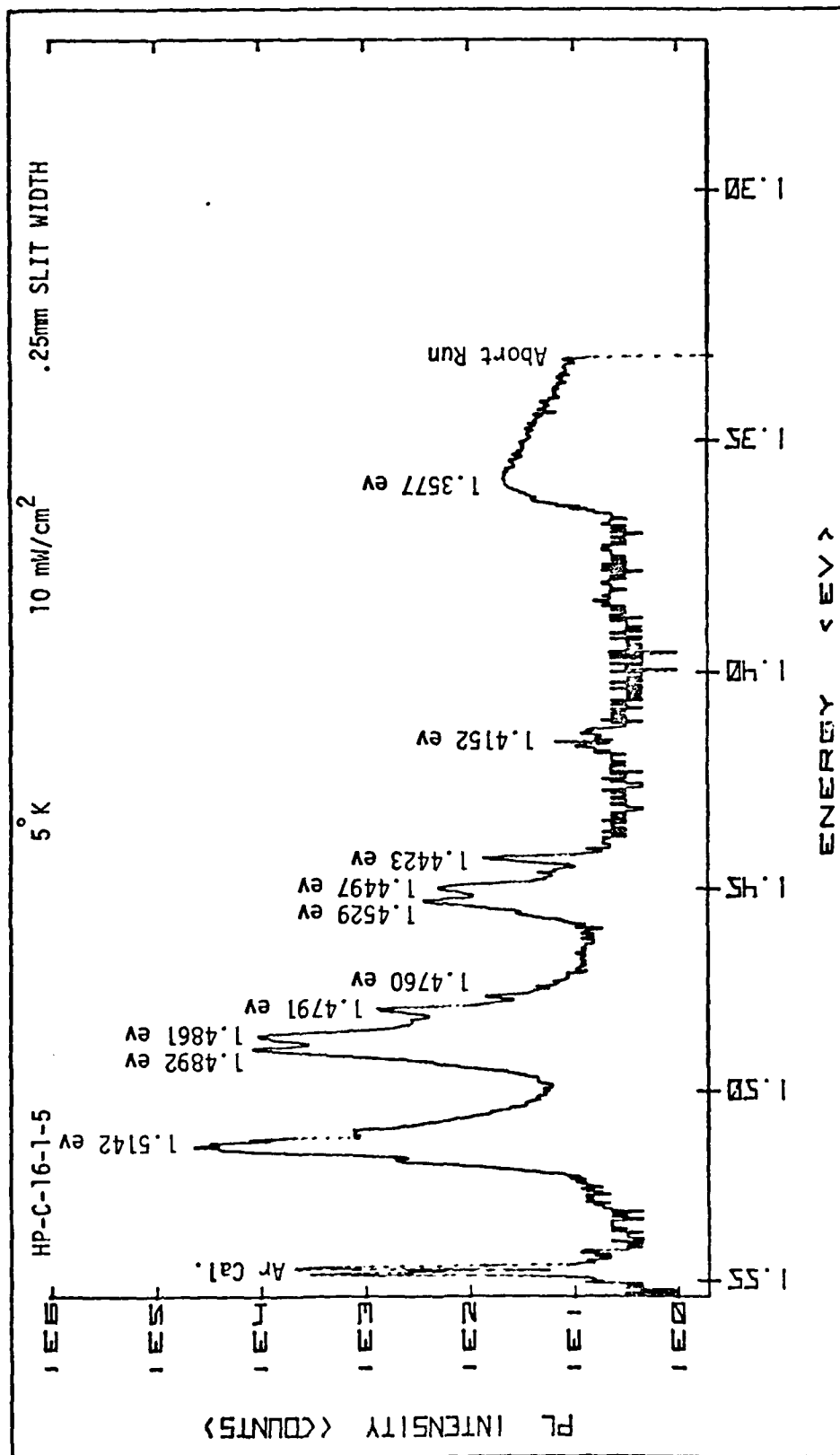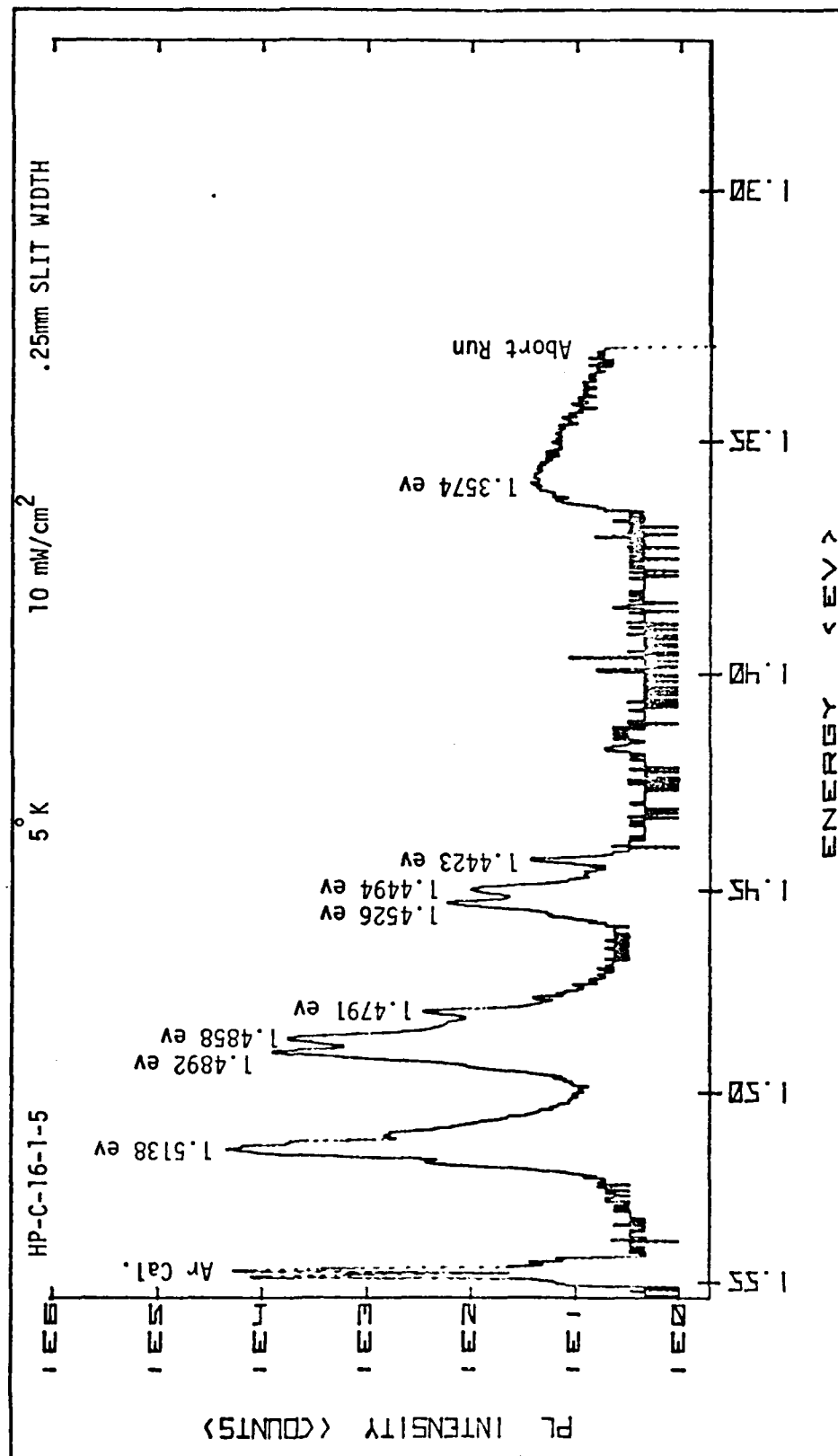
HP-C-16-1-5   5 °K   10mW/cm²   .25mm SLIT WIDTH

Ar Cal.
1.5145 ev
1.4895 ev
1.4861 ev
1.4794 ev
1.4760 ev
1.4529 ev
1.4497 ev
1.4426 ev
1.4169 ev
1.3577 ev
Laser Outage

PL INTENSITY (COUNTS)

ENERGY <EV>

1.55 1.50 1.45 1.40 1.35 1.30

82

83

HP-C-16-1-5

.25mm SLIT WIDTH

10 mW/cm^2

5 K

Ar Cal.

1.5138 ev

1.4892 ev
1.4858 ev
1.4791 ev

1.4526 ev
1.4494 ev
1.4423 ev

1.3574 ev

Abort Run

PL INTENSITY (COUNTS)

ENERGY (EV)

1.55   1.50   1.45   1.40   1.35   1.30

END
DATE
FILMED
2 -81
DTIC
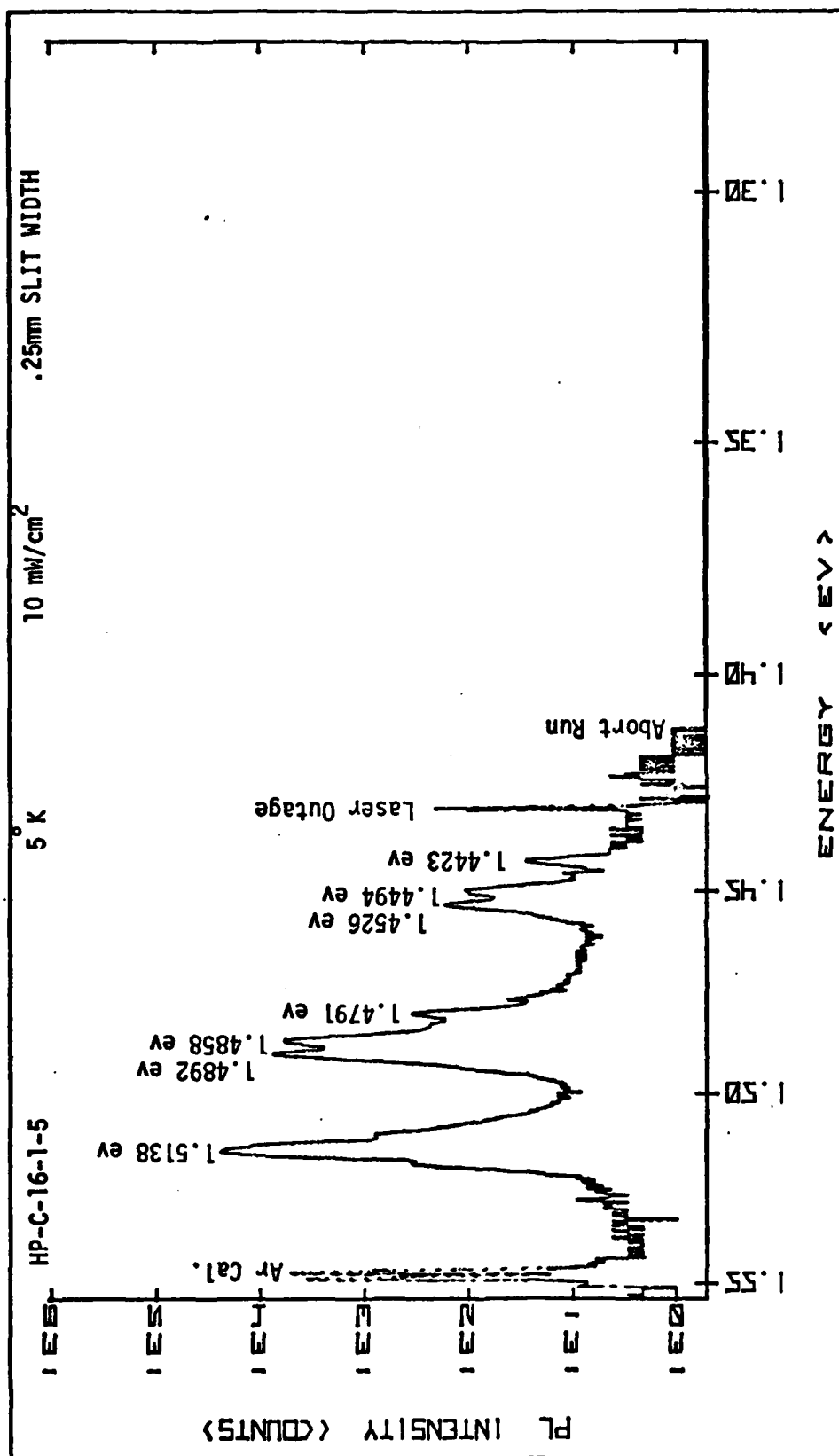
Figure B-12. PL of Virgin VPE GaAs (Not Irradiated)
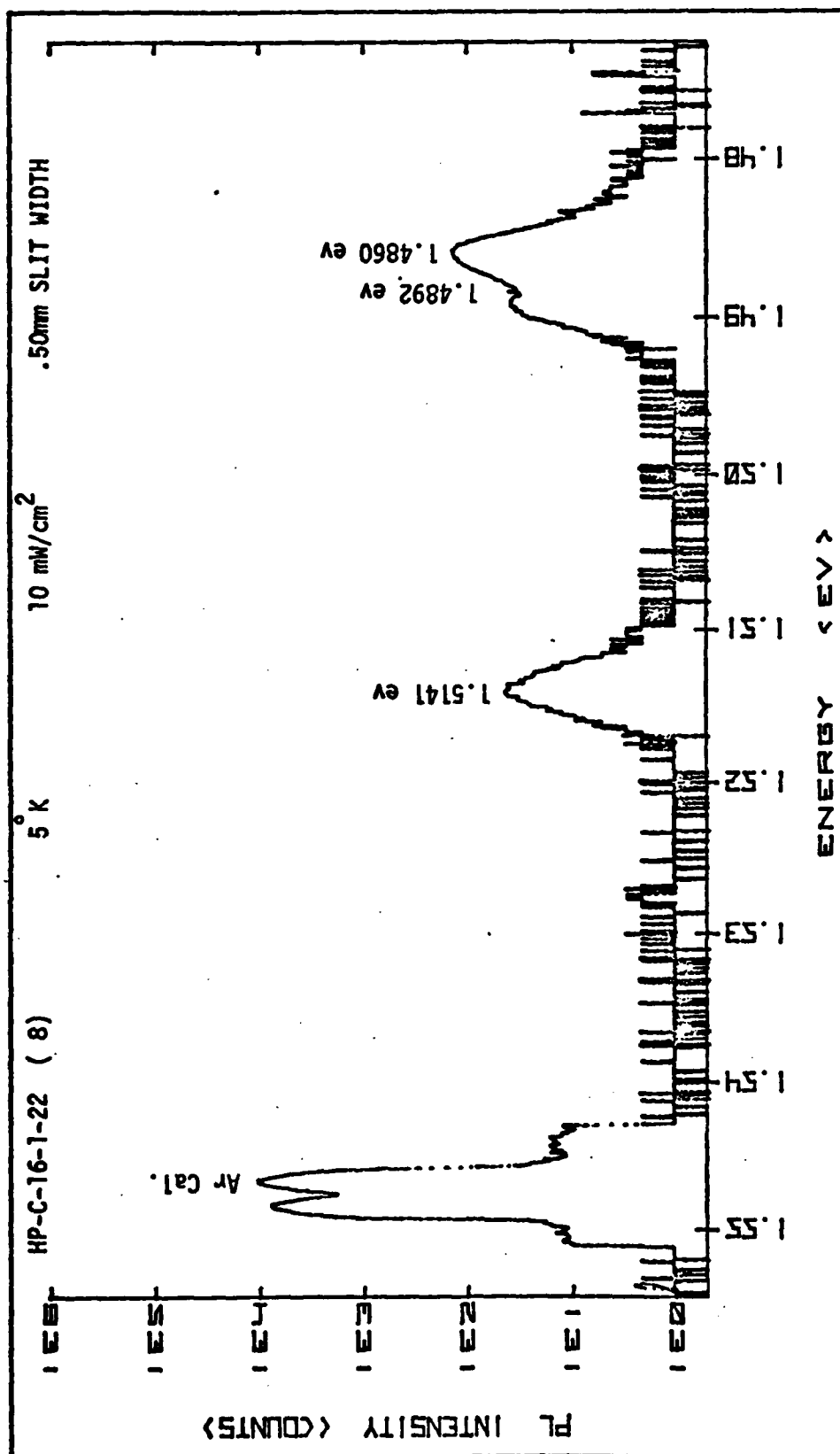
Figure B-13. PL of Implanted (Kr, 10^{14} cm^{-2}) VPE GaAs
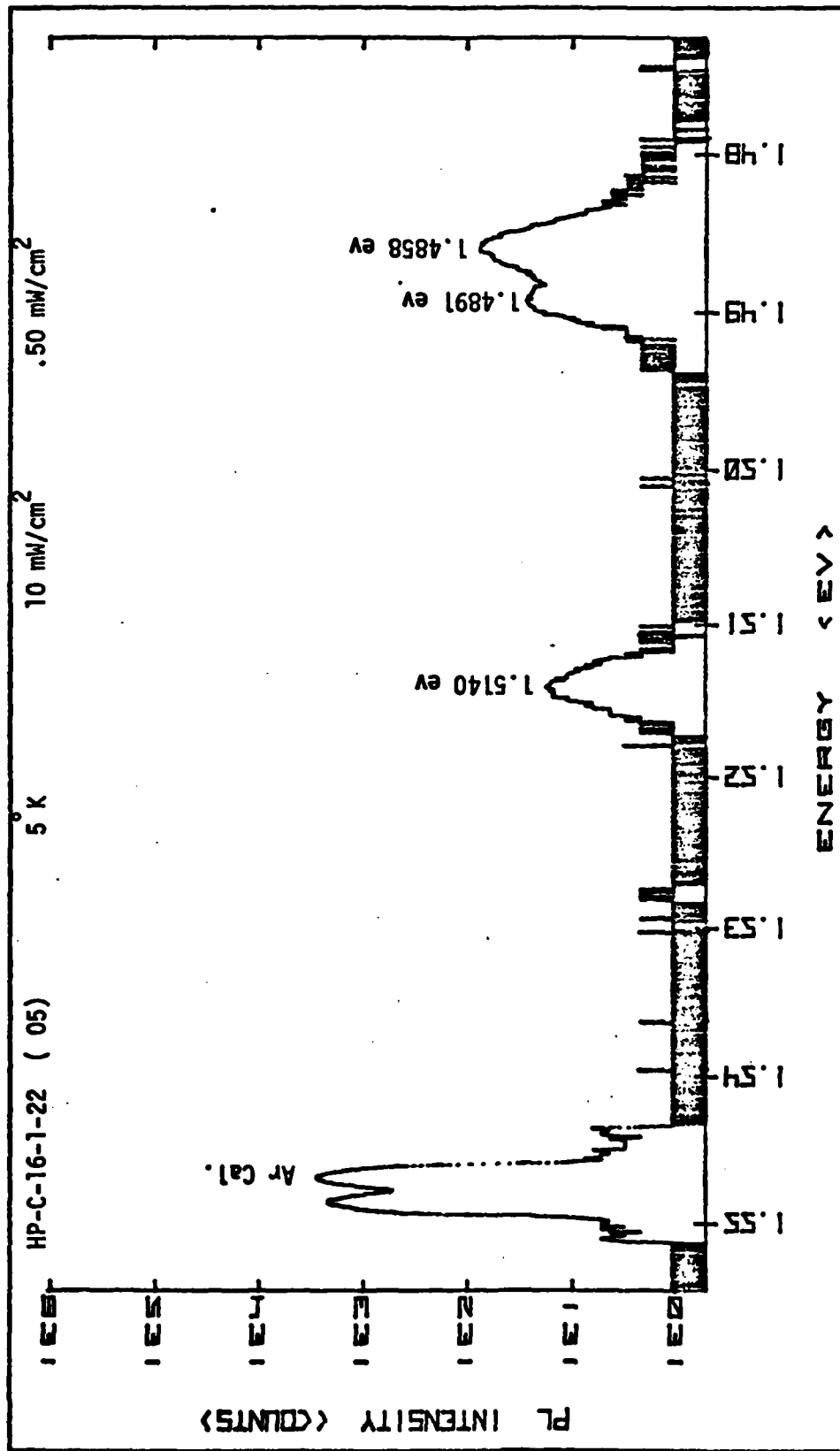
Figure B-14. PL of Implanted (Kr, 10^{14} cm^{-2}) VPE GaAs After Scanning at 520 W/cm

87
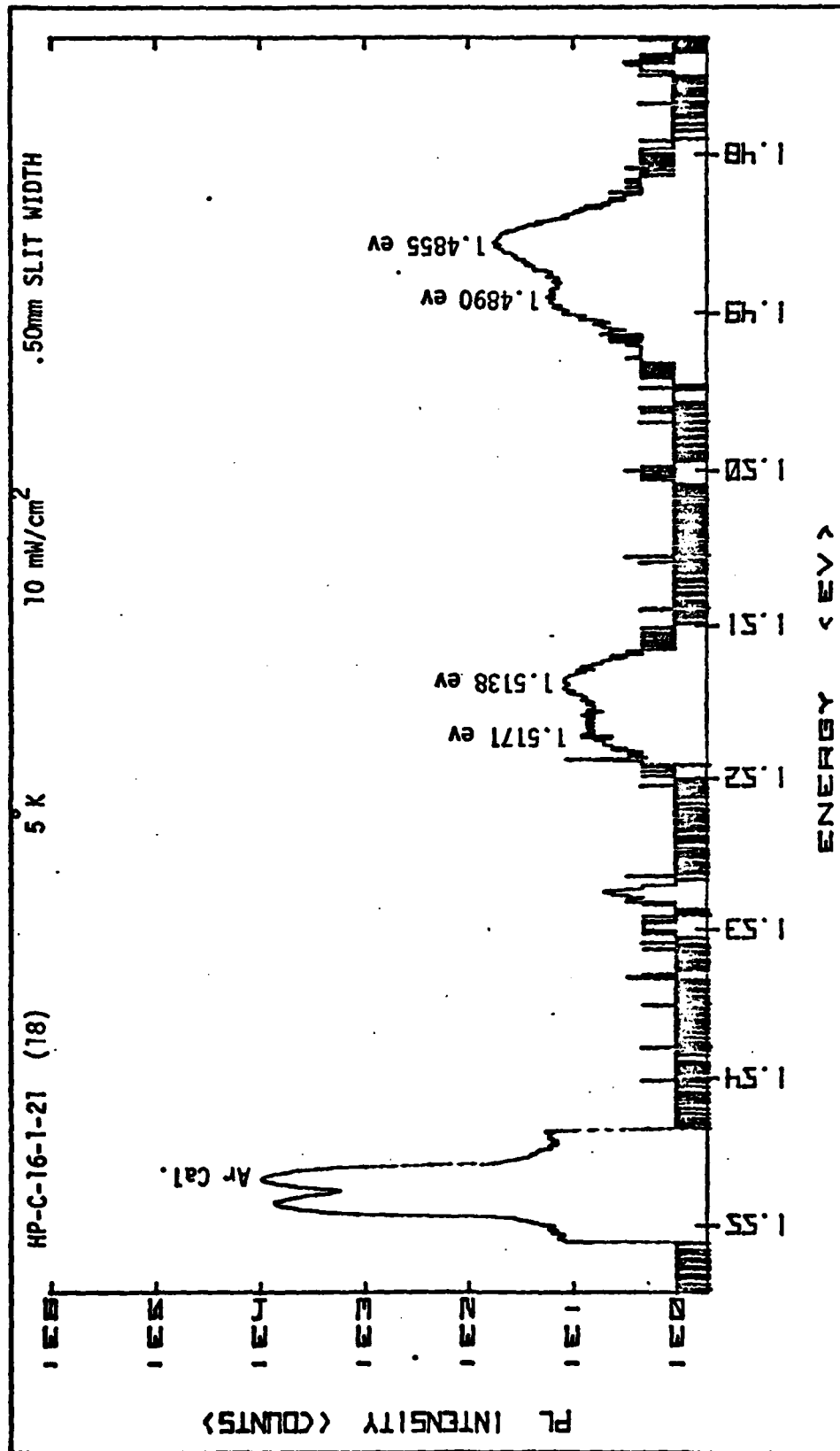
Figure B-15. PL of Implanted (Kr, 10^{14} cm^{-2}) VPE GaAs
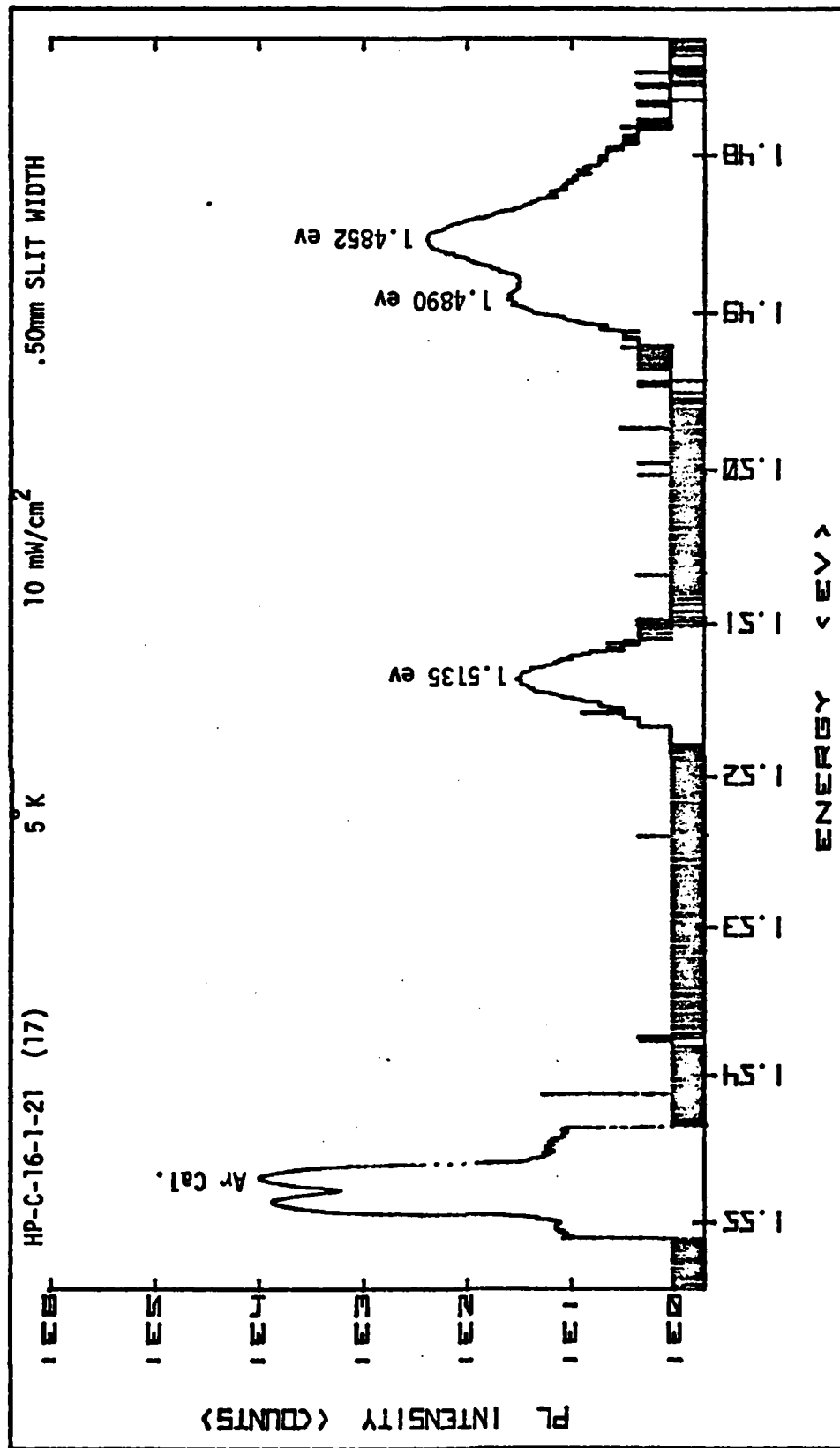
Figure B-16. PL of Implanted (Kr, 10^{14} cm^{-2}) VPE GaAs After Scanning at 520 W/cm
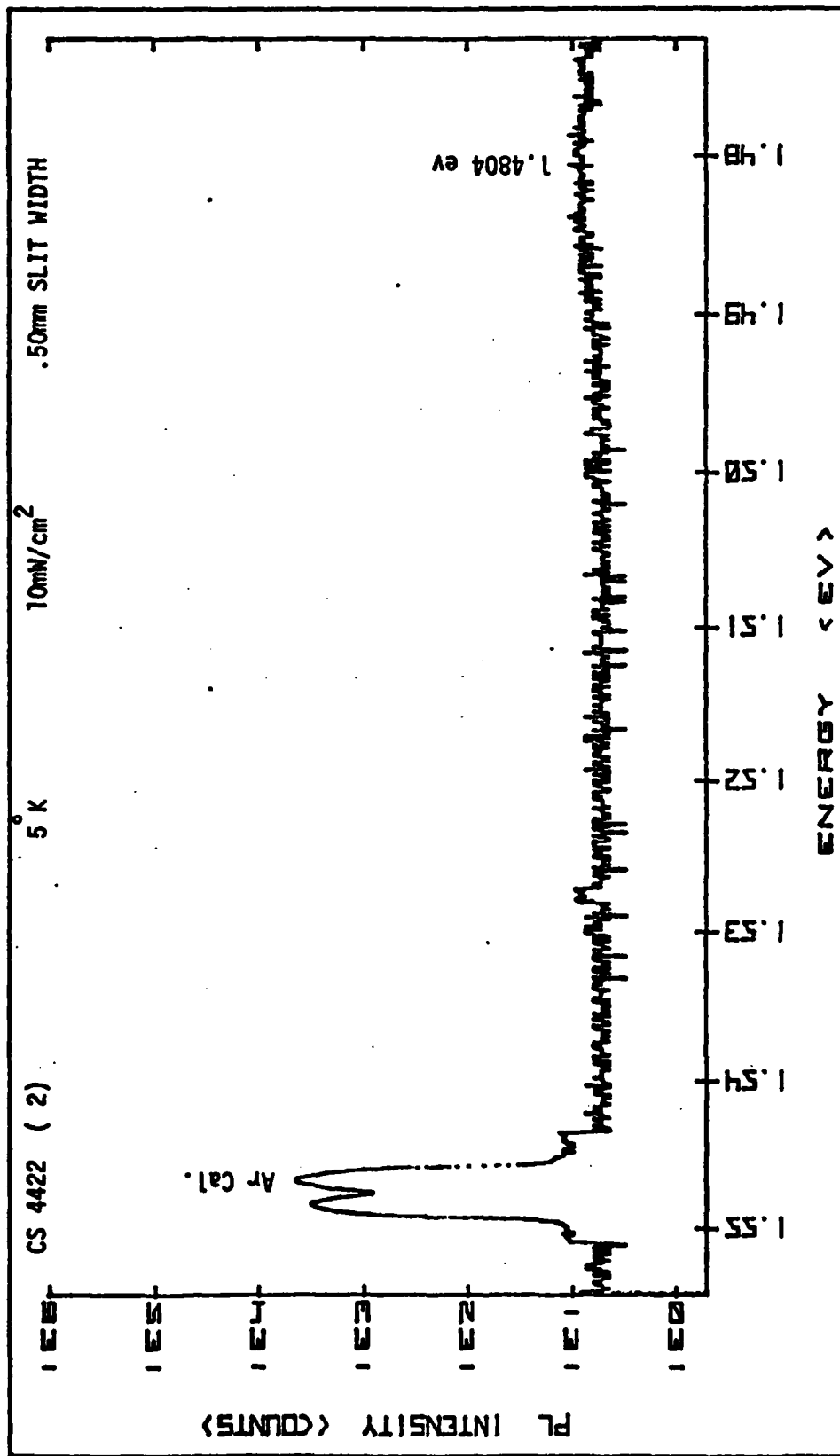
Figure B-17. PL of Implanted (Ge, 10^{13} cm^{-2}) Bridgeman Grown GaAs (Unannealed)
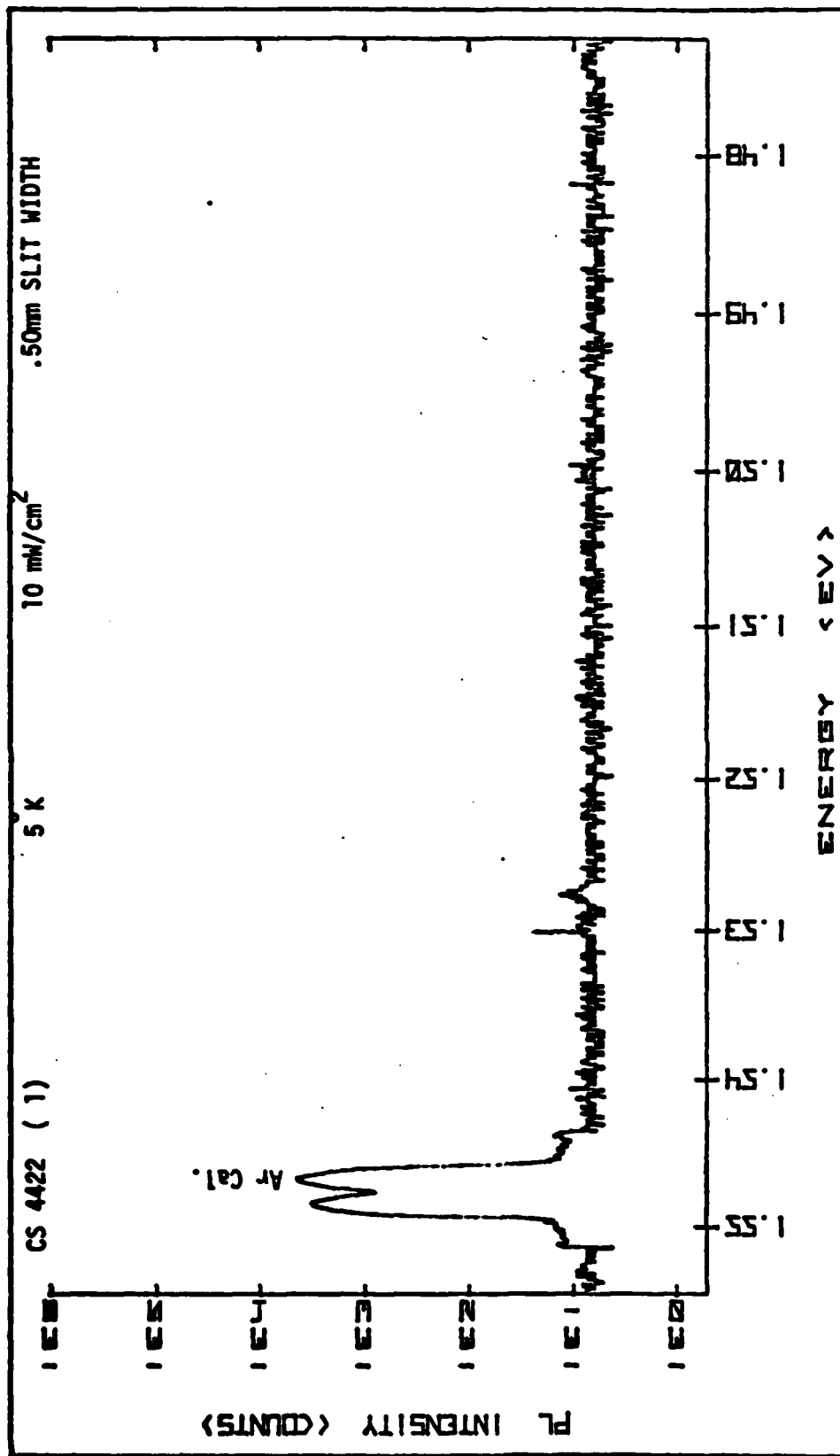
Figure B-18. PL of Implanted (Ge, 10^{14} cm^{-2}) Bridgeman Grown GaAs (Unannealed)
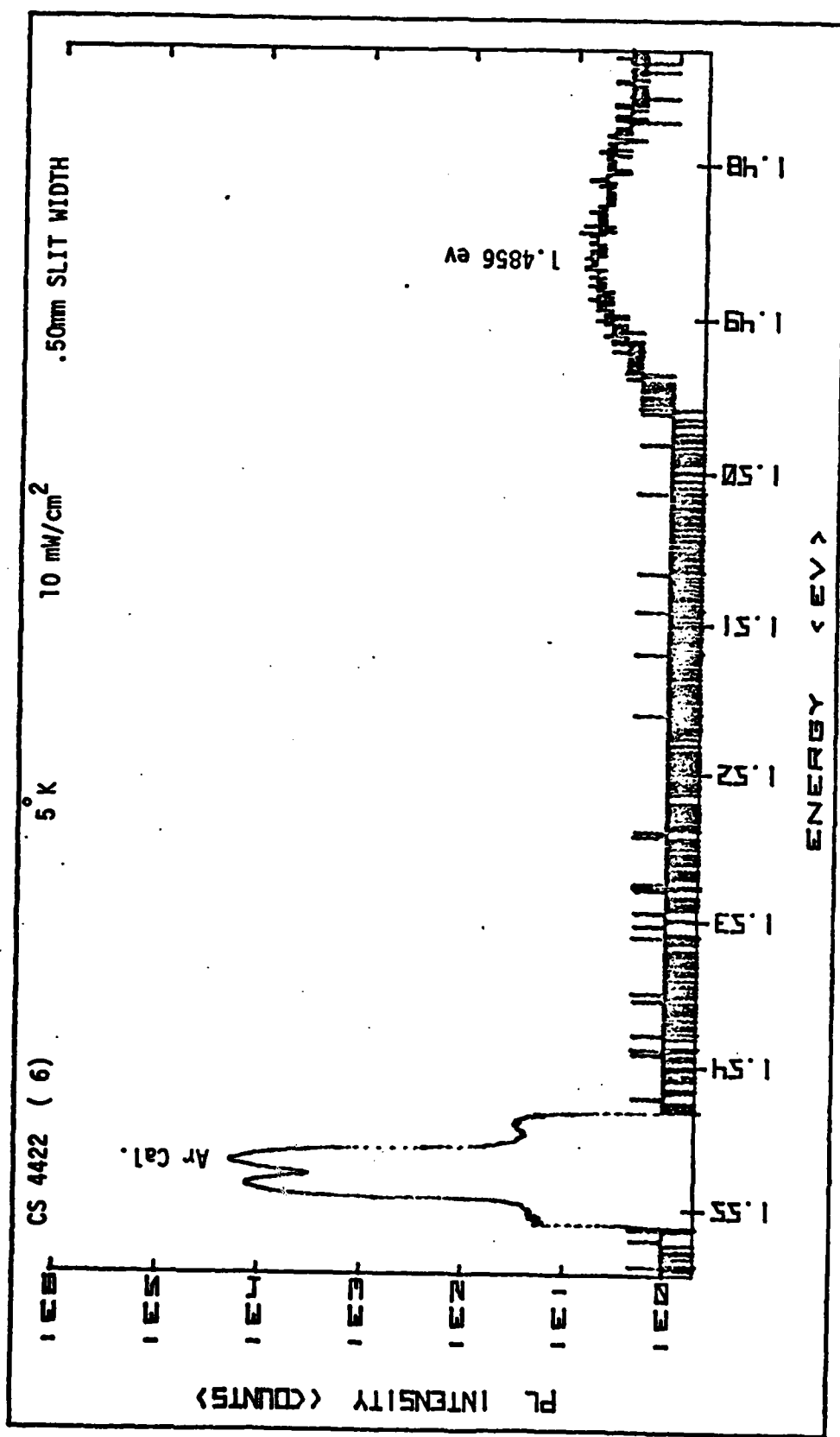
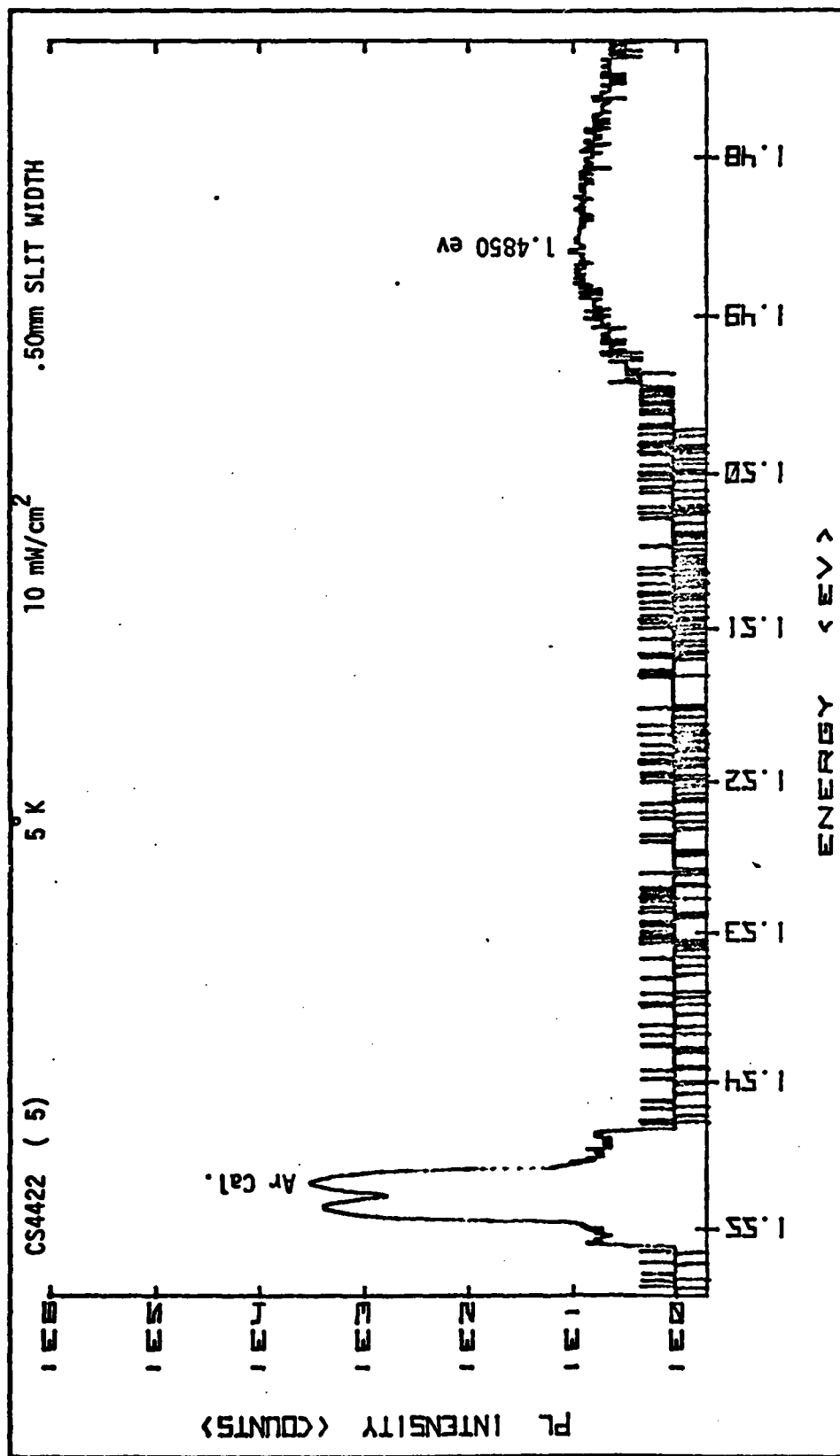Figure B-19. PL of Implanted (Ge, 10^{14} cm^{-2}) Bridgeman Grown GaAs After Scanning with .63 msec Dwell Time

Figure B-20. PL of Implanted (Ge, 10^{14} cm^{-2}) Bridgeman Grown GaAs
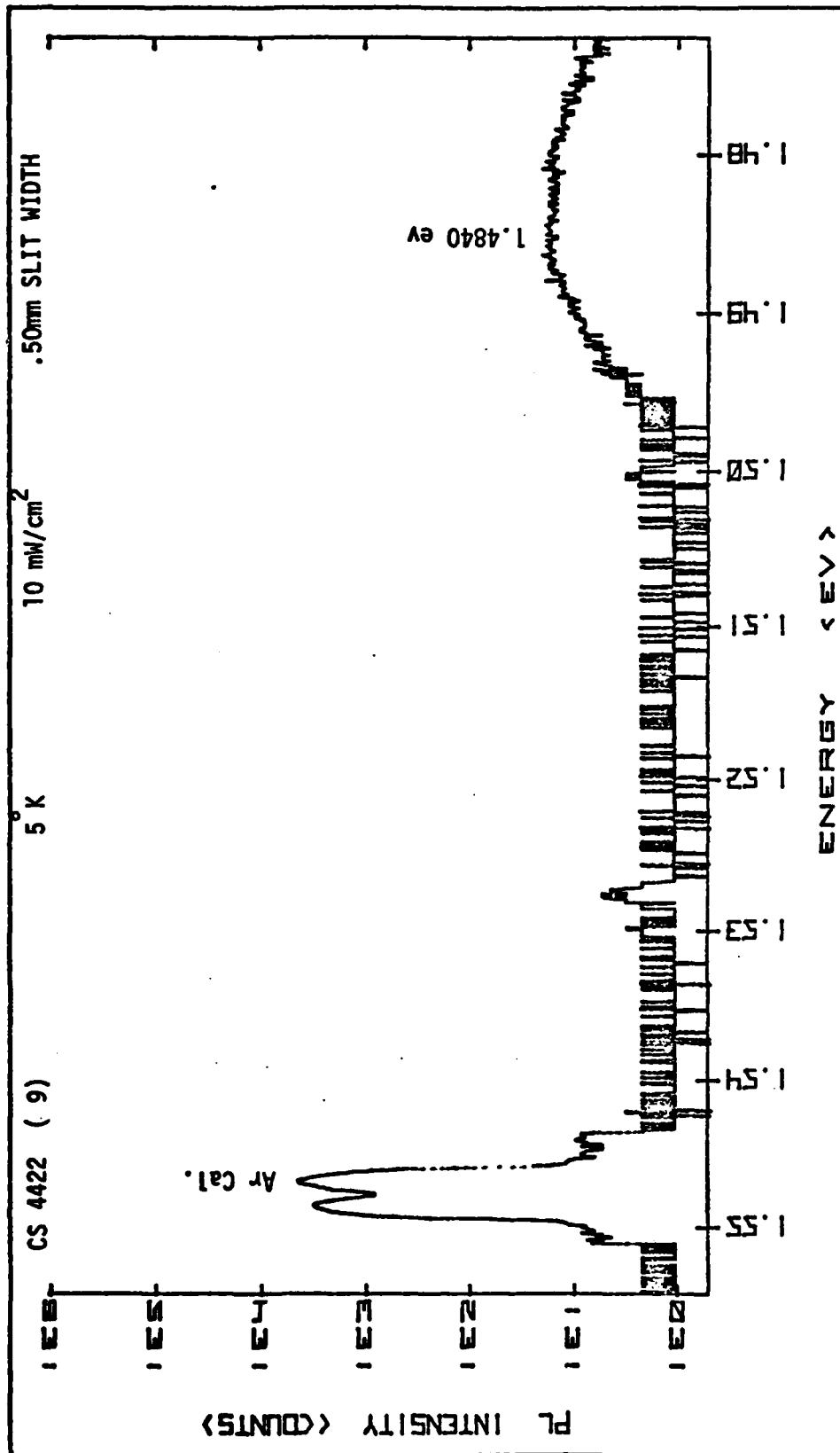After Scanning with 3.23 msec Dwell Time

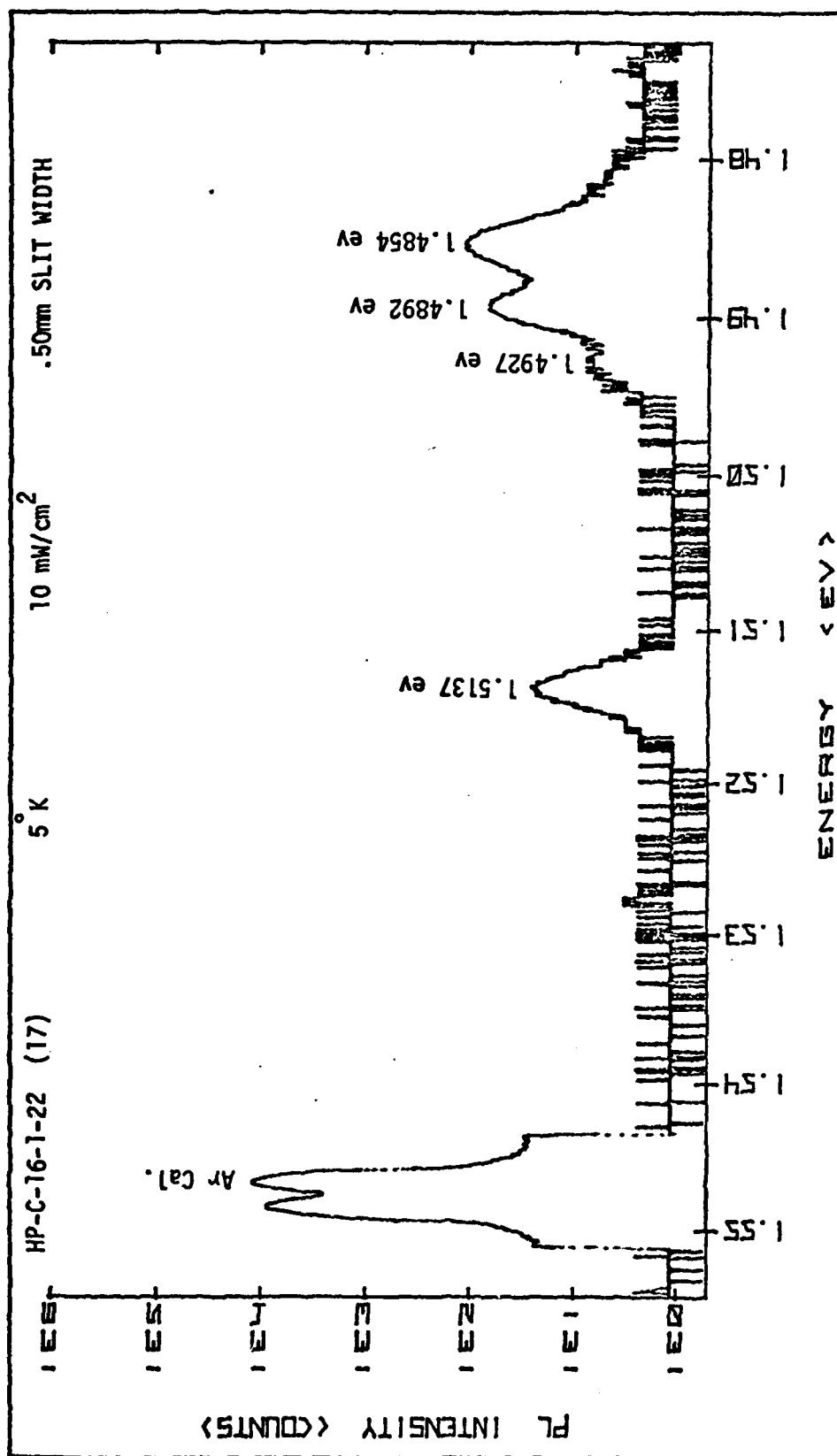Figure B-21. PL of Implanted (Ge, 10^{14} cm^{-2}) Bridgeman Grown GaAs After Scanning with Optimum Scan Pattern

94

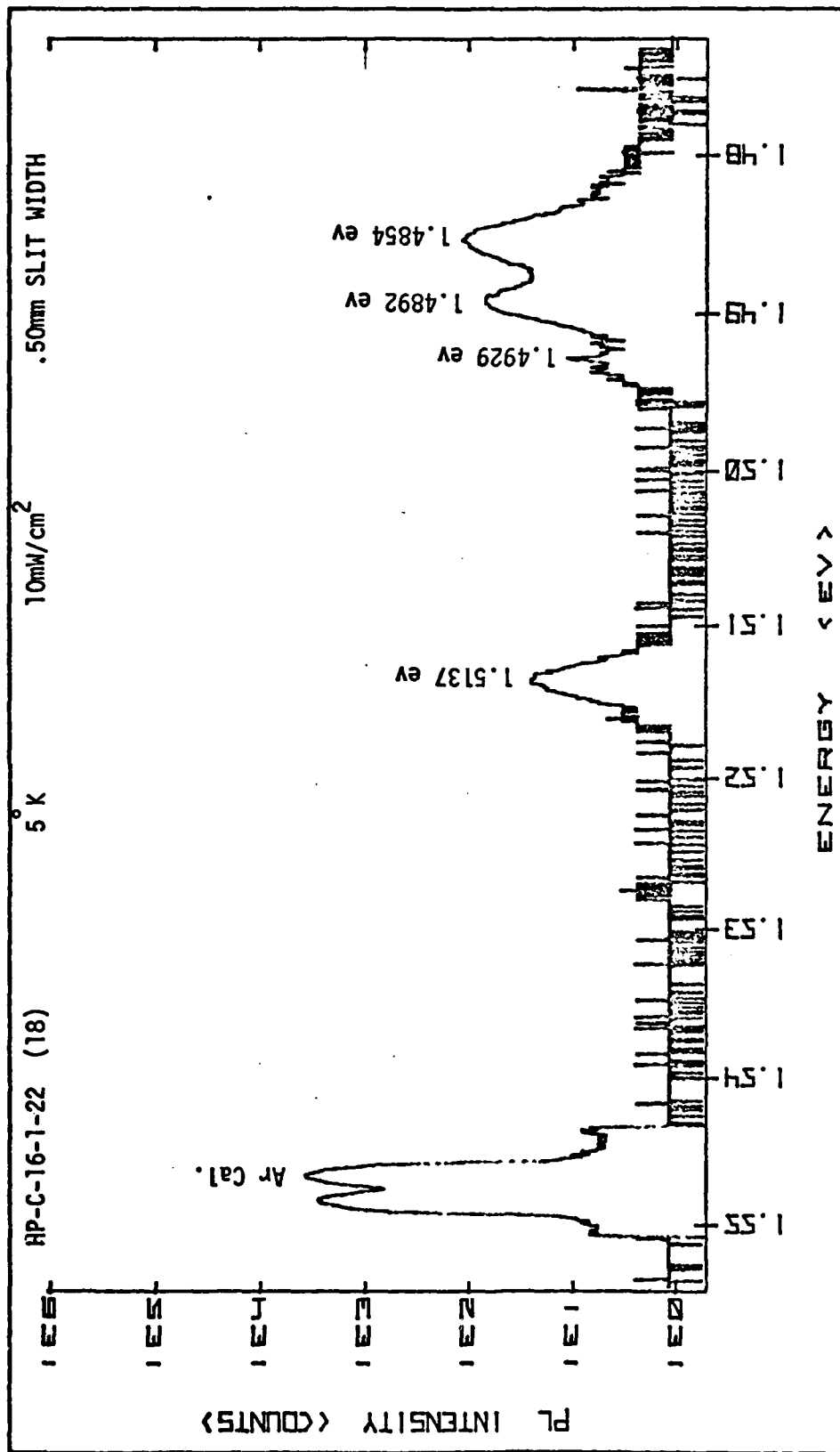Figure B-22. PL of Implanted (Ge, 10^{14} cm^{-2}) VPE GaAs After Scanning at Threshold C (530 W/cm)

Figure B-23. PL of Implanted (Ge, 10^{14} cm^{-2}) VPE GaAs After Scanning at 83% of Threshold C (440 W/cm)
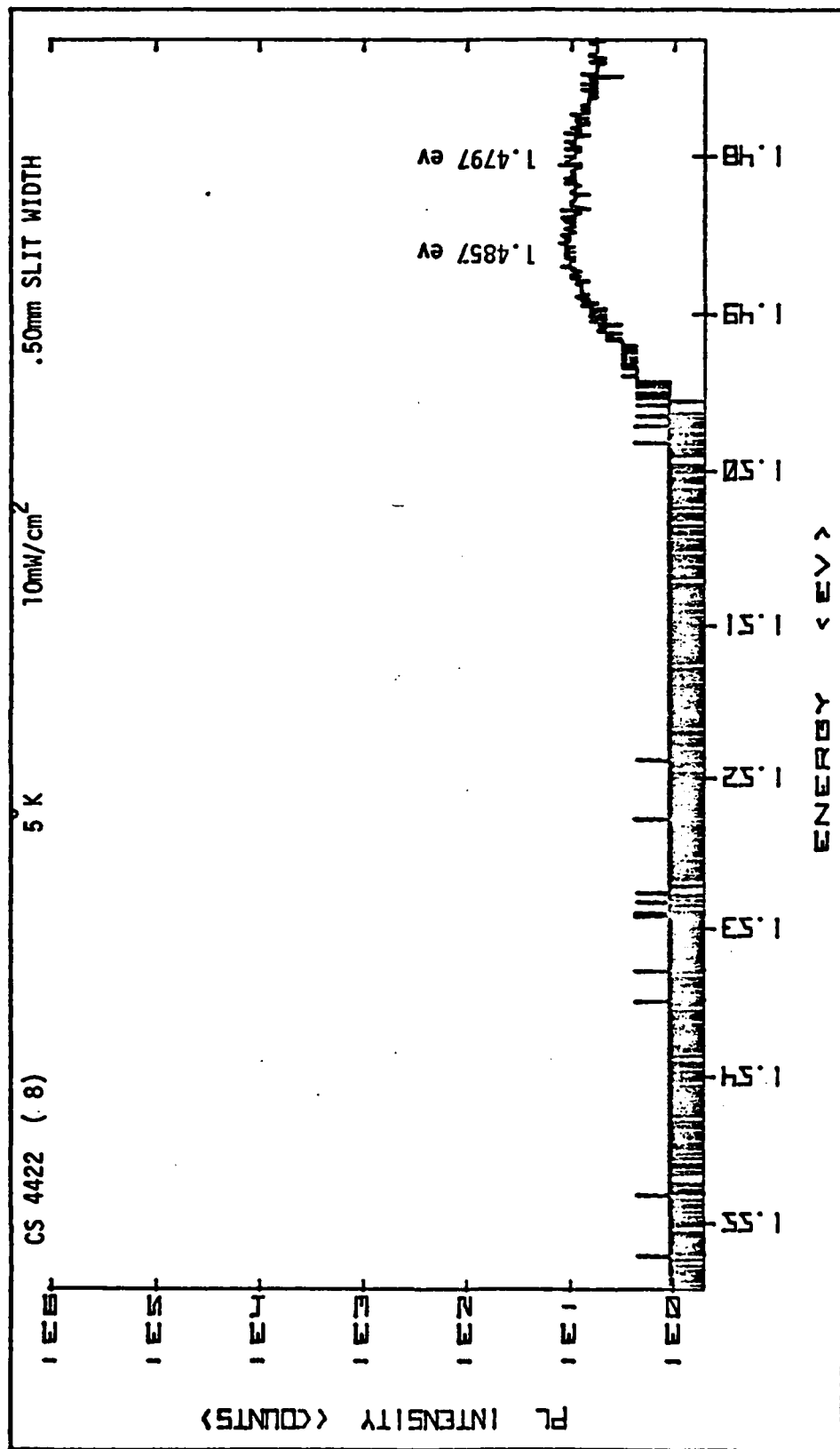
Figure B-24. PL of Implanted (Ge, 10^{13} cm^{-2}) Bridgeman Grown GaAs After Laser Annealing with Baseline Parameters
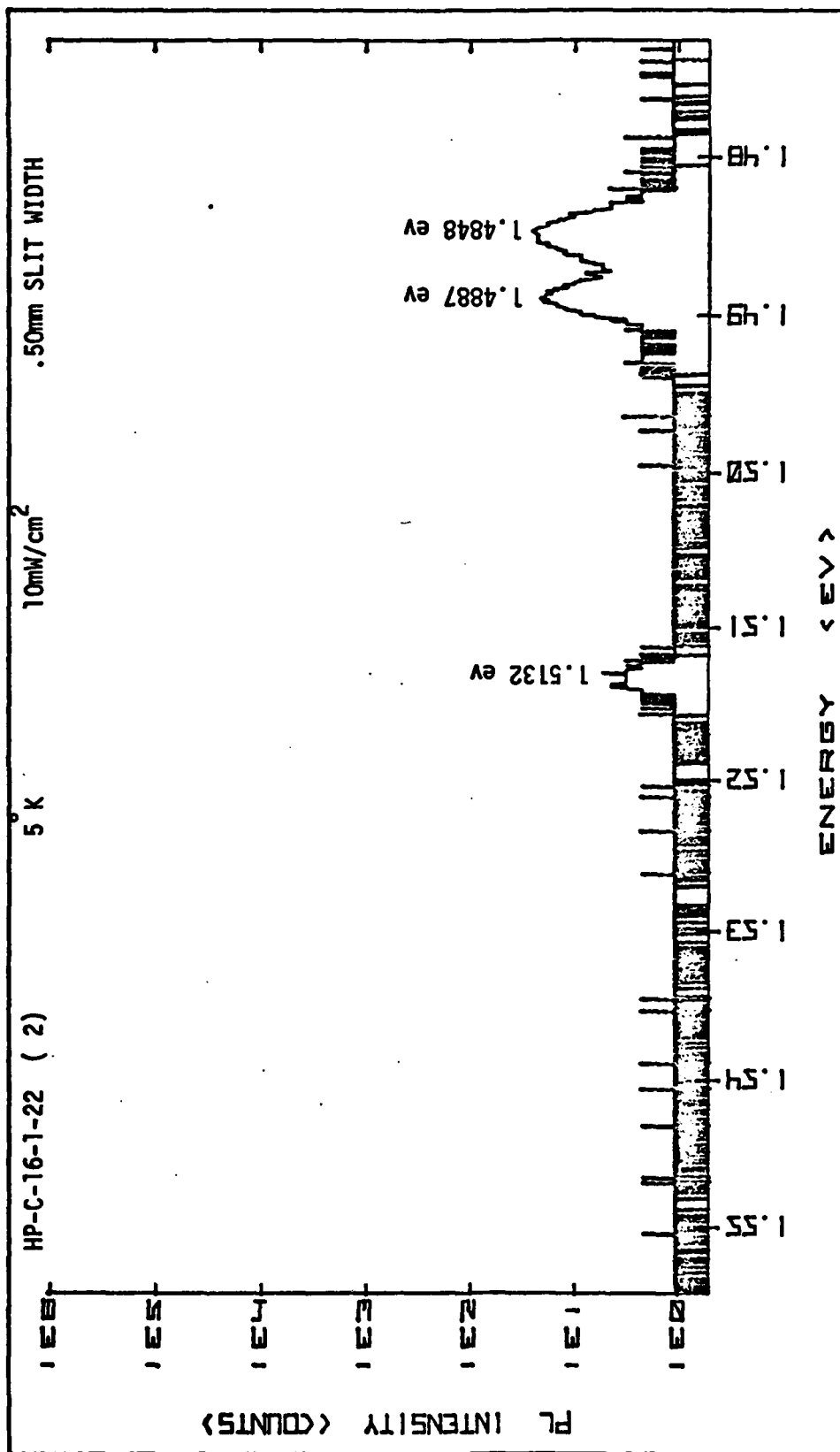
Figure B-25. PL of Implanted (Ge, 10^{15} cm^{-2}) VPE GaAs After Laser Annealing with Baseline Parameters
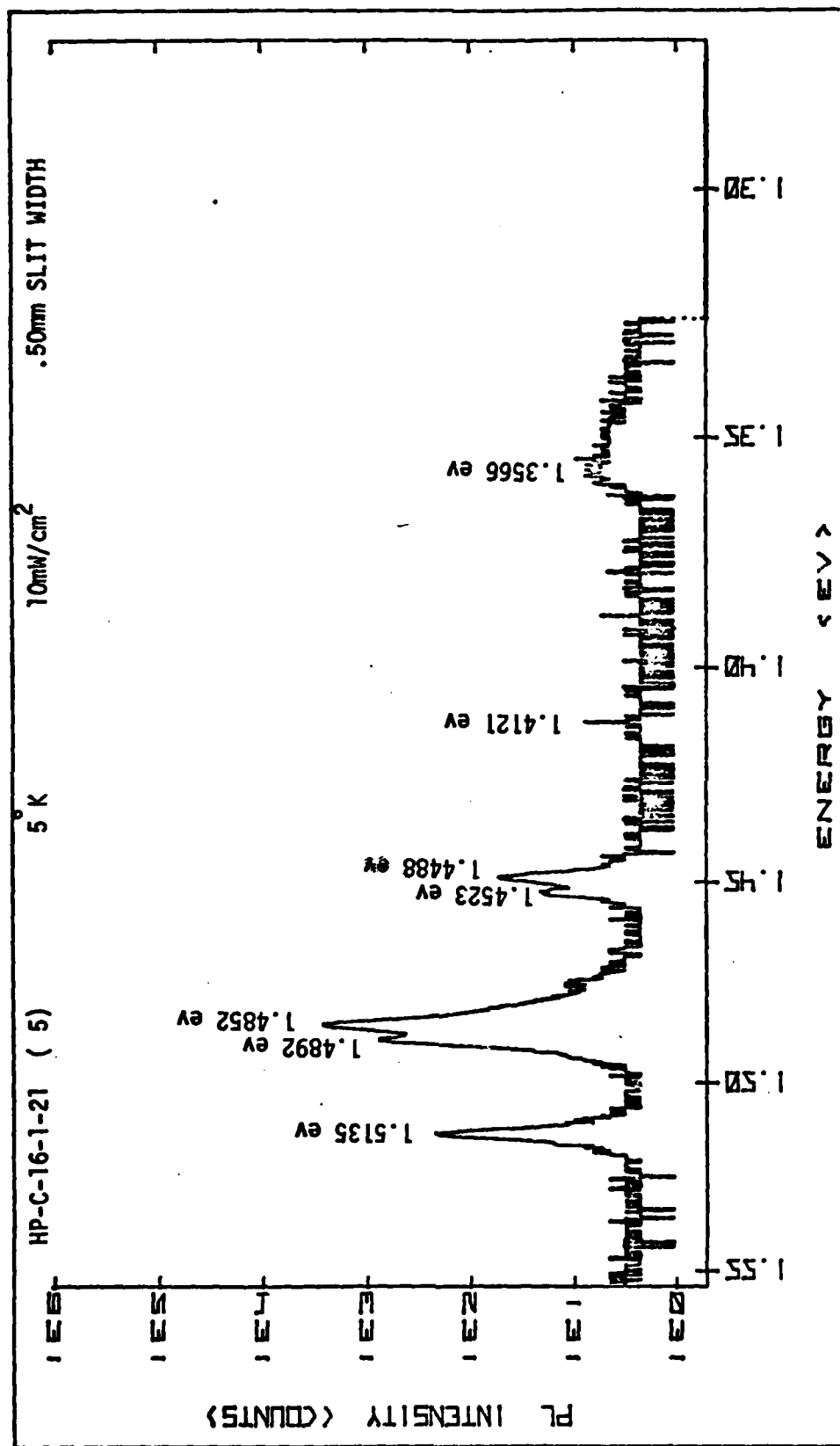
Figure B-26. PL of Implanted (Ge, 10^{14} cm^{-2}) VPE GaAs After Laser Annealing with Optimum Parameters
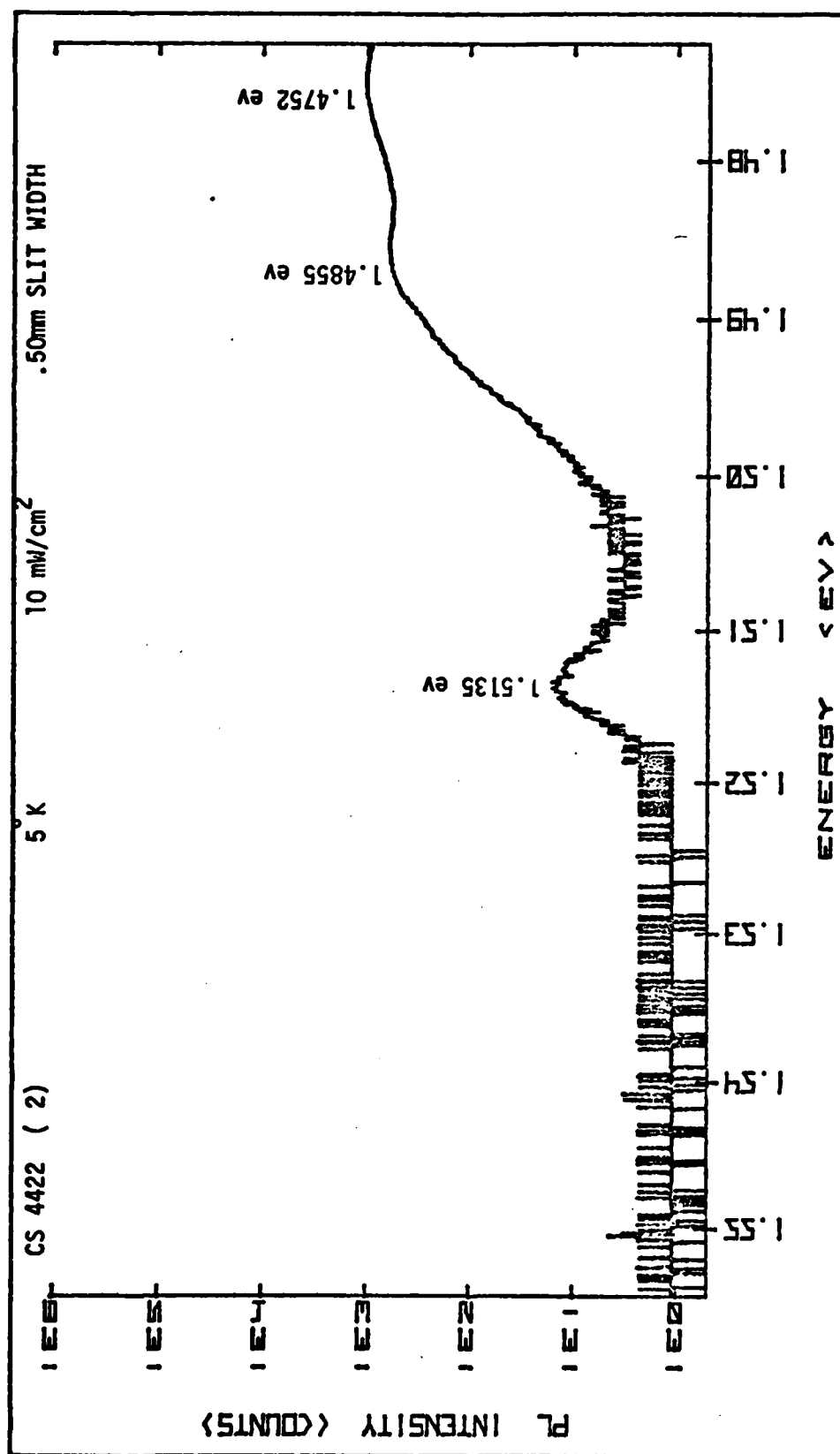
Figure B-27. PL of Implanted (Ge, 10^{14} cm^{-2}) Bridgeman Grown Material
After Thermal Annealing

Vita

James Melvin Heitman was born to Marjorie and Melvin Heitman on 30 October 1946, in Detroit, Michigan. He graduated from Jared W. Finney High School in 1964, and entered Wayne State University in Detroit, Michigan. He received a Bachelor of Science Degree in Electrical Engineering from Wayne State University in April 1969. Upon graduation, he accepted a position as a Project Engineer at the Eastman Kodak Company in Rochester, New York.

In May 1970 he entered the U.S. Air Force. After training at Lackland AFB, Texas and Lowery AFB, Colorado, he was assigned, in April 1971, to the 405B Space Laser Communication Program at WPAFB, Ohio. He received an Honorable Discharge from the Air Force in May 1974, and continued working on the 405B Program in a Civil Service position. In September 1975 he transferred to Cloudcroft, New Mexico, the site of the 405B Space Laser Communication ground station. In September 1977 he returned to the Avionics Lab at WPAFB, where he worked until entering AFIT in October 1979.

Permanent Address: 5000 Croftshire Drive
Kettering, Ohio 45440

REPORT DOCUMENTATION PAGE		READ INSTRUCTIONS BEFORE COMPLETING FORM
1. REPORT NUMBER AFIT/GEO/PH/80-6	**2. GOVT ACCESSION NO.** AD·AC94483	**3. RECIPIENT'S CATALOG NUMBER**
4. TITLE *(and Subtitle)* PHOTOLUMINESCENCE STUDY OF LASER INTERACTION WITH GaAs		**5. TYPE OF REPORT & PERIOD COVERED** MS Thesis
		6. PERFORMING ORG. REPORT NUMBER
7. AUTHOR(s) James M. Heitman		**8. CONTRACT OR GRANT NUMBER(s)**
9. PERFORMING ORGANIZATION NAME AND ADDRESS Air Force Institute of Technology (AFIT-EN) Wright-Patterson AFB, Ohio 45433		**10. PROGRAM ELEMENT, PROJECT, TASK AREA & WORK UNIT NUMBERS**
11. CONTROLLING OFFICE NAME AND ADDRESS Air Force Wright Aeronautical Laboratory Avionics Laboratory (AADR) Wright-Patterson AFB, Ohio 45433		**12. REPORT DATE** December, 1980
		13. NUMBER OF PAGES 112
14. MONITORING AGENCY NAME & ADDRESS*(if different from Controlling Office)*		**15. SECURITY CLASS. *(of this report)*** Unclassified
		15a. DECLASSIFICATION/DOWNGRADING SCHEDULE

16. DISTRIBUTION STATEMENT *(of this Report)*

Approved for public release; distribution unlimited

17. DISTRIBUTION STATEMENT *(of the abstract entered in Block 20, if different from Report)*

18. SUPPLEMENTARY NOTES

Approved for public release; IAW AFR 190-17

FREDERICK C. LYNCH, Major, USAF
Director of Public Affairs   06 JAN 1981

19. KEY WORDS *(Continue on reverse side if necessary and identify by block number)*

Scanned Laser Annealing
Photoluminescence
III-IV compounds
Gallium-Arsenide

20. ABSTRACT *(Continue on reverse side if necessary and identify by block number)*

   A study was made on the effect of scanned CW laser radiation on the
photoluminescence of virgin, VPE and ion-implanted GaAs. The samples were
scanned at room temperature using an argon laser with a beam spot size of
25 microns and a beam dwell time of 1 msec. A flowing cover gas was found
to be essential during scanning for beam powers near the damage threshold.
The damage threshold was primarily a function of laser power and spot size;
dwell time was of secondary importance. Photoluminescence data was taken

DD _{FORM} **1473** EDITION OF 1 NOV 65 IS OBSOLETE

at 5° K using argon laser excitation. Spectra from virgin samples scanned below the damage threshold was similar to that from unscanned samples. For VPE samples implanted at room temperature with Ge at a fluence of 1×10^{14} cm^{-2}, approximately 5% of virgin material luminescence was recovered after laser annealing of both capped and uncapped samples. This is approximately the same percentage achieved after thermal annealing. However, no sign of Ge activation was seen in the laser annealed samples, even though activation was achieved using thermal annealing. Ellipsometry measurements showed that the laser annealed samples had the same index of refraction as found in unimplanted material.

DATE
ILME